Test of Lorentz Invariance Using Sapphire Optical Resonators

Inaugural-Dissertation

zur

Erlangung des Doktorgrades der
Mathematisch-Naturwissenschaftlichen Fakultät
der Heinrich-Heine-Universität Düsseldorf

vorgelegt von

Piergiorgio Antonini

aus Dolo (Italien)

November 2005

Aus dem Institut für Experimentalphysik
der Heinrich-Heine-Universität Düsseldorf

Gedruckt mit der Genehmigung der
Mathematisch-Naturwissentschaftlichen Fakultät der
Heinrich-Heine-Universität Düsseldorf

Referent	:	Prof. Stephan Schiller
Koreferent	:	Prof. Axel Görlitz
Tag der mündlichen Prüfung	:	25. November 2005

Zusammenfassung

Im Laufe dieser Arbeit wurde die Lorentz-Invarianz getestet, indem die Differenz der Resonanzfrequenzen von zwei kryogenen optischen Resonatoren aus Saphir als Funktion der räumlichen Orientierung gemessen wurde.

Die Spezielle Relativitätstheorie ist eine der fundamentalen Theorien in der Physik. Die experimentelle Überprüfung ihrer Prinzipien und Vorhersagen ist nicht nur für die Wissenschaft von großem Interesse, sondern auch für die moderne Technik.

In diesem Experiment werden zwei Nd:YAG-Laser Frequenz-stabilisiert auf die Resonanzfrequenzen zweier gekreuzten ultra-stabiler optischer Resonatoren. Dadurch, dass sie aus reinem Saphir (Al_2O_3) bestehen, zeichnen sie sich durch einen sehr kleinen Wärmeausdehnungskoeffizienten aus. Das reduziert ihre Anfälligkeit für Temperaturschwankungen. Mit einem Puls-Rohr-Kühler sind die Resonatoren auf 3,4 K abgekühlt worden. Diese Technik ist ausgewählt worden, um die Störungen zu vermeiden, die mit dem periodischen Wiederauffüllen bei herkommlichen Flüssighelium-Kryostaten einhergehen. Die vom Kryokühler verursachten Vibrationen konnten durch Vibrationsisolierung, Faserkopplung der Laserstrahlen in die Resonatoren und Dekorrelation der Schwebungsfrequenz mit Hilfe der Fourier-Analyse bei der Kompressionsfrequenz in seinem Relevanz reduziert werden.

Um die Statistik zu verbessern und einen experimentellen Wert für einen zuvor ungemessenen Parameter einer dynamischen Testtheorie zu bestimmen, der für die Lorentz-Invarianz charakteristisch ist, ist der gesamte Aufbau aktiv rotiert worden.

Die systematischen Effekte auf Grund von Veränderungen der Neigung der Resonatoren sind gemessen und dekorreliert worden. Die systematischen Effekte auf Grund von Temperaturschwankungen oder Leistungsschwankungen der einfallenden Laserstrahlen auf die Resonatoren sind mit Hilfe aktiver Regelung verringert worden.

Die Daten sind gemäß der kinematischen Testtheorie von Robertson, Mansouri und Sexl analysiert worden und ergeben eine Verbesserung des vorherigen Ergebnisses um eine Größenordnung. Wir erhalten eine obere Grenze von $(\beta - \delta - 1/2) = (0,5 \pm 3 \pm 0,7) \cdot 10^{-10}$, was einer Verletzung der Lorentz-Invarianz für eine Isotropie des Raums von $\frac{\delta c}{c} = 6,4 \cdot 10^{-16}$ entspricht.

Die Daten sind darüber hinaus auch gemäß einer dynamischen Testtheorie, einer Erweiterung des Standard-Modells der Teilchenphysik, analysiert worden. Dieses Modell zeichnet sich aus durch eine Erweiterung der Maxwell-Gleichungen um Terme, welche die Lorentz-Invrianz verletzen. Ein Ergebnis dieses Experiments war die erstmalige Messung eines Parameters, der für die Lorentzverletzung charakteristisch ist. Dieser Koeffizient kann nur mit einem aktiv rotierenden Aufbau gemessen werden. Für diesen Parameter erhalten wie eine obere Grenze von $|(\tilde{\kappa}_{e-})^{ZZ}| \leq 3 \cdot 10^{-14}$, ein Wert, der durch jüngste Messungen anderer Gruppen bestätigt werden konnte.

Die Ergebnisse der Arbeit wurden publiziert:

1. P. Antonini, M. Okhapkin, E. Göklü and S. Schiller, Phys. Rev. A **71**, 050101(R)

(2005);
2. P. Antonini, M. Okhapkin, E. Göklü and S. Schiller, Phys. Rev. A **72**, 066102 (2005);
3. Schiller *et al.*, e-print physics/0510169, Lecture Notes in Physics, edited by J. Ehlers and C. Lämmerzahl (to be published).

Abstract

In the course of this work a test of Lorentz invariance was performed by comparing the resonance frequencies of two cryogenic sapphire optical resonators as a function of their orientation in space.

The Special Relativity is one of the most fundamental theories in Physics. The need to experimentally test its principles and results is not only of (great) scientific interest, but also technical.

In the experiment presented here two Nd:YAG lasers were frequency-stabilised to the resonance frequencies of two crossed ultra-stable optical resonator. Made of pure sapphire (Al_2O_3), they are characterised by a very small thermal expansion coefficient. This reduces their sensitivity to temperature variations. A pulse-tube cooler was used to cool the resonators down to 3.4 K. This technique was chosen to avoid the disturbances connected to the periodic refills in traditional liquid-helium cryostats. The vibrations induced by the cryo-cooler were reduced by use of vibration insulation, fibre-coupling of the laser beams to the resonators, and decorrelation of the beat frequency by use of Fourier analysis at the frequency of pumping.

In order to improve the statistics and to put an experimental value to a previously unmeasured parameter of a dynamical test theory, which characterises Lorentz invariance, the whole setup was actively rotated.

The systematic effects caused by variations in tilts of the resonators were measured and decorrelated, and systematic effects caused by temperature variations or variations in power of the incident laser bemas on resonators were diminished by use of active control.

The data were analysed in the kinematical test theory of Robertson, Mansouri and Sexl, improving the previous result of one order of magnitude. We set the limit $(\beta-\delta-1/2) = (0.5\pm3\pm0.7)\cdot10^{-10}$, which corresponds to a violation of the Lorentz invariance for the isotropy of space of $\frac{\delta c}{c} = 6.4\cdot10^{-16}$.

The data were also analysed in a dynamical test theory, and extension of the Standard Model of particle physics. This model is characterised by an extension of the Maxwell equations with terms that violates the Lorentz invariance. A result of this experiment was the measurement, for the first time, of one of the parameters that characterise the Lorentz violation. This coefficient can only be measured with an actively rotating setup. We set for this parameter the upper limit: $|(\tilde{\kappa}_{e-})^{ZZ}| \leq 3\cdot10^{-14}$. A value confirmed by more recent measurements by other groups.

The results of the work are published:

1. P. Antonini, M. Okhapkin, E. Göklü and S. Schiller, Phys. Rev. A **71**, 050101(R) (2005);
2. P. Antonini, M. Okhapkin, E. Göklü and S. Schiller, Phys. Rev. A **72**, 066102 (2005);
3. Schiller *et al.*, e-print physics/0510169, Lecture Notes in Physics, edited by J. Ehlers and C. Lämmerzahl (to be published).

Contents

List of Figures

List of Tables

Chapter 1

Theory

1.1 Introduction

This year the 100th anniversary of the theory of Special Relativity is celebrated worldwide, not only in the Physics community. Only very few other scientific theories have had such a big resonance outside the scientists. This is not only because of the outstanding personality of his creator, but also because of the revolutionary character of the theory. Although the results of the theory have always been proved by experiments, there is today a big interest in new experiments to test the validity of the Special and General Relativity. There are several reasons for this interest.

First of all, not only Special and General Relativity describe phenomena like propagation of light, measurements of time and gravitational interactions, Relativity provides the framework in which (at least in principle) every model of physics is based.

Even in the everyday life of the most technological societies Relativity must be taken into account: a common example is the Global Positioning System (GPS) that would make errors at the level of about km per day, without the corrections of Relativity.

Back to Science, Relativity is also important for Metrology: first of all the meter is defined as the distance covered by light in 1/299 792 458 seconds. In addition, all other units of the SI standard (a part from the kelvin) are dependent on Relativity.

Efforts to develop a theory that would unify the Standard Model and Gravitation resulted in Lorentz-violating new theories, such as the Standard Model Extension, explained in details in this thesis. The necessity to test the theory added motivation for new precise tests of Special Relativity in several labs around the world.

The Special Relativity will be treated in this thesis on two ways:

(1) kinematically, when the focus is on the description of the transformation between different inertial systems, and

(2) dynamically, when the speed of light is derived as a consequence of the Maxwell equations.

Already before the invention of the theory of special relativity in 1905 [1], measurements on the speed of light and its dependence on the orientation and motion of the reference frame were performed. New experimental techniques permitted to increase the precision of these experiments significantly over the course of time. The development of laser techniques measurements allowed huge improvements in measurements accuracy [2, 3, 4, 5, 6]. See Fig. 1.1 for a collection of accuracies of experiments on isotropy and dependence on the relative speed of reference frames. of the speed of light.

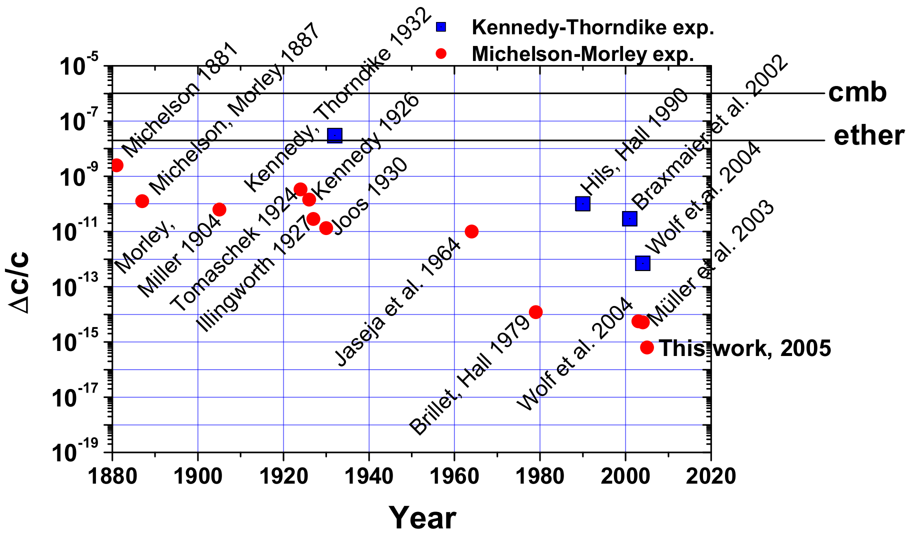

Figure 1.1: Limits for variation of the speed of light for Michelson-Morley and Kennedy-Thorndike experiments. The horizontal line 'cmb' represents the theoretic observable effect in case of a preferred frame in which the lab moves with the velocity of 370 km/s (speed of the Earth respect to the cosmic microwave background). The line 'ether' represents the theoretic observable effect for the classical ether theory, corresponding to the ration $(v/c)^2$, were v is the speed of the Earth respect to the Sun, see Fig. 1.5

The first precision measurement, demonstrating the isotropy of light propagation, was performed by Michelson and Morley in 1887. Local Lorentz Invariance (LLI), isotropy and constancy of the speed of light, is incorporated as a fundamental symmetry into the accepted theories of the fundamental forces, General Relativity [7] and the Standard Model. Numerous experiments have tested LLI with respect to matter and to the electromagnetic field and have upheld its validity until to date [8]. For electromagnetic waves the isotropy of space has so far been verified a the level of a few parts in 10^{15} [2, 3, 4, 5, 6].

New generations of tests of LLI and of other fundamental symmetries like Weak

Equivalence Principle, Local Position Invariance, CPT (charge conjugation, parity inversion, and time reversal) symmetry are seen as one important approach in the quest for a deeper understanding of the forces of nature [8]. They might provide useful inputs for the development of a theory able to describe gravity at the quantum level. In these theories, violations of fundamental symmetries are being considered. Thus, the theoretic models call for improved experiments to either validate LLI at much higher precision levels, or to uncover its limits of validity.

1.1.1 The Michelson-Morley experiment

Michelson-Morley experiment using an interferometer

The Maxwell equations and the Galilei relativity together require the presence of a 'ether', a medium in which the electromagnetic wave of light can propagate. A reference frame (if any) in which the ether would be at rest should be taken as an absolute 'rest frame'. In order to find with which speed and in which direction the Earth was moving through the ether many experiments were planned at the end of the 19^{th} century, but the only one that had high enough sensitivity to reveal that the hypothesis of the ether was wrong was performed by Michelson and Morley in 1887 [9]. As depicted in the left side of Fig. 1.2, in this experiment a beam of light from the source was separated in two parts by a semitransparent mirror (that today is usually called a beam-splitter). Thus a part of the beam follows the path I to mirror M1, and back to the beam-splitter. Then a part of this beam goes on through the beam-splitter back to the source, and the other part is reflected from the beam-splitter and thus sent to the observer. The second path (II) is first deviated by the beam-splitter towards mirror M2, reflected back to the beam-splitter, and the part that is not sent back to the source is superimposed to the beam coming from path I on the observer view. The observer will see the interference pattern produced by the difference of time of arrival between the parts of the two paths that are separated, namely L_1 and L_2.

We can now calculate the displacement of the interference lines as function of the path lengths L_1 and L_2, and of the velocity v of the interferometer through the 'ether'.

For the path I the time needed (in both cases we neglect the parts of the path that are in common) from BS to M1 and back is [10]:

$$t_1 = \frac{L_1}{c+v} + \frac{L_1}{c-v} = \frac{2L_1}{c^2 - v^2} = \frac{2L_1}{c}\frac{1}{1-\dfrac{v^2}{c^2}} \tag{1.1}$$

For the path II we must consider the path covered through the ether:

$$2s = 2\sqrt{L_2^2 + \left(\frac{vt_2}{2}\right)^2} = ct_2$$

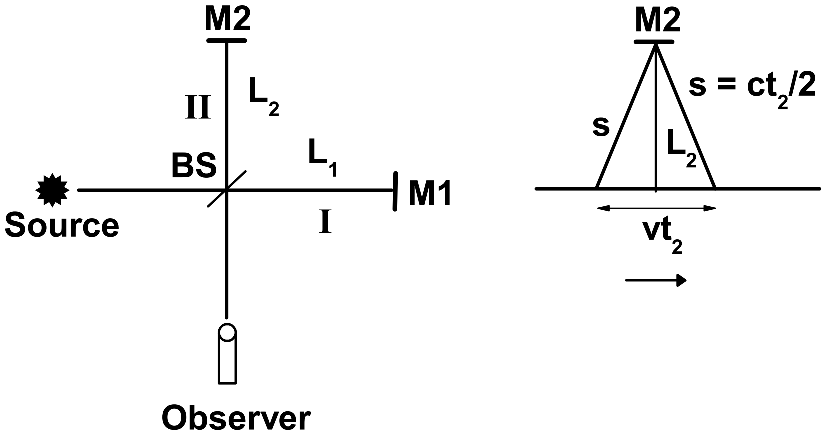

Figure 1.2: **Right:** Scheme of the Michelson interferometer. The beam is divided in two paths I and II by the beam splitter (BS). In the path I the beam goes from BS to mirror M1 and back to BS. In the path II the beam goes from BS to the mirrors M2 and back to the beam-splitter. A part of the two beams is superimposed on the beam-splitter and reach the observer where it produces the interference pattern. The rest goes back to the source. In the real experiment the beams were reflected many times in order to create longer paths that increased the sensitivity of the experiment, see Eq. (1.5). **Left:** The interference pattern of the two pathes depends on the velocity of the interferometer respect to the ether due to the distance vt_2 covered by the interferometer during the time needed by the beam to go from the beam-splitter to the mirror M2 and back.

$$t_2 = \frac{2L_2}{\sqrt{c^2 - v^2}} = \frac{2L_2}{c} \frac{1}{\sqrt{1 - \left(\frac{v}{c}\right)^2}}, \tag{1.2}$$

thus the time difference is:

$$\Delta t = t_2 - t_1 = \frac{2}{c} \left[\frac{L_2}{\sqrt{1 - \left(\frac{v}{c}\right)^2}} - \frac{L_1}{1 - (\frac{v}{c})^2} \right]$$

After a rotation of the interferometer of 90°, the time difference is:

$$\Delta t' = t'_2 - t'_1 = \frac{2}{c} \left[\frac{L_2}{1 - (\frac{v}{c})^2} - \frac{L_1}{\sqrt{1 - \left(\frac{v}{c}\right)^2}} \right]$$

thus the rotation changed this difference by:

$$\Delta t' - \Delta t = \frac{2}{c}\left[\frac{L_1 + L_2}{1-(\frac{v}{c})^2} - \frac{L_1 + L_2}{\sqrt{1-(\frac{v}{c})^2}}\right]$$

we can use the binomial expansion and drop the terms higher than the second-order:

$$\Delta t' - \Delta t \cong \frac{2}{c}(L_1 + L_2)\left[1 + \frac{v^2}{c^2} - 1 - \frac{1}{2}\frac{v^2}{c^2}\right] = \left(\frac{L_1 + L_2}{c}\right)\frac{v^2}{c^2} \tag{1.3}$$

Now the number of fringes that move past the observer are

$$\Delta N = \frac{c[\Delta t' - \Delta t]}{\lambda}, \tag{1.4}$$

the displacement of the interference pattern is found substituting Eq. (1.3) in (1.4):

$$\Delta N \approx \frac{L_1 + L_2}{\lambda}\left(\frac{v}{c}\right)^2 \tag{1.5}$$

where λ is the wavelength of the beam. We can see that the sensitivity of the experiment increases with the lengths of the paths. The paths can be increased only as long as the beams are still coherent through the whole paths.

Michelson Morley experiment using a laser stabilised to a resonator

In the modern Michelson-Morley experiments the interferometers are not anymore used. Instead the resonance frequency of ultrastable resonators in microwave or optic frequencies are used. Two configurations are possible: the comparison of the resonance frequencies of two crossed resonators, Fig. 1.3, or the comparison of the resonance frequency of a stabilised resonator with a stable reference, Fig. 1.4.

The advantages respect to the interferometers are principally two: the interferometers are much more limited by the mechanical stability of the payload on which the source, the beam-splitters and the mirrors lye, and the fact that using a laser or a maser (that produced coherent radiation for a long time) and resonators of very high finesse (related to the quality factor) the photons inside the resonators can bounce several thousands of times, being so equivalent to an interferometer whose arms have a length of order of magnitude of the kilometer, in fact according to Eq. (1.5) the sensitivity depends on the length of the interferometer.

For optical resonators usually the quality of the resonator as an oscillator is expressed as finesse $\mathcal{F}$, which is related to the quality factor Q by the equation:

$$Q = \frac{2L}{\lambda}\mathcal{F}.$$

The finesse in turn is dependent on the optical losses of the resonator (predominantly at the mirror's coating).

The first Michelson-Morley-type experiment using a laser instead of an interferometer was performed by Jaseja *et al.* in 1964 [11]. In that case the accuracy was

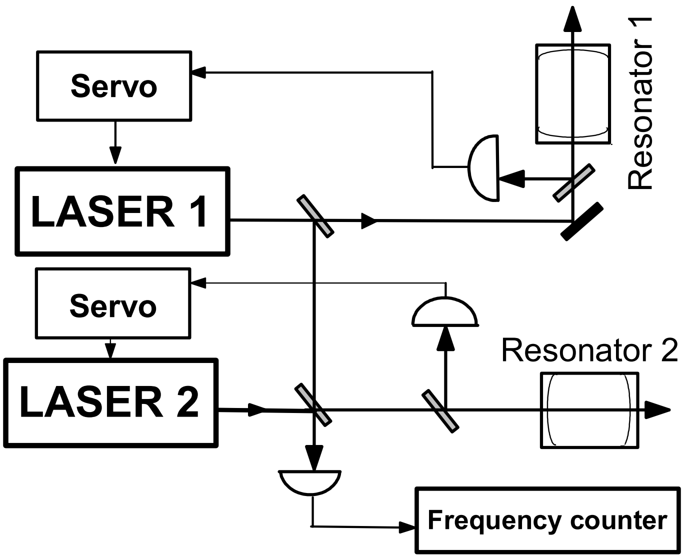

Figure 1.3: Modern Michelson-Morley experiments are performed using laser or microwave generators and ultra-stable resonators instead of interferometers.

limited by the fact that the etalon of length was the laser cavity itself, and a big systematic frequency shift of 275 kHz was observed correlated to the rotation of the setup. For more than twenty years the most accurate experiment was that performed by Brillet and Hall in 1979 [2, 12]. There a He-Ne (wavelength $\lambda = 3.39\ \mu$m) was servostabilised to a highly stable Fabry-Perot resonator. The laser, the servo and the resonator were rotated and the frequency of the stabilised laser compared to the frequency of a second CH_4-stabilised He-Ne laser.

In 2003 Müller *et al.* [5] improved about three times the result of Brillet and Hall, using two crossed sapphire resonators. The use of two resonators doubles the hypothetical signal amplitude, and provides some common-mode rejection of systematic effects. The same cavity used for that experiment were also used for the Kennedy-Thorndike experiment of Braxmaier *et al.* [13] (see Sect. 1.1.2). The fractional frequency shift reported was of $(2.6 \pm 1.7) \cdot 10^{-15}$.

In 2004 Wolf *et al.* [14] improved the measurement using cryogenic sapphire resonators operating in Whispering Galleries modes with a resonance frequency of 11.93 GHz, compared to the frequency of a Hydrogen maser, obtaining a final result of $(1.2 \pm 1.9 \pm 1.2) \cdot 10^{-15}$.

1.1.2 The Kennedy-Thorndike experiment

Less famous than the Michelson-Morley experiment is the Kennedy-Thorndike [15]. The Michelson-Morley experiment is a measurement of the isotropy of the speed of light, that is the dependence of the speed of light on the direction of propagation. The Kennedy-Thorndike experiment (performed for the first time in 1932) is a measurement of the constancy of the speed of light, or its dependence on the speed ('boost') of the lab through the ether. In the classical configuration the principle of the Kennedy-Thorndike experiment was an interferometer with arms of different lengths: the beam of light that is divided into two components and recombined to interfere after that the two components have covered paths of different lengths, their relative phases will depend (according to the ether theory) on the translational velocity of the interferometer through the ether. The modern realisation of the experiment, using lasers and atomic clocks is drawn in Fig. 1.4. It consists of a laser

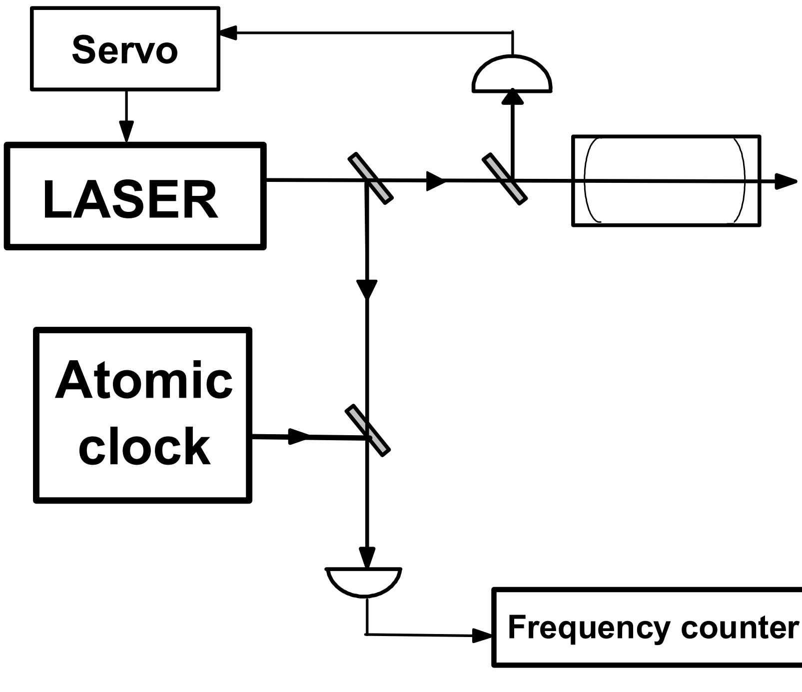

Figure 1.4: One version of the modern Michelson-Morley experiment consists in a laser or a microwave generator locked (servo) to the resonance frequency of a stable cavity. The resonance frequency of the cavity is compared to the output frequency of a stable atomic clock. The same setup can be used for a Kennedy-Thorndike experiment

or a microwave generator locked to the resonance frequency of a stable cavity. The resonance frequency of the cavity is compared to the output frequency of a stable atomic clock, such as a maser, a Cs clock, a laser stabilised to the transition of some molecule, etc. The frequency difference between the resonator and the clock is correlated to the velocity of the lab respect to some reference frame, that could be the Sun system, or the cosmic microwave background.

To measure the dependency on velocity of the frequency difference between the resonator and the clock a variation of the velocity of the experimental apparatus is necessary. There are at least three possibilities, represented in Fig. 1.5:

1. to exploit the variation of velocity v_e of the Earth in its revolution around the Sun, of about 30 km/s. To use the orbital velocity of the Earth implies a measurement that spans over at least six months;

2. to exploit the circumferential velocity v_d of the lab due to the rotation of the Earth (taking into account the latitude). This implies a measurement that spans over one day;

3. to set up the experiment in a satellite. This permits to choose (within the technical possibilities) to choose the most suitable orbit, and possibly to have a drag-free experiment, that is, the experimental setup is in microgravity environment. A description of a possible realisation of this experiment can be found in Sect. 4.1.2.

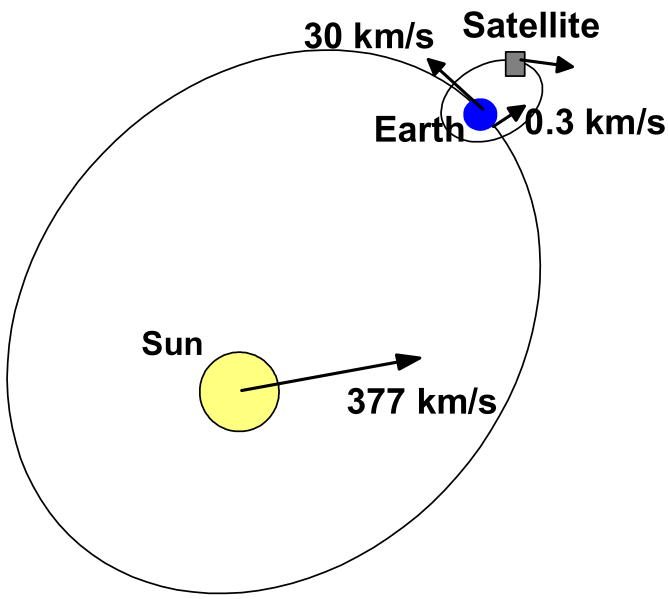

Figure 1.5: To modulate the velocity of the experimental set-up and exploit this modulation for a Kennedy-Thorndike experiment there are at least three possibilities: to exploit the rotation $\Omega_\oplus$ of the Earth around the Sun, or the rotation $\omega_\oplus$ of the Earth around its axis, or to setup an experiment in a satellite. This last solution is a big technical challenge, but the expectations are of an improvements of three order of magnitude respect to the best Earth-based experiments.

In the case of a Earth-based experiment the velocity of the experimental setup can be written as:

$$v(t) = v_s + v_e \sin[\Omega_y(t - t_0)] \cos\phi_E + v_d \sin[\omega_\oplus(t + t_d)] \cos\phi_A$$

where: v_s is the velocity of the Sun in the reference frame, t_0 and t_d are determined by the phase and start date at the begin of the measurement, respectively. Here $\phi_A = 8°$ is the angle between the equatorial plane and the speed of the Sun through the cosmic microwave background (cmb), $\phi_E = 6°$ is the declination between the plane of the Earth's orbit and the direction of the Sun through the cmb, $2\pi/\Omega_\oplus = 1$ year, $2\pi/\omega_\oplus = 1$ sidereal day (23 hours and 56 min.). We are interested in the second order effect, then:

$$\left(\frac{v}{c}\right)^2 \approx \left(\frac{v_s}{c}\right)^2 + \frac{2v_e v_s}{c^2} \sin[\Omega_\oplus(t - t_0)] \cos\phi_E + \frac{2v_d v_s}{c^2} \sin[\omega_\oplus + t_d] \cos\phi_A. \quad (1.6)$$

Using the values: $v_S = 377$ km/s, $v_E = 30$ km/s, $v_P = 330$ m/s, we have:

$$\left(\frac{v}{c}\right)^2 = 1.57 \cdot 10^{-6} + 2.48 \cdot 10^{-7} \sin[\Omega_\oplus(t - t_0)] + 2.74 \cdot 10^{-9} \sin[\omega_\oplus(t + t_d)]. \quad (1.7)$$

We see directly from Eq. (1.7) that an experimental setup designed to exploit the circumferential velocity of the Earth needs a stability two orders of magnitude bigger that an experimental setup that exploits the rotation of the Earth around the Sun. In the second case the experimental setup must remain stable in the time span of one year instead than of a one day. The best experimental results obtained so far were obtained measuring over one year.

1.1.3 The Ives-Stilwell experiment

The Ives-Stilwell experiment measured the time-dilation. The outcome of the experiment is a positive effect, instead of the null effect of the Michelson-Morley and the Kennedy-Thorndike experiments. The scheme of the setup is depicted in Fig.1.6.

The result of the experiment was the displacement of the lines of the H_β lines of hydrogen at 486.1 nm. To get rid of the first-order Doppler effect the measured quantity was the displacement of the centre of mass of the sum of the lines emitted in the direction parallel ($\theta_p = 0$) to the motion of the hydrogen particles with the lines emitted in the direction antiparallel ($\theta_a = \pi$), by means of the mirror M in Fig. 1.6. The hydrogen particles were accelerated at a velocity 0.005 c by means of a potential of 30 kV at the accelerating electrodes A and B in figure.

The respective second-order Doppler shifts are:

$$\nu_0 = \gamma(1 - \beta \cos\theta_{p,a})\nu_0 \quad (1.8)$$

where ν_0 is the transition frequency when the particles are at rest in the frame of the lab. The multiplication of the two equations (1.8) (one for θ_p and one for θ_a) yield the velocity independent relation $\nu_p\nu_a = \nu_0$, if special relativity is valid.

Modern Ives-Stilwell experiments are performed accelerating $^7Li^+$ ions at $v = 0.064\,c$ (13.3 MeV) in a storage ring, using collinear saturation spectroscopy [16].

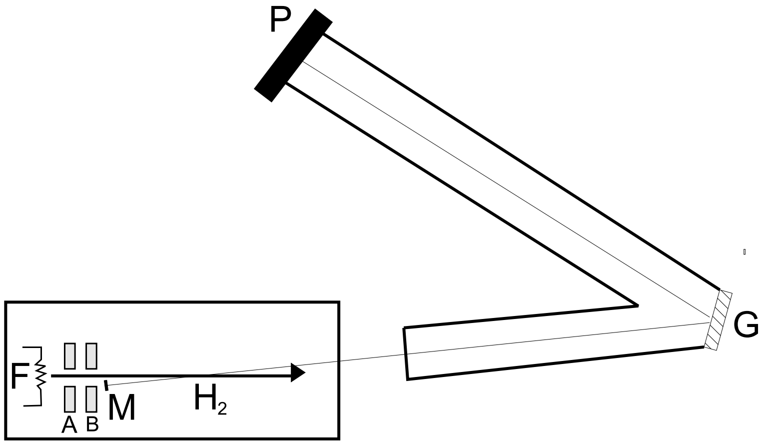

Figure 1.6: The electrodes A and B accelerated the H_2 or H_3 double or triple atomic hydrogen produced in the filament F. The mirror M, placed at 7° respect to the direction of the particles reflected the light emitted antiparallel, superimposing it to the light emitted parallel. A spectrograph G resolved the lines on a photographic plate P.

1.1.4 Local Position Invariance

That experimental setup used in [13] was also used to set a limit on local position invariance (LPI), the gravitational red-shift due to a change in the gravitational potential interacting with the clock. According to the General Relativity, the rate of a clock depends on the gravitational potential: if $\nu(x_1)$ is the rate of a clock collocated in the gravitational potential $U(x_1)$ in the space point x_1, then the rate of the same clock $\nu(x_2)$ in the gravitational potential $U(x_2)$ in the point x_2 is:

$$\nu(x_2) = \nu(x_1)(1 + \frac{U(x_2) - U(x_1)}{c^2}), \tag{1.9}$$

but the rate change does not depend on the type of clock. If LPI is not valid, then the rate change can depend on the type of clock through the parameter α_{clock}:

$$\nu(x_2) = \nu(x_1)(1 + \alpha_{clock}\frac{U(x_2) - U(x_1)}{c^2}), \tag{1.10}$$

with $\alpha_{clock} \neq 1$. To test it two different clocks are compared, exploiting the difference in the gravitational potential due to the different distance between Earth and Sun at different times of the year (or of the orbit of a satellite). Then if the frequency shift depends on the type of clock, this difference is proportional to the gravitational potential:

$$\frac{\Delta\nu_1}{\nu_1} - \frac{\Delta\nu_2}{\nu_2} = \frac{\Delta U}{c^2}(\alpha_{clock1} - \alpha_{clock2}). \tag{1.11}$$

Braxmaier *et al.* comparing a cryogenic optical resonator (one of the two used for this work) to a Nd:YAG laser locked to a transition of the I_2 molecule set a limit for $(\alpha_{res} - \alpha_{mol}) \leq 4 \cdot 10^{-2}$. The most precise measurement for the relation of

Eq. 1.10 is $\alpha_{clock} \leq 7 \cdot 10^{-5}$ [17], comparing the frequencies of a hydrogen maser in a satellite at 10 000 km above the Earth surface and a maser at ground.

1.2 Kinematic test theories

Violations of LLI can be interpreted using so-called test theories. A kinematic test theory commonly applied is that by Robertson, Mansouri and Sexl (RMS) [18, 19, 20, 21]. Here, light propagation is described relative to a preferred frame ('ether frame') Σ in which there is no preferred direction and thus the speed of light c_0 is rectilinear, isotropic and constant. Usually the frame in which the cosmic microwave background is isotropic is assumed to be this frame. Lorentz transformations between a laboratory frame S and Σ are replaced by general linear transformations which depend on the velocity $\vec{v}$ of the lab frame with respect to Σ and on three phenomenological parameters.

1.2.1 The Robertson test theory

In a paper appeared in 1949 [18], H. P. Robertson stated that three second-order experiments (second-order in (v/c)) enable to replace the Einstein's (second) postulate on universality of c. These three experiments are the Michelson-Morley [9], the Kennedy-Thorndike [15] and the Ives-Stilwell [22, 23] experiments.

Robertson postulated the existence of a reference frame Σ, an Einstein's 'rest system', in which light is propagated rectilinearly and isotropically in vacuum with a constant speed c. He also postulated that the 3-dimensional space is Euclidean, that all clocks that are at rest in Σ are synchronised, and that the speed of light in free space is independent of the motion of the source. Also assigned is a metric $d\sigma^2$ defined by:

$$d\sigma^2 = \Sigma\gamma_{\mu\nu}d\xi^\mu d\xi^\nu = d\tau^2 - (d\xi^2 + d\eta^2 + d\zeta^2)/c^2 \tag{1.12}$$

for the coordinates $(\tau; \xi, \eta, \zeta)$. Here τ is the time coordinate and the other three the spatial coordinates. This metric is useful to:

1. measure time intervals;
2. measure space intervals;
3. characterise all beams of lights passing through an event E as the generator of the cone $d\sigma = 0$ with E as vertex.

Next he postulated a second reference frame S, a 'moving system', which is moving with a constant velocity $d\xi^\alpha/d\tau = v^\alpha$, of magnitude $v < c$. The frame S is provided of the coordinates $(x^i) = (t; x, y, z)$, and also the spatial 3-dimensional space (x, y, z) in S be Euclidean. No other assumption is made concerning the velocity of light or other physical law in S, that will be derived from results of experiments and from the laws postulated in Σ.

We must then find the transformation $T : (t; x, y, z) \rightarrow (\tau; \xi, \eta, \zeta)$ that relates the measurements on S with the measurements in Σ. This transformation should only depend on the relative velocity v^α between the two systems, and reduce to identity when $v^\alpha \mapsto 0$. Moreover, limiting ourselves in the space-time neighborhood of a given event, the transformation T can be assumed linear.

Choosing that event as the common origin of the coordinates, the transformation simplifies:

$$T = \xi^\mu = \sum_{i=0}^{3} a_i^\mu x^i \tag{1.13}$$

For the clock synchronisation will be assumed the Einstein's clock synchronisation, described at the end of this section.

Defining $d\sigma = 0$ as the light cone we determine the normalisation imposed on the coefficients of T. We can write the metric (1.12) in the coordinates x^i as:

$$d\sigma^2 = g_{ij} dx^i dx^j \tag{1.14}$$

with

$$g_{ij} = \gamma_{\mu\nu} a_i^\mu a_j^\nu$$

the repeated indexes imply summation over their range. Proper choice of orientation of the axis and Einstein's synchronisation lead to the form

$$\begin{pmatrix} a_0^0 & va_1^1/c^2 & 0 & va_3^1/c^2 \\ va_0^0 & a_1^1 & 0 & a_3^1 \\ 0 & 0 & a_2^2 & a_3^2 \\ 0 & 0 & 0 & a_3^3 \end{pmatrix} \tag{1.15}$$

for the transformation T.

We can write the metric (1.14) as:

$$d\sigma^2 = g_0^2 dt^2 - [g_1^2 dx^2 + g_2^2 (dy^2 + dz^2)]/c^2 \tag{1.16}$$

where

$$\left.\begin{array}{rcl} g_0 & = & a_0^0 \sqrt{1 - v^2/c^2} \\ g_1 & = & a_1^1 \sqrt{1 - v^2/c^2}, \\ g_2 & = & a_2^2 \end{array}\right\} \tag{1.17}$$

In order to completely define the transformation T we need the dependence of the three parameters a_0^0, a_1^1 and a_2^2, or alternatively g_0, g_1 and g_2 on the magnitude of v. We know that they must reduce to 1 when $v \mapsto 0$, and the fact that the light paths in S are generators of the cones $d\sigma^2 = 0$ only establish the ratios between these parameters, using observations involving the speed of light.

The result of the Michelson-Morley experiment, stating that the total time required for light to traverse a distance l and back is independent of its direction implies for the above mentioned parameters, that

$$g_2(v) = g_1(v), \tag{1.18}$$

or

$$a_2^2 = a_1^1\sqrt{1 - v^2/c^2} \tag{1.19}$$

and is equivalent to a length contraction of $\sqrt{1 - v^2/c^2}$.

The result of the Kennedy-Thorndike experiment, stating that the total time required for light to traverse a closed path in S is independent of the velocity v of S relative to Σ delivers $g_1/g_0 = 1$.

Equations (1.16), (1.18) and (1.19) give then:

$$\left.\begin{array}{l} g_0(v) = g_1(v) = g_2(v) := g(v) \\ a_0^0 = a_1^1 = \frac{g(v)}{\sqrt{1-v^2/c^2}} \\ a_2^2 = g(v) \end{array}\right\} \tag{1.20}$$

This means that the Michelson-Morley and Kennedy-Thorndike experiments together imply that the two-way speed of light in vacuum, measured in S, is equal to c, independently of its direction and of the relative velocity between S and Σ. The metric becomes then

$$ds^2 = d\sigma^2/g^2(v) = dt^2 - \frac{1}{c^2}(dx^2 + dy^2 + dz^2) \tag{1.21}$$

Using Eq. (1.16) and (1.17) the transformation assumes the usual Lorentz form

$$T := \left\{\begin{array}{lcl} \tau & = & \frac{g(t+vx/c^2)}{\sqrt{1-v^2/c^2}} \\ \xi & = & \frac{g(vt+x)}{\sqrt{1-v^2/c^2}} \\ \eta & = & gy \\ \zeta & = & gz \end{array}\right. \tag{1.22}$$

No experiment involving only the velocity of light in S is useful to determine the unknown parameter $g(v)$. Einstein postulated it to be unity. The Ives-Stilwell experiment [22, 23], stating that the frequency of a moving atomic clock is altered by the factor $\sqrt{1 - u^2/c^2}$, being u the velocity of the clock to respect to the observer, determines the parameter $g(v)$ as unity, within the experimental accuracy, see Sect. 1.1.3.

Conclusion of the Robertson theory was then that the three experiments together replace almost completely the Einstein's postulates with experimental results, delivering the metric:

$$ds^2 = d\sigma^2 = dt^2 - \frac{1}{c^2}(dx^2 + dy^2 + dz^2). \tag{1.23}$$

The Einstein's synchronisation

Einstein defined simultaneity by postulating the constancy of the speed of light. To define the Einstein synchronisation, consider two points A and B. The clock in A can only be used to measure time differences between events that happen near A, and the clock in B can only be useful near B. This defines an 'A time' and a 'B time'. To have a common time both for A and B, we *define* that the time for a light signal to go from A to B and the time to go from B to A are equal. If we put a mirror in B and send a light signal from A to B at $t = 0$, that comes back to A at time $t = t_0$, then the time at which the signal reaches B is *defined* as $t_0/2$. This defines a procedure for synchronising clocks in all the space. A corollary for this definition is that the speed of light in vacuum has always the same value [24]. This is the Einstein's synchronisation.

1.2.2 The Mansouri-Sexl test theory

The Robertson's theory is too general to be used to compare different kind of experiments concerning the isotropy and constancy of the speed of light. A more practical test theory was achieved by the development of the Robertson's theory by Reza Mansouri and Roman U. Sexl in a series of three papers in 1977 [19, 20, 21].

There as 'ether frame' was considered the cosmic background microwave radiation. In the same year of the publication of these papers, moreover, an anisotropy of the cosmic background radiation was measured by Smooth *et al.* [25]. This anisotropy was interpreted as Doppler shift produced by the motion of the Earth relative to the inertial frame in which the radiation is assumed to be isotropic. This motion is given by the motion of the Sun (377 km/s) $\pm$ the motion of the Earth around the Sun (30 km/s). This gives a point to considering as reference frame that one in which the microwave background radiation is isotropic.

Mansouri and Sexl considered these assumptions:

(L1) The velocity of light is independent of the motion of the source;

(Σ1) In the preferred frame Σ the Einstein synchronisation and the synchronisation by slow clock transport agree;

(S1) There is no preferred direction in Σ.

The conditions (Σ1) and (S1) imply in the three dimensional case that the velocity of light is isotropic in Σ. The condition (Σ1) does not define Σ uniquely. Then the second frame S is considered having a velocity $v < c$ with respect to Σ. It also implies that the time dilation factor be exactly the Special Relativity factor $a(v) = \sqrt{1 - (v/c)^2}$ in the transformation between the two systems:

$$\begin{array}{rcl} T_S & = & a(v)T_\Sigma + e(v)Z_S \\ X_S & = & d(v)X_\Sigma \\ Y_S & = & d(v)Y_\Sigma \\ Z_S & = & b(v)(Z_\Sigma - vT_\Sigma) \end{array} \tag{1.24}$$

that must be linear because the world-line of a free falling body is a straight line in the space-time in each inertial system.

The function $e(v)$ defines the clock synchronisation. With the Einstein synchronisation it is $e(v) = -v/(c^2(1-v^2))$. As consequence of the isotropy of space, the functions a, b and d are even in v. This theory restricts itself only to kinematic aspects, and becomes cumbersome for very high velocities, but for $v \ll c$ we can write:

$$\begin{array}{rcl} a(v) & = & 1 + \alpha(\frac{v}{c})^2 + \mathcal{O}\left(\frac{v^4}{c^4}\right) \\ b(v) & = & 1 + \beta(\frac{v}{c})^2 + \mathcal{O}\left(\frac{v^4}{c^4}\right) \\ d(v) & = & 1 + \delta(\frac{v}{c})^2 + \mathcal{O}\left(\frac{v^4}{c^4}\right) \end{array} \tag{1.25}$$

The relativity implies:

$$\alpha = -\tfrac{1}{2}, \beta = \tfrac{1}{2}, \delta = 0.$$

Some calculations yield the final equation, that is the useful relation of the test theory:

$$\boxed{\frac{c}{c(\theta)} = 1 + \left(\beta + \delta - \frac{1}{2}\right)\left(\frac{v}{c}\right)^2 \sin^2\theta + (\alpha - \beta + 1)\left(\frac{v}{c}\right)^2 + \mathcal{O}\left(\frac{v^4}{c^4}\right)} \tag{1.26}$$

where the coefficient $A = (\beta + \delta - \frac{1}{2})$ can be constrained with a Michelson-Morley-like experiment, and the coefficient $B = (\alpha - \beta + 1)$ with Kennedy-Thorndike. The parameter α is measured with Ives-Stilwell-like experiments.

The parameter α is measured in the Ives-Stilwell experiment through the equation (1.8), in the form:

$$\frac{\nu_p \nu_a}{\nu_0} = 1 + 2\alpha(\beta^2 + 2\vec{\beta}_{lab} \cdot \vec{\beta}) + \mathcal{O}\left(\frac{v^4}{c^4}\right) \tag{1.27}$$

where $\vec{\beta}_{lab} = \vec{v}_{lab}/c$, and the other quantities were already defined in Sect. 1.1.3.

It was measured using laser collinear saturation spectroscopy on fast ions in a storage ring in Heidelberg by Saathoff *et al.* [16]. They obtained a limit of $2.2 \cdot 10^{-7}$ for deviations from the time-dilation factor $\gamma = \frac{1}{\sqrt{1-(\frac{v}{c})^2}}$.

The best measurement for the MM parameter A was $(2.2 \pm 1.5) \cdot 10^{-9}$ [5], obtained with a non-rotating setup, that was improved in this work to $(0.5 \pm 3 \pm 0.7) \cdot 10^{-10}$ [26]. Wolf *et al.* recently published a similar value of $(-0.9 \pm 2.0) \cdot 10^{-10}$, measured with a rotating setup consisting in rotating microwave sapphire cryogenic resonators, over a time span of 18 days.

The most stringent measurement on the KT parameter B to date is $B = (1.6 \pm 3.0) \cdot 10^{-7}$ [14].

In the Robertson theory the above coefficients correspond to:

$A = |1 - \frac{g_1(v)}{g_2(v)}|$ and $B = |1 - \frac{g_1(v)}{g_0(v)}|$.

1.3 Data analysis in the RMS framework

The parameter $(\beta - \delta - \frac{1}{2})$ from Eq.(1.26) is obtained by fitting the functions:

$$\begin{aligned} 2B(t) = (1/2 - \beta + \delta)(v^2/c_0^2)(\gamma_3 \cos \omega_\oplus T_\oplus + \\ \gamma_4 \cos 2\omega_\oplus T_\oplus + \sigma_3 \sin \omega_\oplus T_\oplus + \sigma_4 \sin 2\omega_\oplus T_\oplus)\ , \end{aligned} \tag{1.28}$$

$$\begin{aligned} 2C(t) = (1/2 - \beta + \delta)(v^2/c_0^2)(\gamma_0 + \gamma_1 \cos \omega_\oplus T_\oplus + \\ \gamma_2 \cos 2\omega_\oplus T_\oplus + \sigma_1 \sin \omega_\oplus T_\oplus + \sigma_2 \sin 2\omega_\oplus T_\oplus), \end{aligned} \tag{1.29}$$

the expressions for the γ_i and σ_i are given in the Table 1.1

Table 1.1: The values of the γ_i and σ_i appearing in Eqs.(1.28) and (1.29).

$\gamma_0 =$	$\frac{1}{4}\sin^2\chi(3\cos^2\Theta - 1)$		
$\gamma_1 =$	$\frac{1}{2}\cos\Phi\sin 2\Theta\sin 2\chi$	$\sigma_1 =$	$\gamma_1 \tan\Phi$
$\gamma_2 =$	$\frac{1}{4}\cos 2\Phi\cos^2\Theta(\cos 2\chi - 3)$	$\sigma_2 =$	$\gamma_2 \tan 2\Phi$
$\gamma_3 =$	$\sigma_3 \tan\Phi$	$\sigma_3 =$	$\cos\Phi\sin\chi\sin 2\Theta$
$\gamma_4 =$	$-\sigma_4 \tan 2\Phi$	$\sigma_4 =$	$\cos^2\Theta\cos\chi\cos 2\Phi$

$T_\oplus$ is the time since the beginning of the data plus an offset that accounts for a time difference since the coincidence of the lab's y axis with the $\hat{Y}$ axis of the Sun-centered system [27]. The direction of the Sun's velocity $\vec{v}$ relative to the cosmic microwave background is given by the right ascension $\Phi = 168°$ and the declination $\Theta = -6°$. The systematics are modeled adding a contribution $b_{syst} \sin 2\theta + c_{syst} \cos 2\theta$ to Eq.(1.66), and fit b_{syst}, c_{syst}, $\beta - \delta - \frac{1}{2}$. Effectively, this means that only the modulation of the $\{2B, 2C\}$ amplitudes by Earth's rotation contributes to the fit result for $(\beta - \delta - \frac{1}{2})$.

1.4 The Standard Model Extension

Nowadays the strongest theoretic efforts on Relativity are on the *dynamical* aspects. In fact, the kinematical test theories require the definition of a preferred reference frame (the cosmic microwave background, for example), and the transformations could depend on the choice of the reference frame. Moreover, the kinematical test theories give no explanation for the violation of Lorentz invariance, they only give the parameters to quantify the violation.

Dynamical test theories, like the Standard Model Extension, include a Lagrangian that yields modified Maxwell or Dirac equations. The coefficients do depend on the choice of the reference frame, but there is no necessity to define a preferred frame. A Sun-centred reference frame is chosen only for practical reasons, and the coefficients show a temporal dependency due to the motion of the lab relative to the Sun. For a definition of a reference frame see Sect. 1.4.2 below.

The unification of the fundamental forces in nature is expected to occur in the Plank scale, that is the natural scale for a fundamental theory that includes gravity, where quantum physics and gravity could meet. The Planck mass is defined by $m_P = \sqrt{\frac{hc}{G}} = 5.45604{\cdot}10^{-8}\text{kg} \simeq 10^{19}\text{GeV}$. This is the only combination of h, c and G that results in a quantity with the dimensions of a mass. At low energy scale, relative to Planck scale, observable violations of Lorentz invariance are described by an extension of the Standard Model of physics, the Standard Model Extension (SME). Among the possible mechanisms that could originate Lorentz violations one is in the context of string and field theories. A Lorentz violation would be expected to take place at the order of magnitude of $m_w/m_P \simeq 10^{-17}$, where $m_w \simeq 100$ GeV is the electroweak scale, or even smaller.

A spontaneous breaking of the Lorentz symmetry can occur in string theory [28]. The idea there is that in order to have strings describe the 4-dimensional conventional space-time, it is necessary that some metamorphosis occur that compactifies the 26 dimension (for strings) or the 10 (for the superstring) of the Poincaré symmetry. The Lorentz invariance could be broken by the generation for Lorentz tensors of negative square masses and from static tensor-tensor-scalar couplings.

1.4.1 The modified Maxwell equations

A comprehensive dynamical test theory of Local Lorentz Invariance (LLI) violation has been developed, the Standard Model Extension (SME) [29, 27]. It is based on the Lagrangian of the Standard Model, extended by terms that violate LLI and CPT. These terms describe possible violations in the behaviour of both matter and fields, and contain a large number of unknown parameters, that in principle can be determined experimentally. Moreover, the SME contains the Robertson-Mansouri-Sexl kinematical test theory as a special case [27].

The SME allows for violations of Lorentz and CPT symmetries that the Standard Model and Einstein's Relativity do not. In fact the Standard Model allows for violations of C, or P, or T, or CP, but not of CPT or Lorentz Invariance (isotropy and constancy of speed of light). The Standard Model Extension allows for violations of CPT. The CPT theorem, that links Lorentz and CPT symmetries can be used to show that particles and antiparticles must have some common properties, such as mass, size of charge, magnetic moment. Violations of CPT, allowed by the SME would explain differences between the spectra of hydrogen and antihydrogen [30], an effect forbidden in the Standard Model. This effect has not yet been experimentally demonstrated.

The Standard Model Extension extends the minimal SU(3)×SU(2)×U(1) gauge invariant Standard Model, where the Maxwell equations can be written through the Lagrangian:

$$\mathcal{L}_{mw} = -\frac{1}{4}F_{\mu\nu}F^{\mu\nu}$$

where $F_{\mu\nu} = \partial_\mu A_\nu - \partial_\nu A_\mu$.

In particular, the extended Lagrangian of the electromagnetic field is given by

$$\mathcal{L} = -\frac{1}{4}F_{\mu\nu}F^{\mu\nu} + \frac{1}{2}(k_{AF})^\kappa \epsilon_{\kappa\lambda\mu\nu}A^\lambda F^{\mu\nu} - \frac{1}{4}(k_F)_{\kappa\lambda\mu\nu}F^{\kappa\lambda}F^{\mu\nu}. \tag{1.30}$$

The coefficient $\frac{1}{2}(k_{AF})^\kappa$ is real, has the dimension of a mass, and is CPT odd. This coefficient is associated with negative contributions to the energy, thus it is a potential source of instability. Theoretic [29, 27] and experimental [31] results allow to set it as zero, then for the following

$$\frac{1}{2}(k_{AF})^\kappa \epsilon_{\kappa\lambda\mu\nu}A^\lambda F^{\mu\nu} = 0.$$

We can express the Lagrangian of the photon sector in terms of the potentials $(\vec{A}, \phi)$ and of the fields $(\vec{E}, \vec{B})$:

$$\begin{aligned}
\mathcal{L} &= \frac{1}{2}\left(\vec{E}^2 - \vec{B}^2\right) + \frac{1}{2}\alpha\left(\vec{E}^2 + \vec{B}^2\right) + \frac{1}{2}\beta_E^{jk}E^jE^k \\
&+ \frac{1}{2}\beta_B^{jk}B^jB^k + \frac{1}{2}\beta_{EB}^{jk}E^jB^k \\
&+ k_{AF}^0\vec{A}\cdot\vec{B} - \phi\vec{k}_{AF}\cdot\vec{B} + \vec{k}_{AF}\cdot\left(\vec{A}\times\vec{E}\right).
\end{aligned} \tag{1.31}$$

The equations of motion, remembering that we set

$$\frac{1}{2}(k_{AF})^\kappa \epsilon_{\kappa\lambda\mu\nu}A^\lambda F^{\mu\nu} = 0,$$

are [27]:

$$\partial_\alpha F_\mu^\alpha + (k_F)_{\mu\alpha\beta\gamma}\partial^\alpha F^{\beta\gamma} = 0 \tag{1.32}$$

and these are the Lorentz-breaking extensions of the usual Maxwell equations (in absence of sources) $\partial_\mu F^{\mu\nu} = 0$.

In order to get the observables, it is useful to observe an analogy with the conventional electrodynamics: if we define the fields $\vec{D}$ and $\vec{H}$ by the matrix equation

$$\begin{pmatrix} \vec{D} \\ \vec{H} \end{pmatrix} = \begin{pmatrix} 1+\kappa_{DE} & \kappa_{DB} \\ \kappa_{HE} & 1+\kappa_{HB} \end{pmatrix} \begin{pmatrix} \vec{E} \\ \vec{B} \end{pmatrix} \tag{1.33}$$

where $\vec{E}$ and $\vec{B}$ are the electric and magnetic fields obtained solving the modified Maxwell equations (1.32).

The matrices κ_{DE}, κ_{HB}, κ_{DB} and κ_{HE} are defined in terms of k_F as

$$\begin{aligned}
(\kappa_{DE})^{jk} &= -2(k_F)^{0j0k} \\
(\kappa_{HB})^{jk} &= \frac{1}{2}\epsilon^{ipq}\epsilon^{krs}(k_F)^{pqrs} \\
(\kappa_{DB})^{jk} &= -(\kappa_{HE})^{kj} = (k_F)^{0jpq}\epsilon^{kpq}.
\end{aligned} \tag{1.34}$$

The modified Maxwell equations can now be written in the familiar form of the Maxwell equations in homogeneous anisotropic media:

$$\vec{\nabla} \times \vec{H} - \partial_0 \vec{D} = 0 \tag{1.35}$$
$$\vec{\nabla} \times \vec{E} + \partial_0 \vec{B} = 0 \tag{1.36}$$
$$\vec{\nabla} \cdot \vec{D} = 0 \tag{1.37}$$
$$\vec{\nabla} \cdot \vec{B} = 0 \tag{1.38}$$

The advantage of this substitution is that in this formalism many results of the conventional electrodynamics still holds.

For the observables of interest here, we better introduce the coefficients:

$$(\tilde{\kappa}_{e+})^{jk} = \frac{1}{2}(\kappa_{DE} + \kappa_{HB}^{jk}) \tag{1.39}$$
$$(\tilde{\kappa}_{e-})^{jk} = \frac{1}{2}(\kappa_{DE} - \kappa_{HB}^{jk}) - \frac{1}{3}\delta^{jk}(\kappa_{DE}^{ll}) \tag{1.40}$$
$$(\tilde{\kappa}_{o+})^{jk} = \frac{1}{2}(\kappa_{DB} + \kappa_{HE}^{jk}) \tag{1.41}$$
$$(\tilde{\kappa}_{o-})^{jk} = \frac{1}{2}(\kappa_{DB} - \kappa_{HE}^{jk}) \tag{1.42}$$
$$(\tilde{\kappa}_{tr})^{ll} = \frac{1}{3}(\kappa_{DE}^{ll}) \tag{1.43}$$

Eqs. (1.39) to (1.42) define 3×3 matrices, while Eq. (1.43) defines a single coefficient. The subscripts 'e' and 'o' are for (parity) even or odd respectively, the signs $\pm$ for the respective sum or difference in their definitions, and the subscript $_{tr}$ for 'trace'.

These parameters are the useful ones to compare the results of different experiments: typical laboratory experiments with electromagnetic resonators search for rotation-violating parity even observables ($\tilde{\kappa}_{e+}$) and ($\tilde{\kappa}_{e-}$). Observables depending on the leading order on the velocity are sensitive to the parity odd coefficients, and the last (1.43) is the only one to play role in the second order in the velocity.

The condition on the double trace of $(k_F)_{\kappa\lambda\mu\nu}$ implies the tracelessness of $\kappa_{DB} = (\kappa_{HE})^T$. Thus κ_{DE} and κ_{HB} have eleven independent elements and the matrix $\kappa_{DB} = -(\kappa_{HE})^T$ eight, for a total of nineteen independent coefficients of k_F.

The coefficient $(k_F)_{\kappa\lambda\mu\nu}$ is dimensionless and CPT even. It describes violations of LLI and has 19 independent coefficients. Their values are dependent on the frame of reference; a frame in which the Sun is stationary is chosen for practical reasons. It can be decomposed into two Lorentz-irreducible pieces, one with 10 coefficients, that describe polarization-dependent effects, the second with the remaining nine, analogous to the trace-free Ricci-tensor. The 10 components of the first part can be restricted to the level of 10^{-32} using astronomical observations of the polarization of distant light sources [32], and in the following will be set as zero.

Of the remaining 9 coefficients of the k_F, one ($\tilde{\kappa}_{tr}$) describes an asymmetry of the one-way speed of electromagnetic waves [33], while the others describe different aspects of violations of constancy, *i.e.* a dependence on the direction of propagation and on the speed of the laboratory frame of reference. These eight coefficients can be arranged in two traceless 3×3 matrices: the antisymmetric $(\tilde{\kappa}_{o+})^{ij}$ that describes violation of boost invariance and therefore enters observable quantities weighted by the ratio $\beta_\oplus \simeq 10^{-4}$ of Earth's orbital velocity and the speed of light, and the symmetric $(\tilde{\kappa}_{e-})^{ij}$ quantifying anisotropy of c.

These eight coefficients can in principle be determined by measuring the dependence of the resonance frequency of an electromagnetic resonator (assuming that particles satisfy LLI). If the electromagnetic resonator is stationary in the lab fixed on Earth, seven coefficients can be determined by taking advantage of the rotation and orbital motion of Earth. Three experiments, using ultra-stable cryogenic resonators for microwaves and optical waves, have been performed recently along this line. Lipa *et al.* [4] took data for ~100 days and could constrain four coefficients of $\tilde{\kappa}_{e-}$ and four linear combinations of three coefficients of $\tilde{\kappa}_{o+}$. Müller *et al.* [5] performed an experiment where the measurement duration was extended to a sufficient duration (over 1 year) that the measurement of the 7 coefficients was achieved. Wolf et al. [6] extended the measurement time further and improved significantly on the limits.

The eighth coefficient, $(\tilde{\kappa}_{e-})^{ZZ}$, was first determined with the work described in this thesis [26].

1.4.2 Definition of the reference frame

In order to derive the equations that quantify the change of beat frequency between the two resonators, let us define the reference frame in which they will be calculated. The lab cannot be considered as inertial. For practical reasons a Sun-centred system will be taken as the inertial system. In fact over the time elapsed during a measurement this system can be considered as not accelerating.

In this system, described on [27, 34, 35], we define a $\hat{X}$ axis pointing towards the vernal equinox on the celestial sphere, in the Earth's equatorial plane together with its orthogonal $\hat{Y}$, and $\hat{Z}$ parallel to Earth's rotation axis, but along the centre of the Sun. The Earth's equatorial plane, on which the vectors $\hat{X}$ and $\hat{Y}$ lie, is at an angle of $\eta \approx 23°$ to the Earth's orbital plane. The time T is measured by a clock at rest in the Earth, with origin $T = 0$ in the vernal equinox of the year 2004. In

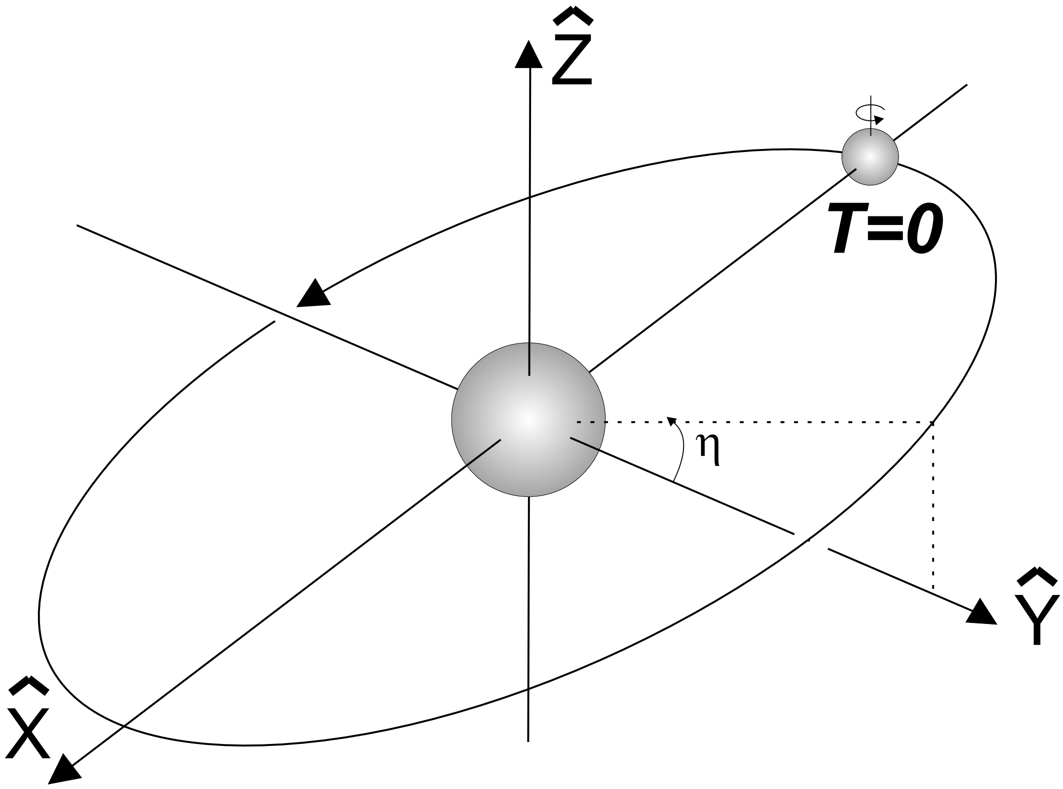

Figure 1.7: The definition of the coordinate system: the time point T = 0 correspond to the position of the Earth in the vernal equinox.

the laboratory frame we define the x axis pointing south, the y east and z axes to complete the orthogonal reference system (vertically upwards). The time scale is defined setting $T_\oplus$ as origin of the lab time when the axis $\hat{Y}$ and y coincide.

Due to the Earth's movement in space, the values of the coefficients defined in Eqs. (1.33) change accordingly to the position of the Earth, that is they show a time dependence, that is to be taken into account.

We define $\omega_\oplus \simeq 2\pi/(23\text{h}56\text{min})$ the Earth's sidereal angular frequency and $\Omega_\oplus$ the angular frequency of the Earth's orbital motion, and $\beta_\oplus$ its speed. The angle χ is the colatitude of the laboratory. We assume the orbit circular, the rotation from the Sun-centred system to the laboratory frame is given by [27]:

$$R^{jJ} = \begin{pmatrix} \cos\chi\cos\omega_\oplus T_\oplus & \cos\chi\sin\omega_\oplus T_\oplus & -\sin\chi \\ -\sin\omega_\oplus T_\oplus & \cos\omega_\oplus T_\oplus & 0 \\ \sin\chi\cos\omega_\oplus T_\oplus & \sin\chi\sin\omega_\oplus T_\oplus & \cos\chi \end{pmatrix}. \tag{1.44}$$

The velocity 3-vector of the lab in the Sun-centred frame is then:

$$\vec{\beta} = \beta_\oplus \begin{pmatrix} \sin\Omega_\oplus T \\ -\cos\eta\cos\Omega_\oplus T \\ -\sin\eta\cos\Omega_\oplus T \end{pmatrix} + \beta_L \begin{pmatrix} -\sin\omega_\oplus T_\oplus \\ \cos\omega_\oplus T_\oplus \\ 0 \end{pmatrix}. \tag{1.45}$$

The matrices κ in the lab system will be transformed in this way:

$$(\kappa_{DE})^{jk}_{lab} = T_0^{jkJK}(\kappa_{DE})^{JK} - T_1^{(jk)JK}(\kappa_{DB})^{JK} \tag{1.46}$$

$$(\kappa_{HB})^{jk}_{lab} = T_0^{jkJK}(\kappa_{HB})^{JK} - T_1^{(jk)JK}(\kappa_{DB})^{JK} \tag{1.47}$$

with [36]

$$T_0^{jkJK} = R^{jJ}R^{kK} \qquad \text{and} \qquad T_1^{(jk)JK} = R^{jP}R^{kJ}\epsilon^{KPQ}\beta^Q. \tag{1.48}$$

The speed β_L is the speed of the lab due to the rotation of the Earth, thus $\beta_L \lesssim 1.5\cdot 10^{-6}$. If the experiment is actively rotated, the rotation of the experiment must be added.

1.4.3 Experiments with optical resonators

In the case of an experimental setup made of a laser locked to the resonance frequency of an optical resonator in vacuum, as is the case of this work, we must find the relationship between a change of that frequency with a hypothetical violation of the Lorentz invariance. Following ref. [27], from the Eq. (1.33) the change in frequency can be written in the frame fixed to the lab, as

$$\frac{\delta\nu}{\nu} = (\mathcal{M}_{DE})^{jk}_{lab}(\kappa_{DE})^{jk}_{lab} + (\mathcal{M}_{HB})^{jk}_{lab}(\kappa_{HB})^{jk}_{lab} + (\mathcal{M}_{DB})^{jk}_{lab}(\kappa_{DB})^{jk}_{lab} \tag{1.49}$$

where the $(\mathcal{M}_{DE})_{lab}$, $(\mathcal{M}_{HB})_{lab}$ and $(\mathcal{M}_{DB})_{lab}$ are constant matrices that characterise the apparatus, and that we will now determine.

For a given resonator, let $\vec{E}_0, \vec{B}_0, \vec{D}_0, \vec{H}_0$ be the fields associated with a mode resonant into the resonator, of angular frequency ω_0. If the coefficient k_F is nonzero, then in presence of a Lorentz violations these fields will be perturbated. Let us call $\vec{E}, \vec{B}, \vec{D}, \vec{H}$ the perturbated fields, and $\delta\nu = \delta\omega/2\pi$ the change in the resonant frequency. Some manipulation yields the fractional resonant frequency shift as

$$\begin{aligned} \frac{\delta\nu}{\nu} = & -\left(\int_V d^3x(\vec{E}_0^* \cdot \vec{D} + \vec{H}_0^* \cdot \vec{B})\right)^{-1} \\ & \times \int_V d^3x(\vec{E}_0^* \cdot \vec{D} - \vec{D}_0^* \cdot \vec{E} - \vec{B}_0^* \cdot \vec{H} + \vec{H}_0^* \cdot \vec{B} \\ & - i\omega_0^{-1}\vec{\nabla}\cdot(\vec{H}_0^* \times \vec{E} - \vec{E}_0^* \cdot \vec{H})) \end{aligned}$$

where V is the volume of the resonator. The expected violations of Lorentz invariance are small, then the last term is negligible [27] and we can expand the last equation in the coefficients $(k_F)_{\kappa\lambda\mu\nu}$. For a resonator in vacuum we may write $\vec{D}_0 = \vec{E}_0, \vec{H}_0 = \vec{B}_0$, and using (1.33) have:

$$\begin{aligned} \vec{D} - \vec{E} &\simeq \kappa_{DE} \cdot \vec{E}_0 + \kappa_{DB} \cdot \vec{B}_0 &(1.50)\\ \vec{H} - \vec{B} &\simeq \kappa_{HE} \cdot \vec{E}_0 + \kappa_{HB} \cdot \vec{B}_0. &(1.51)\end{aligned}$$

The fractional frequency shift is:

$$\frac{\delta\nu}{\nu} = -\frac{\int_V d^3x(\vec{E}_0^*\kappa_{DE}\vec{E}_0 - \vec{B}_0^*\kappa_{HB}\vec{B}_0) + 2\mathrm{Re}(\vec{E}_0^*\kappa_{DB}\vec{B}_0)}{\int_V d^3x(\vec{E}_0 \cdot \vec{D}_0^* + \vec{B}_0 \cdot \vec{H}_0^*)}. \tag{1.52}$$

The denominator corresponds to 4 times the time-averaged energy stored in the resonator.

To apply the Eq. (1.52) to the case of an optical resonator in vacuum we write the unperturbed fields as

$$\begin{aligned} \vec{E}_0(x) &= \vec{E}_0 \cos(\omega_0 \hat{N} \cdot \vec{x} + \phi) e^{-i\omega_0 t} &(1.53)\\ \vec{B}_0(x) &= i\hat{N} \times \vec{E}_0 \sin(\omega_0 \hat{N} \cdot \vec{x} + \phi) e^{-i\omega_0 t} &(1.54)\end{aligned}$$

where $\hat{N}$ is a unit vector pointing along the axis of the resonator, ϕ a phase, $\vec{E}_0$ a vector perpendicular to $\hat{N}$ that specifies the polarisation. The resonant frequency is $\omega_0 = n\pi/L$, where n is the mode number (the number of half-wavelengths that fit into the resonator) and L the length of the resonator.

The fractional frequency shift caused by the Lorentz violation is given by substitution of Eqs. (1.54) and (1.54) into Eq. (1.52):

$$\frac{\delta\nu}{\nu} = -\frac{1}{2|\vec{E}_0|^2}\left[\vec{E}_0^* \cdot (\kappa_{DE})_{lab} \cdot \vec{E}_0 - (\hat{N} \times \vec{E}_0^*) \cdot (\hat{N} \times \vec{E}_0)\right]. \tag{1.55}$$

From this equation we can finally extract the matrices $(\mathcal{M}_{DE})_{lab}$, $(\mathcal{M}_{HB})_{lab}$ and $(\mathcal{M}_{DB})_{lab}$ of Eq. (1.49):

$$\begin{aligned} (\mathcal{M}_{DE})^{jk}_{lab} &= -\frac{\mathrm{Re}(E_0^*)^j(E_0)^k}{2|\vec{E}_0|^2} &(1.56)\\ (\mathcal{M}_{HB})^{jk}_{lab} &= \frac{\mathrm{Re}(\hat{N} \times \vec{E}_0^*)^j(\hat{N} \times \vec{E}_0)^k}{2|\vec{E}_0|^2} &(1.57)\\ (\mathcal{M}_{DB})^{jk}_{lab} &= 0 &(1.58)\end{aligned}$$

It is so shown that in the presence of a Lorentz violation the frequency of an optical resonator depends on the orientation of the resonator (through the vector

$\hat{N} = (\cos\theta, \sin\theta, 0)$ if θ is the angle between the x axis and the vector $\hat{N}$) and the polarisation of the light ($\vec{E}_0$).

The matrices $(\mathcal{M}_{DE})_{lab}$, $(\mathcal{M}_{HB})_{lab}$ and $(\mathcal{M}_{DB})_{lab}$ are constant if the resonator is fixed in the lab, but they vary in time if the resonator is rotating.

Since the definition of the frame, Sect. 1.4.2, the matrices can be rewritten in the form:

$$\begin{aligned}
(\mathcal{M}_{DE})^{33}_{lab} &= \frac{\sin^2\theta}{2} && (1.59)\\
(\mathcal{M}_{HB})_{lab} &= \frac{1}{2}\begin{pmatrix} \sin^2\theta & -\sin\theta\cos\theta & 0 \\ -\sin\theta\cos\theta & \cos^2\theta & 0 \\ 0 & 0 & 0 \end{pmatrix} && (1.60)\\
(\mathcal{M}_{DB})^{jk}_{lab} &= 0 && (1.61)
\end{aligned}$$

This means that for every resonator the frequency shift (Eq. 1.49) is:

$$\begin{aligned}
\frac{\delta\nu}{\nu} &= -\frac{1}{4}[2(\kappa_{DE})^{33}_{lab} - (\kappa_{HB})^{11}_{lab} - (\kappa_{HB})^{22}_{lab}] \\
&\quad -\frac{1}{2}(\kappa_{HB})^{12}_{lab}\sin(2(\theta+\Delta\theta)) \\
&\quad -\frac{1}{4}[(\kappa_{HB})^{11}_{lab} - (\kappa_{HB})^{22}_{lab}]\cos(2(\theta+\Delta\theta))
\end{aligned}$$

so that for two orthogonal resonators the frequency shift is given by the difference between the two expressions of the previous equation for each resonator ($\Delta\theta_1 = 0, \Delta\theta_2 = \pi/2$):

$$\frac{\delta(\nu_1-\nu_2)}{<\nu>} = -(\kappa_{HB})^{12}_{lab}\sin(2\theta) - \frac{1}{2}[(\kappa_{HB})^{11}_{lab} - (\kappa_{HB})^{22}_{lab}]\cos(2\theta) - \cos 2(\theta) \quad (1.62)$$

with $<\nu>= (\nu_1-\nu_2)/2 \simeq \nu$.

For two orthogonal resonators that rotate in the lab, the vectors $\hat{N}_i$ can be written as:

$$\hat{N}_1 = \begin{pmatrix} \cos\theta \\ \sin\theta \\ 0 \end{pmatrix} \qquad \hat{N}_2 = \begin{pmatrix} \cos(\theta+\pi/2) \\ \sin(\theta+\pi/2) \\ 0 \end{pmatrix} \quad (1.63)$$

and the electric fields:

$$\vec{E}_1 = \vec{E}_2 = \begin{pmatrix} 0 \\ 0 \\ 1 \end{pmatrix} \quad (1.64)$$

Since the lab is not an inertial frame, we must transform the matrices in the Sun-centred system matrices, using the rotation R^{jJ} (1.44), and Eqs. (1.47), (1.47):

$$\frac{\delta(\nu_1(t)-\nu_2(t))}{\nu} = B(t)(\sin 2\theta - \sin 2(\theta+\pi/2)) + C(t)(\sin 2\theta - \sin 2(\theta+\pi/2)), \quad (1.65)$$

that is:

$$\frac{\delta(\nu_1(t)-\nu_2(t))}{\nu} = 2B(t)\sin 2\theta(t) + 2C(t)\cos 2\theta(t), \tag{1.66}$$

where $\nu_1 \approx \nu_2 \approx \nu$ ($2.8 \cdot 10^{14}$ Hz) is the average frequency.

Each amplitude $2B(t)$ and $2C(t)$ is a linear combination of the eight coefficients, weighted by time-harmonic factors. The amplitude $B(t)$ contains frequency components at 0, $\omega_\oplus$, $2\omega_\oplus$, $\omega_\oplus \pm \Omega_\oplus$ and $2\omega_\oplus \pm \Omega_\oplus$, while $C(t)$ contains in addition one component at the frequency $\Omega_\oplus$. Here $\omega_\oplus$ is Earth's sidereal angular frequency and $\Omega_\oplus$ is Earth's orbital frequency. For the determination of the individual $\tilde{\kappa}_{o+}$ coefficients a measurement extending over of at least 1 year is necessary: it requires the ability to resolve the contribution of Earth's orbital motion in order to discriminate between frequency coefficients differing by $\Omega_\oplus$.

The coefficients B and C in Eq. (1.66) can be written as:

$$\begin{aligned} B &= B_0 + B_1\sin(\omega_\oplus T_\oplus) + B_2\cos(\omega_\oplus T_\oplus) && (1.67)\\ &+ B_3\sin(2\omega_\oplus T_\oplus) + B_4\cos(2\omega_\oplus T_\oplus) && (1.68)\end{aligned}$$

$$\begin{aligned} C &= C_0 + C_1\sin(\omega_\oplus T_\oplus) + C_2\cos(\omega_\oplus T_\oplus) && (1.69)\\ &+ C_3\sin(2\omega_\oplus T_\oplus) + C_4\cos(2\omega_\oplus T_\oplus) && (1.70)\end{aligned}$$

The variables $\omega_\oplus$ and $T_\oplus$ were defined in Sect. 1.4.2.

The definitions of the coefficients B_i and C_i are reported in Sect: 1.4.4.

1.4.4 Values of Bs and Cs

The following values of the coefficients Bs and Cs of Eqs. (1.67) and (1.69) are taken from [27] and [36]:

$$\begin{aligned}
B_1 &= \frac{1}{2}\sin\chi\tilde{\kappa}_{e-}^{XZ} + \frac{1}{2}\beta_\oplus\sin\chi[\cos\eta\sin\Omega_\oplus T\tilde{\kappa}_{o+}^{XY} - \sin\eta\cos\Omega_\oplus T\tilde{\kappa}_{o+}^{YZ}]\\
B_2 &= -\frac{1}{2}\sin\chi\tilde{\kappa}_{e-}^{YZ} - \frac{1}{2}\beta_\oplus\sin\chi[-\cos\eta\cos\Omega_\oplus T\tilde{\kappa}_{o+}^{XY} + \sin\eta\cos\Omega_\oplus T\tilde{\kappa}_{o+}^{XZ}]\\
B_3 &= \frac{1}{4}\cos\chi[\tilde{\kappa}_{e-}^{YY} - \tilde{\kappa}_{e-}^{XX}] - \frac{1}{2}\beta_\oplus\cos\chi[\sin\Omega_\oplus T\tilde{\kappa}_{o+}^{YZ} - \cos\eta\cos\Omega_\oplus T\tilde{\kappa}_{o+}^{XZ}]\\
B_4 &= \frac{1}{2}\cos\chi\tilde{\kappa}_{e-}^{XY} - \frac{1}{2}\beta_\oplus\cos\chi[\sin\Omega_\oplus T\tilde{\kappa}_{o+}^{XZ} + \cos\eta\cos\Omega_\oplus T\tilde{\kappa}_{o+}^{YZ}]
\end{aligned}$$

$$
\begin{aligned}
C_0 &= \frac{3}{8}\sin^2\chi\tilde{\kappa}_{e-}^{ZZ} - \frac{1}{4}\beta_\oplus \sin^2\chi[\sin\Omega_\oplus T\tilde{\kappa}_{e-}^{YZ} + \cos\eta\cos\Omega_\oplus T\tilde{\kappa}_{o+}^{XZ} + 2\sin\eta\cos\Omega_\oplus T\tilde{\kappa}_{o+}^{XY}] \\
C_1 &= -\frac{1}{2}\sin\chi\cos\chi\tilde{\kappa}_{e-}^{YZ} - \frac{1}{2}\beta_\oplus\cos\chi\sin\chi[-\cos\eta\cos\Omega_\oplus T\tilde{\kappa}_{o+}^{XY} + \sin\eta\cos\Omega_\oplus T\tilde{\kappa}_{o+}^{XZ}] \\
C_2 &= -\frac{1}{2}\sin\chi\cos\chi\tilde{\kappa}_{e-}^{XZ} - \frac{1}{2}\beta_\oplus\cos\chi\sin\chi[\sin\Omega_\oplus T\tilde{\kappa}_{o+}^{XY} - \sin\eta\cos\Omega_\oplus T\tilde{\kappa}_{o+}^{YZ}] \\
C_3 &= \frac{1}{4}(1+\cos^2\chi)\tilde{\kappa}_{e-}^{XY} - \frac{1}{4}(1+\cos^2\chi)\beta_\oplus[\sin\Omega_\oplus T\tilde{\kappa}_{o+}^{XZ} + \cos\eta\cos\Omega_\oplus T\tilde{\kappa}_{o+}^{YZ}] \\
C_4 &= -\frac{1}{8}(1+\cos^2\chi)[\tilde{\kappa}_{e-}^{YY} - \tilde{\kappa}_{e-}^{XX}] + \frac{1}{4}(1+\cos^2\chi)\beta_\oplus[\sin\Omega_\oplus T\tilde{\kappa}_{o+}^{YZ} - \cos\eta\cos\Omega_\oplus T\tilde{\kappa}_{o+}^{XZ}]
\end{aligned}
$$

1.4.5 The coefficient $(\tilde{\kappa}_{e-})^{ZZ}$

From the coefficients of Sect. 1.4.4, we see that the contribution of $(\tilde{\kappa}_{e-})^{ZZ}$ to the beat frequency signal is

$$\boxed{\frac{\delta(\nu_1(t)-\nu_2(t))}{\nu} = \frac{3}{4}(\tilde{\kappa}_{e-})^{ZZ}\sin^2\chi\cos 2\theta(t) + ...}, \tag{1.71}$$

where χ is the colatitude of the laboratory, 38.8° for Düsseldorf.

From (1.71) follows that the this particular Lorentz-violating coefficient $(\tilde{\kappa}_{e-})^{ZZ}$ is only measurable if the resonators are actively rotated.

Three high precision experiments using ultra-stable cryogenic resonators for microwaves or optical waves have been performed recently [4, 5, 6]. These experiments were not rotating, so they could measure only seven of the eight coefficients.

The eighth coefficient, $(\tilde{\kappa}_{e-})^{ZZ}$, was first determined in the experiment described here. A value of $|(\tilde{\kappa}_{e-})^{ZZ}| < 2\cdot 10^{-14}$ was reported in [26].

A modification of the Coulomb potential as consequence of the Lorentz violation results in a length change of the resonators, thus in a change of the resonance frequency. In principle this effect must be taken into account, because it could complicate the interpretation of the results of the experiment [37]: from Eq. (2.1) it can be seen that the resonance frequency does not depend only on the speed of light, but also on the length of the resonator. This effect is in fact negligible for sapphire resonators [38].

Chapter 2

The experimental setup

It was mentioned in Sect. 1.4.5 that active rotation of the experimental setup is necessary to measure the coefficient $(\tilde{\kappa}_{e-})^{ZZ}$.

Another advantage of active rotation is that the rotations are faster than the Earth's rotation, implying less restrictive conditions to the stability of the resonators, in contrast to stationary experiments, which must be stable over 12 h. Variations of the beat frequency that are much slower than the rotation period can then be eliminated in the data analysis. A rotating experiment offers the possibility to determine two data points $B(t_i)$ and $C(t_i)$ for every rotation (t_i is the mid-time of the rotation period). Thus, a rotating experiment offers a significant increase in data acquisition rate and thus a reduction of statistical noise. An overall measurement time of 1 year or longer is still necessary for a precise determination of all individual coefficients.

For these reasons the cryostat was mounted on a rotating stage, that permitted to rotate continuously and in a controlled way the resonators.

In the next sections the experimental setup will be described.

2.1 Overview

The experimental setup can be seen on Figs. 2.1 and 2.2. Inside a cryostat two optical resonators made of sapphire were cooled down to 3.4 K by a pulse-tube cooler. In this way the very small coefficient of thermal expansion of sapphire could be exploited. Two Nd:YAG laser were frequency locked to the resonance frequency of the TEM_{00} modes of the resonators.

The relationship between the resonance frequencies of the modes of a resonator and the speed of light permits to test directly the speed of light, as long as the distance between the mirrors, L, remains constant, at least inside the desired experimental error. The relationship is:

$$F = \frac{nc}{2L}, \tag{2.1}$$

where $n \in \mathbb{N}$ is the number of half-wavelengths that fit in the resonator, c the speed of light. In order to minimise the systematic errors in the measurements, it is necessary to minimise variations in L. L depends on temperature and mechanical stresses on the resonator, like variations in the pressure of the environment, which was minimised by working in vacuum.

The beams of the lasers were coupled to the resonators via two 4-meters long polarisation-maintaining single-mode fibres. The beat frequency between the two lasers was compared to the output frequency of a hydrogen maser by a frequency counter that was phase locked to the maser. A computer-controlled rotation stage rotated the cryostat continuously over a range of 90°. The angle of rotation of the resonators was recorded and correlated to the beat frequency in search of violations of the Lorentz invariance. Variations of the angle of tilt of each resonator relative to the direction of gravity were minimised before each measurement, and measured to decorrelated them from the beat frequency.

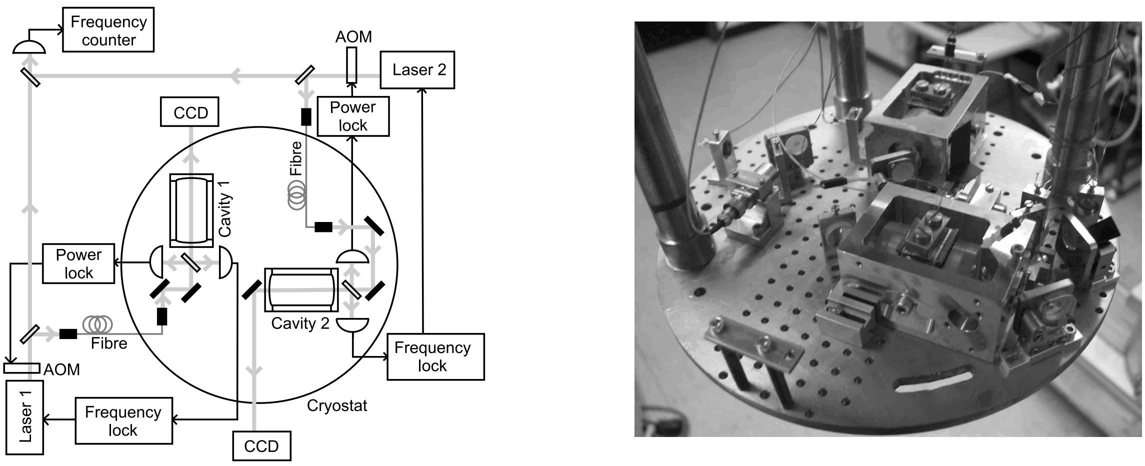

Figure 2.1: The experimental setup. **Left:** Two Nd:YAG lasers are frequency-locked to two sapphire optical resonators located in a cryostat. The beams are fed to the resonators via optical fibers. The TEM modes of the resonators are observed by means of two CCD cameras. Acousto-optic modulators (AOM), stabilize the power of the beams fed to the resonators. All components shown are mounted on a rotating table. **Right:** View of the cryogenic optical components. The two resonators are contained in invar housings. On top of the resonators are copper blocks that contain temperature sensors and heating resistors for temperature stabilization. This is a configuration used in the first measurements, small modifications led to a slightly different configuration. The copper base plate is rigidly connected to the room-temperature top flange of the cryostat vacuum housing.

A part of the laser beams was superimposed on a fast photodiode producing a heterodyne signal at the beat frequency ($\nu_1 - \nu_2$) between the two lasers, about 700 MHz. This frequency was down-mixed with a frequency generator to a frequency of about 10 MHz, to exploit the better accuracy of the counter at lower frequencies.

The frequency generator was phase locked to the hydrogen maser output frequency (5 MHz). The down-loaded frequency was measured with a frequency counter, also phase-locked to the reference output of a hydrogen maser.

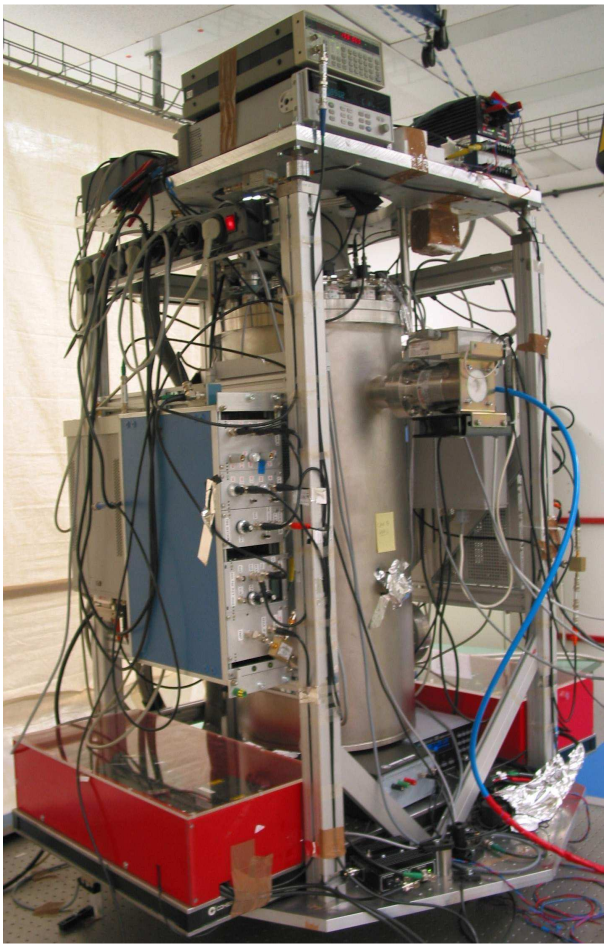

Figure 2.2: The experimental setup. The octagonal table lies on a rotation stage. Over the octagon an aluminium frame holds the cryostat, into which the pulse-tube cooler cools two sapphire optical resonators and the optics and photodiodes necessary for the laser stabilisation to the resonance frequency of the resonators. All the electronics for the laser stabilisation, the frequency counter and the laser themselves were mounted to the rotating setup, in order to minimise systematic effects caused by the rotations. The laser beams were sent to the resonators via cryogenic optical fibres. The setup was mounted on a heavy optical table (3 m $\times$ 1.5 m).

2.2 The cryogenics

The cryogenic system consisted of a two-stage pulse-tube cooler and a cryostat. The pulse-tube cooler reached a temperature of about 3 K in its second stage. The cryogenic resonators were then temperature stabilised at 3.4 K.

2.2.1 The cryostat

The cryostat integrated a pulse-tube cooler with the optical experiment. It was designed to accede the optical resonators both with free laser beams through anti-reflection-coated BK7 windows and through optical fibers.

A schematic drawing of the cryostat, with the pulse-tube cooler is shown in Fig. 2.3.

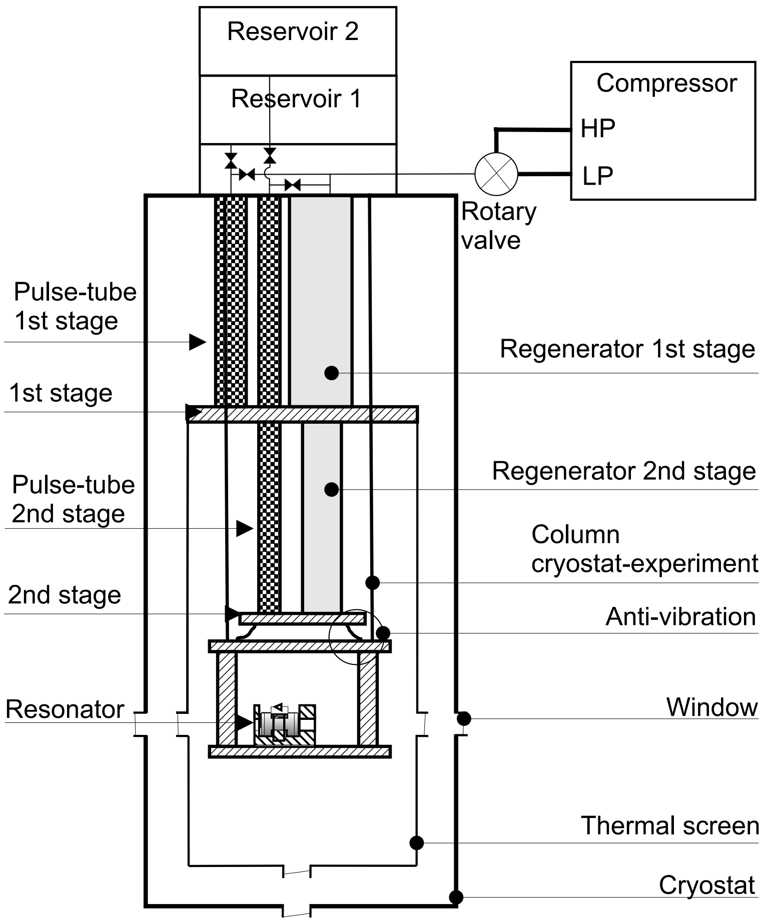

Figure 2.3: A schematic drawing of the cryostat. It was provided with three antireflection coated windows: two in a horizontal configuration, and one on the bottom part, along the axis of the cryostat that could be used to monitor the TEM mode of a third resonator. In this figure only one resonator is showed. The different parts of the pulse-tube cooler are also depicted. HP and LP: high- and low-pressure side of the compressor.

A copper screen was connected to the first stage of the cooler (about 40 K), that enveloped the second stage and the experiment. Anti-reflection coated BK7 1/2 inch windows were mounted also in this screen, in correspondence of the optical resonators, providing at the same time access for the beams emitted by the optical resonators and thermal screen between the walls of the cryostat (at 300 K) and the experiment (at 3.4 K). The screen and the tubes of the cooler were wrapped into super-insulation aluminized foils to insulate them from radiations form the cryostat walls. The second stage and the experiment were not provided of copper screen in order to reduce the mass and the radiated surface, but were wrapped in 20 superinsulation foils, in the way shown in Fig. 2.4.

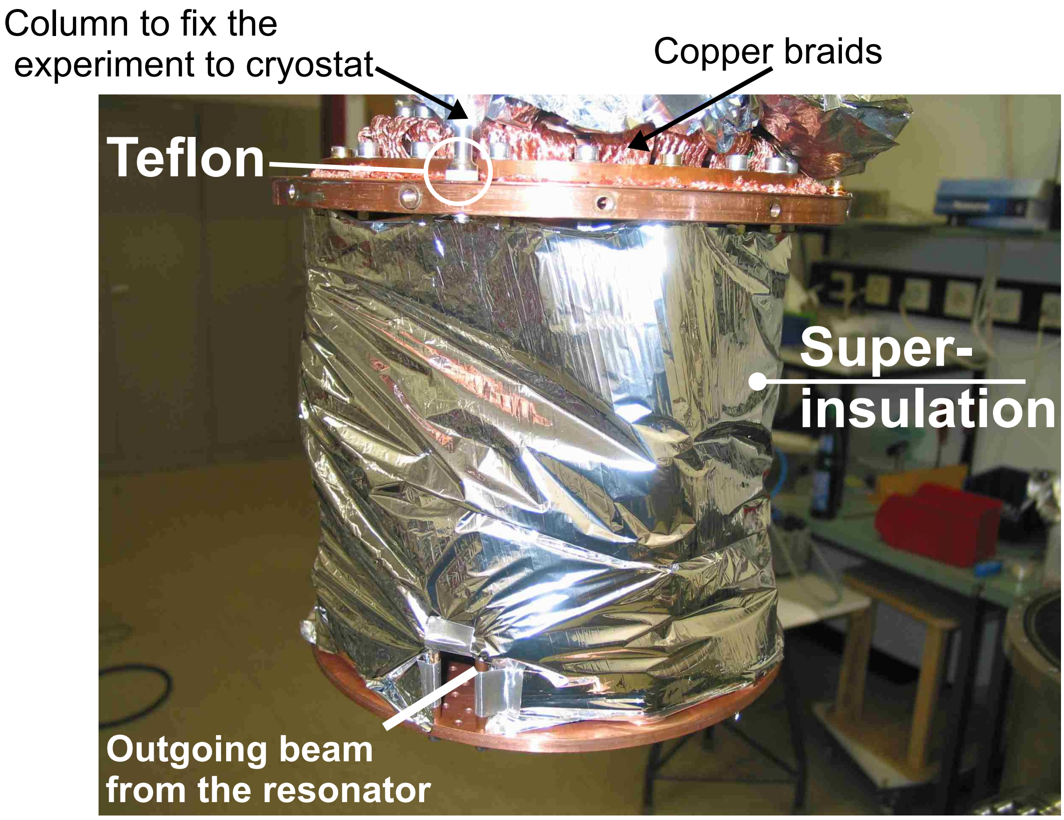

Figure 2.4: The second stage and the optical resonators were wrapped into superinsulation foils.

During the experimental runs the external windows were covered with superinsulation foils, to avoid that non-uniform radiation inside the lab could result in a angle-dependent systematic effect due to transmission of the radiation through the windows.

2.2.2 Pulse-tube cooler

A schematic of the pulse-tube cooler (PTC) used for this work was shown in Fig. 2.3. Here its working principle will be explained.

The pulse-tube cooler (aka pulse tube refrigerator, or orifice pulse-tube cooler) is the evolution of the Gifford-McMahon (GM) refrigerator. The most important difference between the GM and the pulse-tube is the absence of the moving displacer in the latter. This greatly reduced the vibrations that made the GM unsuitable for many applications.

The stages of operation of a one-stage PTC are [39]:

1. A compressor compresses the room temperature helium gas, and a rotary valve let the gas in the cooler;

2. the heated compressed gas column flows through the regenerator, the pulse tube and the orifice to the reservoir. During this travel it exchanges the heat Q_H at the hot end of the pulse tube;

3. the rotary valve connects the cooler to the low pressure side of the compressor, to expand adiabatically the helium gas in the pulse-tube;

4. the cooled low-pressure gas in the tube is forced towards the cold end of the pulse-tube by the flow from the reservoir into the tube via the orifice. As it passes through the cold-end exchanger it picks up the heat Q_C.

The regenerator acts to precool the incoming high-pressure pulse before it reaches the cold end. It is normally composed of a stack of metal gauze discs or spheres. The material for the regenerator is of great importance for the efficiency of the cooler. ErNi, Er_3Ni, $ErNi_{0.9}Co_{0.1}$ or Pb are commonly used for their large volumetric specific heat at low (4 K) temperatures [40]. The reservoir volume (1.2 litre) is sufficient to reduce pressure oscillations during the flow. The result of the pressure cycling is to transfer heat from the cold end toward the closed (hot) end. A scheme of a one-stage PTC is depicted in Fig. 2.5.

Pulse-tube coolers are usually described as 'low vibrations' or 'low noise' devices, especially respect to the older generation of mechanical coolers, like the Gifford-McMahon (GM) refrigerators. This is motivated by the absence of the moving displacer in the cold tube. It is true that the pulse-tube coolers are much quieter and less vibrating that the GM refrigerators. For this reason they find a spread use in applications that need cryogenic temperatures and low vibrations, *e.g.* SQUIDs (super conducting quantum interference devices) or Mössbauer spectroscopy. Nevertheless, the cold head of such a cooler still presents vibrations at the frequency of the helium wave and its harmonics, although as small as $1.5 \cdot 10^{-4}$ g [41].

Pulse-tube coolers do not use liquid cryogens, but waves of helium gas. This avoids the deformations due to refills, and the closed cycle of helium gas makes so that the only costs are due to the electrical power to the 6 kW helium compressor.

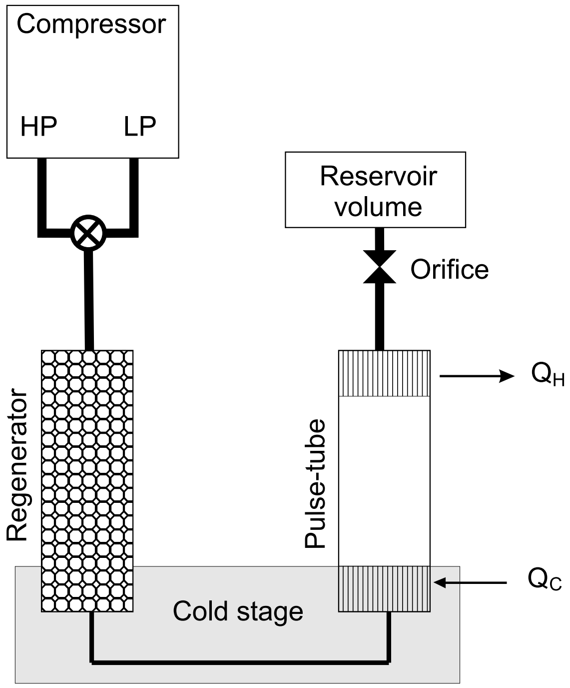

Figure 2.5: Schematic diagram of an one-stage pulse tube cooler. HP is the high-pressure side of the compressor, LP is the low-pressure side of it. Q_C is the heat that the cooler picks up, and Q_H the heat that the cooler gives to the environment. The symbol $\otimes$ is for the rotary valve, HP and LP for the high- and low-pressure sides of the compressor.

Moreover, the absence of moving parts in the cold side makes them suitable for applications that need low magnetic interference, as SQUIDs.

The pressure modulations generated in a pulse-tube cooler cause a periodical deformation of the regenerator and pulse tubes. These vibrations were measured by Lienerth *et al.* [42] in a one-stage pulse-tube cooler at level of 6 μm, and with a vibration compensation reduced to 0.5 μm.

A part from vibrations and noise, a possible problem of a pulse-tube cooler is an instability in its temperature. One of the main reasons of instability is a DC-flow, that is a small continuous flow of gas through the tubes, instead of a pure cylindrical column that travels back and forth inside the cooler [43]. The DC flow is a small amount (mg/s, instead of g/s of the AC-flow) of unregenerated room temperature gas that reaches the cold stage, increasing the heat load.

When this happens the profile of the gas column degrades, and this eventually results in an increasing of the working temperature of the cold stage (up to 15 K), accompanied by an instability of the order of a few kelvin. This probably happens due to some contamination of the helium gas (that has to be of purity grade 5.0) that enters into the helium cycle, most probably in the rotary valve. The rotary valve itself can contaminate the helium gas if it becomes too hot, outgassing the lubricants that serve for its rotation. When this happens the cooler must be switched off and both cooler and compressor must be evacuated and new helium gas must be filled. A cam-operated valve was proposed [44] to overcome this problem, but it has not yet a commercial application.

A compressor with a big adsorber is necessary to ensure a long duty time. The adsorber blocks impurities in the helium cycle.

The cooling powers of the two stages of the pulse-tube cooler used for this experiment are shown in Fig. 2.6. The values of the cooling powers were measured applying a heat load to the stages, and measuring the temperatures as function of the heating power. It can be noted that the increase of temperature in one stage causes the decrease of temperature in the other.

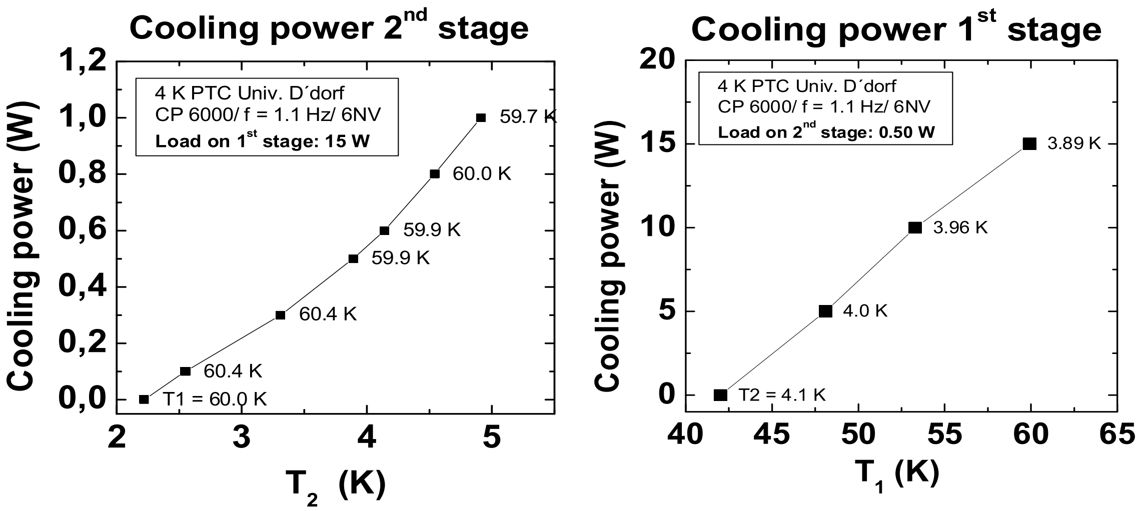

Figure 2.6: The cooling power of the two stages of the pulse-tube cooler. The values were obtained applying a heat load through a resistive heater to the cold end of each stage.

The next Figures show the temperature stability of the first stage, in a time scale of few hours (Fig. 2.7) and a week (Fig. 2.8).

The Fig. 2.9 plots the same temperature recorded six months before. It can be seen that the behaviour is quite different. Such differences in the behaviour if the cooler caused drifts in the frequency measurements, that were difficult to control.

The rotating table could rotate over 360°, but due to the helium connections between the compressor and the pulse-tube cooler the cryostat mounted on the table only rotate a maximum of 180°. To reduce forces on the rotating frame containing the cryostat due to tension of these connections, the cryostat was rotated only within

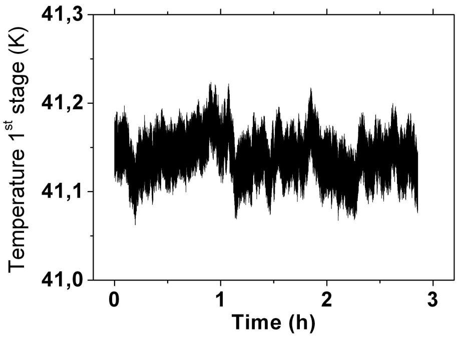

Figure 2.7: Temperature of the 1^{st} stage over a time span of 3 hours. These data and the data used for the next plot were recorded in February 2005, during the measurements used for the test of Lorentz invariance.

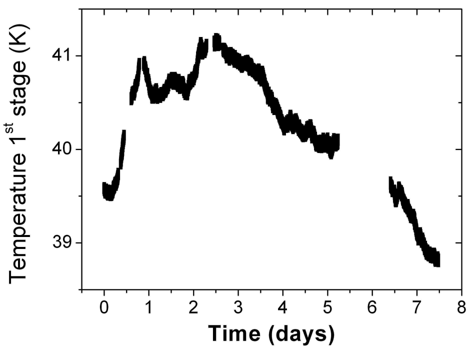

Figure 2.8: Temperature of the 1^{st} stage over a time span of one week.

a range of 90°, which was enough for the scope of this experiment.

Heat sink

To avoid a thermal short-cut between the feed-through (at 300 K) and the experiment (at 3.4 K), the coaxial cables connecting the photodiodes to the preamplifiers, the wires for the temperature sensors and for the resistive heaters had to be anchored to several points of the regenerators, in order to gradually decrease their temperatures. This to avoid that a wire with too high temperature could give an unnecessary thermal load to the second stage of the pulse-tube cooler, degrading the stability of the system.

The heat sink of the optical fibers was more problematic. Mechanical deformation of the optical fibers causes phase shifts that resulted in frequency shifts. Since the quantity of interest in our experiment was the difference between the frequencies of the two lasers, great care was taken to avoid this effect.

With a set-up consisting of two separated fibers, heat-sinked in several points of the cooler, it was noted that the difference frequency between the two lasers suffered of some modulations correlated with the temperatures of these points. Due to its complicated thermodynamics, the temperatures of some points of the cooler can change within several kelvin even at regime. Thus in the final set-up the optical fibers were heat-sinked only at the cold end of the first stage (whose temperature was constant within 0.5 K in one day, see Figs. 2.8 and 2.10) and at the cold end of the second stage (that was temperature stabilized). For some time the first stage was also temperature stabilized, but that did not improve the results of the experiment.

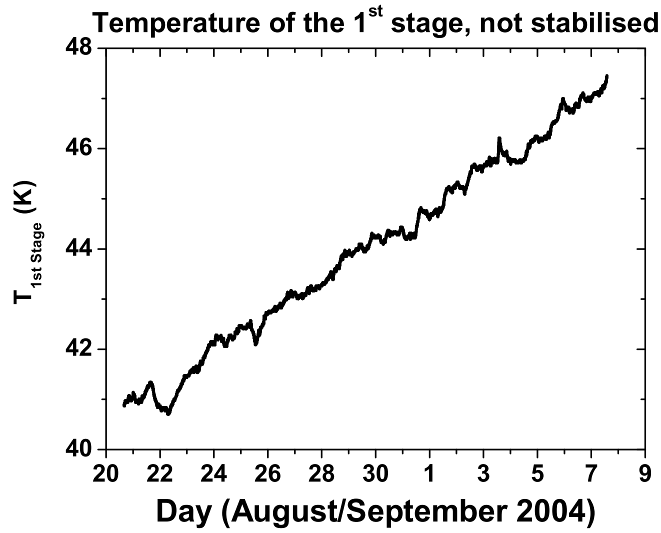

Figure 2.9: Temperature of the 1^{st} stage in the time span of 20 days.

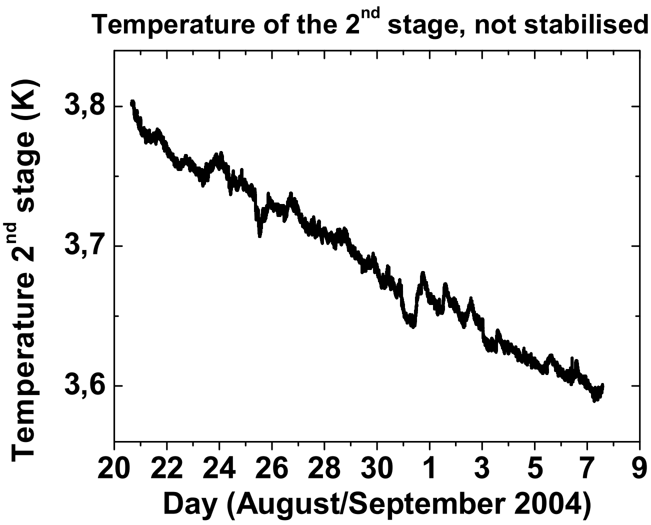

Figure 2.10: Temperature of the 2^{nd} stage in the time span of 20 days.

2.3 The resonators

The two optical resonators were made of pure sapphire (Al_2O_3). Each consists of a 3 cm long cylindrical spacer with inner diameter 0.1 cm, outer diameter 0.26 cm, c axis of the sapphire crystal parallel to the axis of the cylinder and two sapphire mirrors (1 m radius) that were optically contacted to each spacer. The mirrors were coated for high reflection at 1064 nm. The resonators [45] were high-reflection coated for wavelengths around 1 μm.

The free spectral range is defined as

$$FSR = \frac{c}{2L} = \frac{3 \cdot 10^8 \mathrm{m/s}}{2 \cdot 3 \cdot 10^{-2} m} = 5\,\mathrm{GHz}$$

where c is the speed of light, and L the distance between he mirrors. The linewidth $\Delta\nu$ of the resonators was measured as 100 kHz, the beamwaist 200 μm.

These resonators were already used for laser stabilization [45, 46] and relativity tests [47, 13].

Sapphire was chosen because of its very low thermal expansion coefficient, that makes the resonators less sensitive to changes in the environment temperature. For crystals, the thermal expansion coefficient drops as T^3 for $\mathrm{T} \mapsto 0$. The coefficient for sapphire interpolated at 3.4 K using the value from [48] is $(7.67 \pm 0.15) \cdot 10^{-11}\,\mathrm{K}^{-1}$.

The thermal expansion coefficient for the resonators was measured in [45]. This value is not the coefficient for sapphire, because it also involves the interaction of the resonator with its holder. Interpolating the value found at 4.2 K to 3.4 K we find: $\alpha = 2.86 \cdot 10^{-11}$ K^{-1}, a value three times smaller.

2.3.1 Elastic distortions due to inclination

A tilt of a resonator changes its length for two reasons:

1. the change of the component of the gravitational force in the direction orthogonal to the axis of the resonator;

2. the appearance of a component of the gravitational force in the direction of the axis.

To estimate the magnitude of the effects, imagine a solid in absence of gravity. Be in this case its length L and its hight h. If now the gravity force $F_\perp$ is applied, the solid will be compressed of the quantity:

$$\Delta h = \frac{F_g h}{ES} \tag{2.2}$$

where E is the Young's modulus (300 GPa for sapphire) and S the surface of the solid on the plane parallel to the direction of gravity. The relative contraction will be:

$$\frac{\Delta h}{h} = \frac{F}{ES}. \tag{2.3}$$

But $F_g = mg = g\rho V = g\rho LS$, being m the mass of the material the solid is made of, ρ its density (4 g/cm^3 for sapphire), and V the volume. The relative expansion in the orthogonal direction (from zero gravity to Earth's gravity) is, for sapphire:

$$\frac{\Delta L}{L} = \nu \frac{\rho LSg}{ES} = \nu \frac{\rho Lg}{E} = 4 \cdot 10^{-9}, \tag{2.4}$$

being ν the Poisson's number (about 0.16 for sapphire [49]). This effect is depicted in Fig. 2.11.

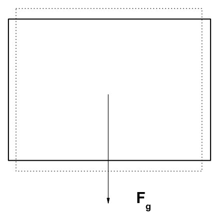

Figure 2.11: When the force of gravity F_g acts on a solid that in absence of gravity has the dimensions represented by the dashed line, the solid is compressed in the direction of the force of the quantity Δh, and as consequence the solid becomes longer in the orthogonal direction of the quantity $\nu\Delta h$, here ν is the Poisson's number, see text for details.

Orthogonal component of the gravity, $F_\perp$

When the solid is tilted the component $F_\perp$ of the force decreases of $(1 - \cos\alpha)$, consequently the solid will expand in the L direction of the same quantity, see Fig. 2.12. That is, for a tilt of 1 μrad:

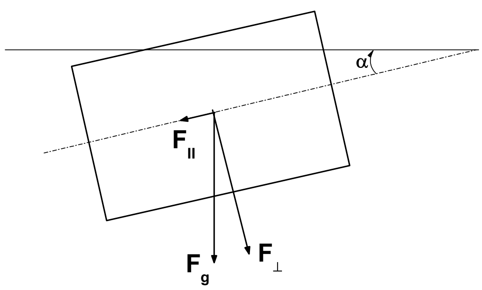

Figure 2.12: The tilt of the solid decreases the component $F_\perp$ of the force that compresses the solid in the h direction, as consequence the solid will expand in the L direction of the quantity $(1 - \cos\alpha)$, respect to the solid in a perfectly horizontal position.

$$\frac{\Delta L}{L} = 6.4 \cdot 10^{-10}(1 - \cos\alpha) = 6.4 \cdot 10^{-10} \cdot 5 \cdot 10^{-13} = 3.2 \cdot 10^{-22}. \tag{2.5}$$

This effect is negligible.

Parallel component of the gravity, F_{II}

The effect that plays a role in the tilt of the resonators is the appearance of the component parallel to the optical axis of the resonator, F_{II} in Fig. 2.12. To understand what happens, imagine the resonator laying on its centre. In case of tilt, the lower part will be pulled away from the centre by the gravity, causing an elongation, whereas the upper part will be compressed towards the centre, reducing thus the length of the resonator. In case of a perfectly symmetric mount the two length changes compensate exactly, otherwise the relative length change will be [50]

$$\frac{\Delta L}{L} = \frac{\rho g L}{E}\left(\lambda - \frac{1}{2}\right). \tag{2.6}$$

The parameter λ is zero if the resonator is mounted at the lower end (compression), 1 if mounted at the other end (expansion) and 1/2 if mounted exactly in the centre (perfect compensation).

For this experiment the sensitivity of the beat frequency (and then via Eq. (2.1) of the length of the resonators) was measured as $(\Delta\nu/\nu)/\Delta\alpha = 0.06\mathrm{Hz}/\mu\mathrm{rad}$, that corresponds to $(\Delta L/L)/\Delta\alpha = 2.2 \cdot 10^{-16}/\mu\mathrm{rad}$, see Sect. 2.9.1 for details.

This correspond to the parameter $\lambda = 0.5 + 0.04$, that is the mounting is symmetric within 8%.

2.4 Resonator mounting

To reduce the transfer of vibrations from the pulse-tube cooler cold end to the experiment, a vibration isolation in the same style as [42] was used. The optics of the experiment (the housings for the optical resonators, fibers outcouplings, mirrors, beam-splitters and photodiodes) where mechanically fixed to a OFHC[1] copper disc rigidly connected the internal part of the cryostat by use of three stainless steel rods, 350 mm long, 10 mm diameter. The copper disc was then thermally decoupled from these rods by use of Teflon insulating material. Flexible copper braids thermally connected the copper disc to the cold end of the second stage of the pulse-tube cooler.

How to fix the resonators to the cold end of the pulse-tube cooler was a crucial part of the work. A schematic drawing of the housing is shown in Fig. 2.16. The housings were coated with a 5 μm-thick layer of gold. Gold was used to obtain good contact surface between the resonators and the housing. The resonators were then fixed to the housing using for each a thin copper strap. The straps were not tightly blocked, to avoid the risk of squeezing the resonators with the contraction of the straps during cooling down. The resonators were placed as symmetric as possible on the housings, for the reasons explained in Sect. 2.3.1.

The optical setup inside the cryostat can be seen in Fig. 2.13 and Fig. 2.14.

Fig. 2.13 shows the setup in an older configuration. The resonator housings were not gold-coated. Indium foils provided thermal coupling between the resonators and their housings,and temperature control was realised using two independent control loops heating two heating resistors,each connected to a resonator, visible as copper blocks on the top of the resonators.

Fig. 2.14 shows the setup used for the measurements analysed in this work. The indium foils between resonators and housings were removed. The cooper blocks on the resonators were also removed. The housings were gold coated. This improved the stability of the resonators, and thus the quality of the measurements.

[1]OFHC: oxygen-free high conductivity.

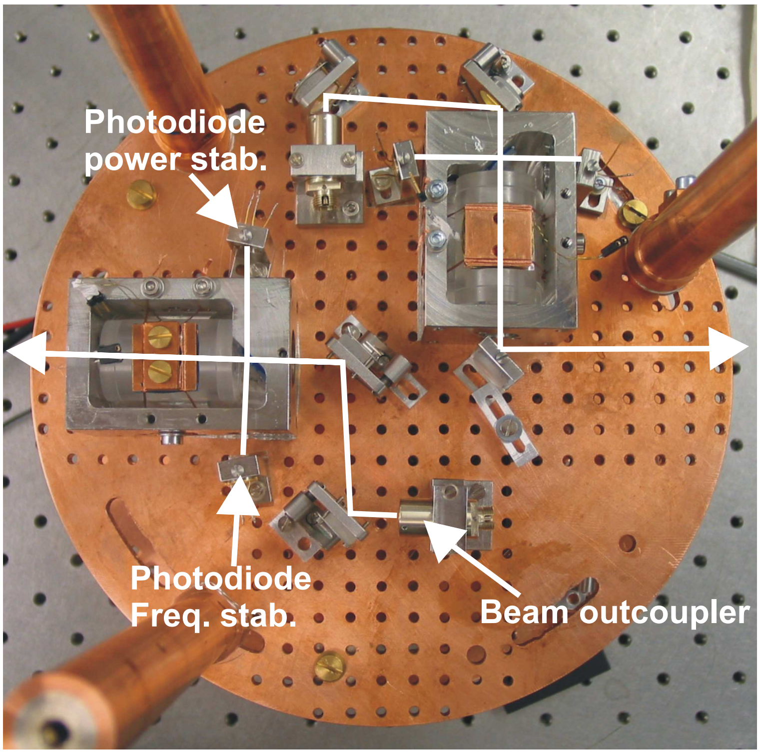

Figure 2.13: Upper view of the housing, before they were gold-coated. The beamsplitters were glued to the housings. It is possible to see the photodiodes used for the frequency- and power-stabilisation, as well as the beam outcouplers for the optical fibres, and the mirrors for the mode-matching of the beams to the resonators, cfr. with the schematic Fig. 2.1.

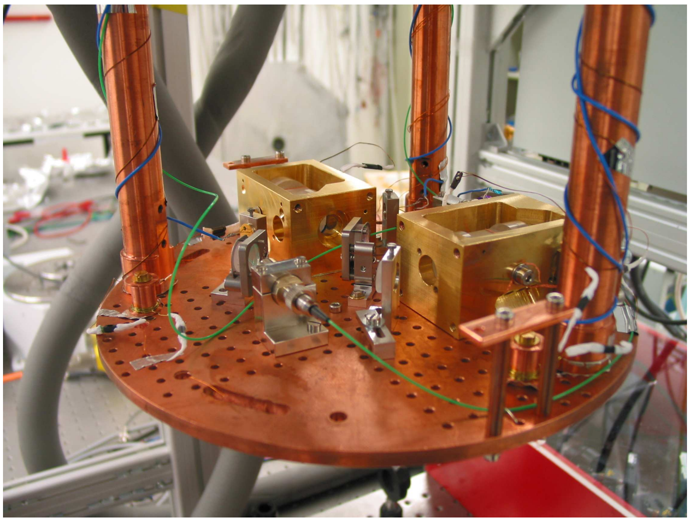

Figure 2.14: In the last configuration the resonators holders were coated with 5 μm gold, and the copper blocks on the resonators were eliminated. The beamsplitters were reglued to the housings after the coating process. The temperature stabilisation was provided by a resistive heater under the copper plate.

2.4.1 Temperature stabilisation and temperature sensitivity

Without any temperature stabilisation, the cold part of the experiment, connected to the second stage of the pulse-tube cooler has short-time (10 s) temperature stability of 4 mK. The temperature of the stage has instabilities at the level of 50 mK over 10 hours. These come from instabilities of the system itself, and from a dependence of the temperature of the stage from the temperature in the lab.

The dependence of the temperatures of the first and the second cold stages on the temperature of the lab were measured. Acting on the air conditioning system of the lab the temperature around the experiment was changed of 1.4 K, and a temperature change on the first stage of 2.1 K was measured. As it can be seen in Fig. 2.15, the second stage also follows the temperature changes of the room. This is not surprising, because the pulse-tube cooler exchanges heat with the air around the cryostat, then the efficiency of the cooler increases when the lab is colder. It was then found 1.5 mK/K for the second stage.

The temperature of the resonators were stabilised using a resistive heater screwed under the copper disc on which the resonators lay, Fig. 2.16. The heater was placed equidistant from the two resonators, and a temperature sensor (Cernox by Lakeshore) in thermal contact with one of the two resonator's housings was used to monitor the temperature, controlled by a commercial cryogenic temperature controller.

The root Allan Variance of the temperatures of the experiment with the temperature controller on is shown in Fig. 2.17

The stabilization of the resonators through a commercial temperature controller was at level of 1 mK for short times, and less than 45 μK for integration times of 300 s.

We measured a dependence of the beat frequency on *simultaneous* changes of the temperature of both resonators of the order of 1.5 Hz/mK. The temperature controller stabilised the temperature of the whole cryogenic optical setup, not of the two resonators separately. A temperature change of 1 mK of only one resonator would result in a relative frequency change of $1 \cdot 10^{-3} \cdot 2.86 \cdot 10^{-11} = 2.86 \cdot 10^{-14}$ which corresponds to about 8 Hz. We see then that we have a common mode rejection of the temperature at level of $8/1.5 = 5$ times.

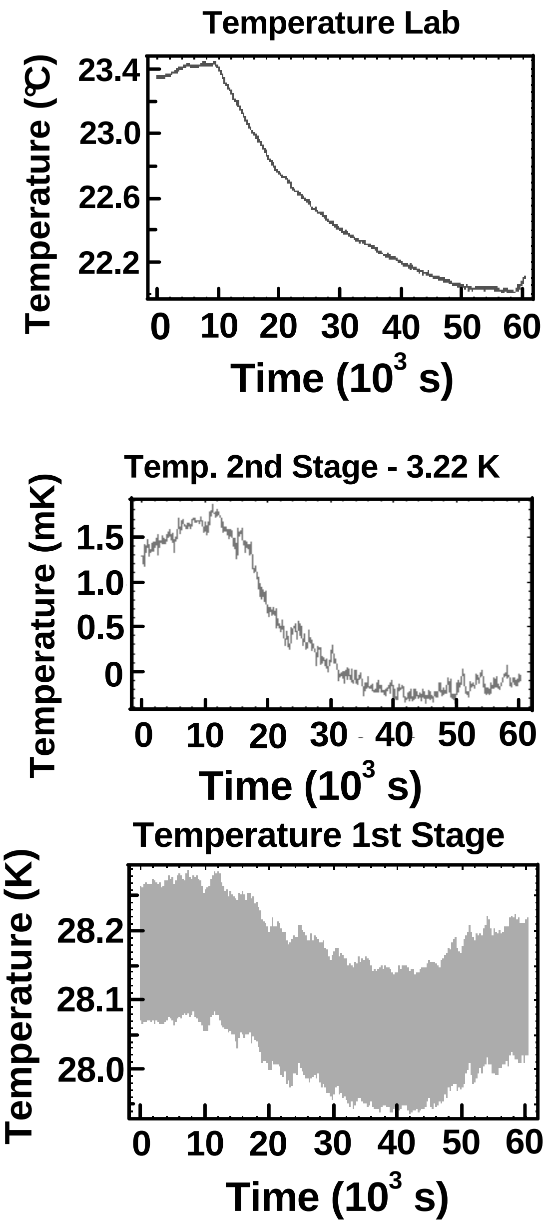

Figure 2.15: Changes of the temperature of the lab result in changes of the temperatures of the first and second stages, due to increasing efficiency of the cooler when the temperature around the cryostat is decreased

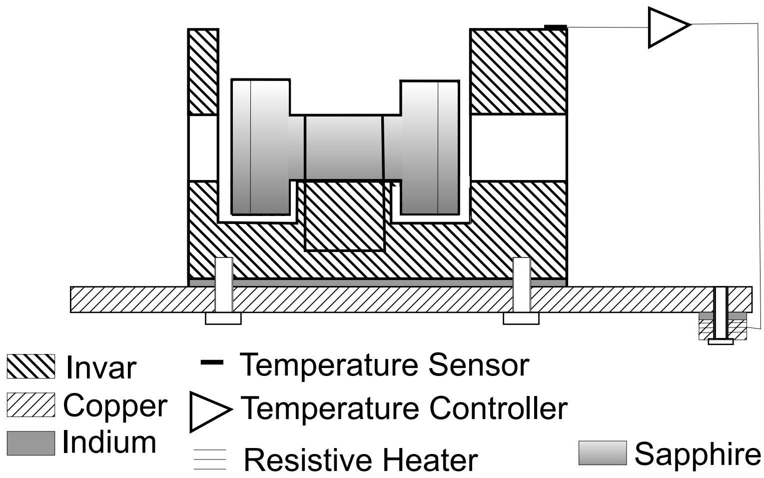

Figure 2.16: The temperature stabilisation of the resonators. The resonators were placed in an invar housing, and fixed to it by means of a copper wire. A temperature sensor fixed to the housing of the resonator B monitored the temperature, controlled by means of a resistive heater placed under the copper plate that held both housing.

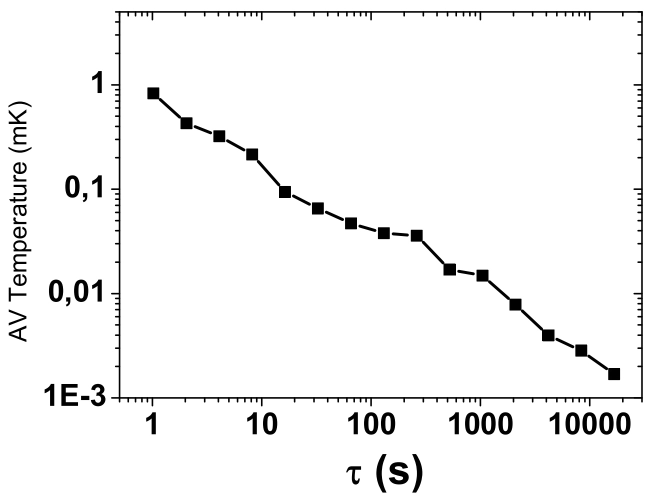

Figure 2.17: The root Allan Variance of the temperature of the cold part of the experiment. The plateau between 100 and 200 s is due to the time constant of the temperature controller.

2.5 The Lasers

Two diode-pumped monolithic non-planar ring oscillator 1064 nm Nd:YAG lasers were locked to the resonance frequencies of the two resonators by means of a first-harmonic Pound-Drever-Hall reflection locking scheme [51].

The laser stablisation can be analysed as a feedback system. The gain of the different parts of the system determine the ability of the stabilisation system to suppress the noises that act do deviate the frequency of the laser from the resonance frequency of the resonator.

The Fig. 2.18 is a schematic of the laser stabilisation. The controlled quantity is the laser frequency ν, perturbed by the noises $S_{f,laser}$ (the spectral density of frequency noise associated with the laser). Other noises are added by the control system: $S_{v,discr}$, the noise of the resonator (produced by the changes in length of the resonator, discussed below), $S_{v,servo}$, the noise introduced by the servo.

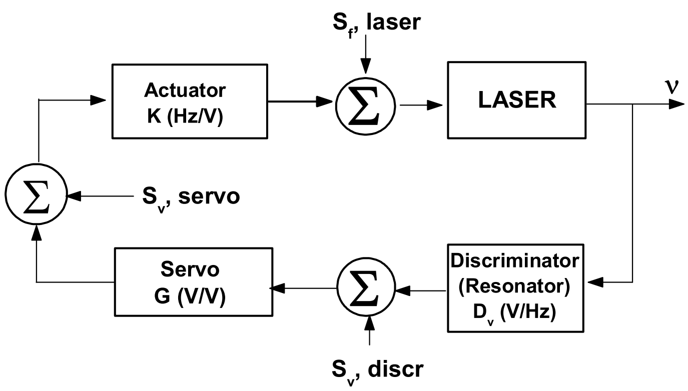

Figure 2.18: The frequency stabilisation of a laser can be treated in the control theory. The output quantity is the laser frequency, perturbed by the noise produced by the laser $S_{f,laser}$, by the resonator $S_{v,discr}$, and by the servo itself $S_{v,servo}$. From [52].

The spectral density of frequency noise is a measure of the rms laser frequency fluctuation in a 1 Hz bandwidth, therefore has the units of Hz/$\sqrt{\text{Hz}}$.

The resonator is the discriminator, that determines the desired value of frequency, and produces a signal in volts proportional to the frequency difference between the laser and the resonance frequency. The proportionality is the gain of the discriminator, D_V, in V/Hz. This error signal is amplified and compensated in the servo, with a gain G(V/V), which is frequency dependent. This amplified voltage is negatively fed back to the laser through the actuator to the laser. In order to have a negative feed-back the phase is the important quantity.

The total closed-loop linear spectral density of frequency noise is [52]:

$$S_{f,cl} = \frac{\sqrt{S_{f,laser}^2 + |KS_{v,servo}|^2 + |KGS_{v,discr}|^2}}{|1 + KGD_v|}, \tag{2.7}$$

that in the limit of very high servo gain becomes

$$S_{f,cl} = \frac{S_{v,discr}}{D_v}. \tag{2.8}$$

That is, in this limit the noise properties of the system are dominated by the noise of the discriminator (the resonator).

Let us now analyse the different sources of noise.

Shot noise

The limiting frequency stability is:

$$\sigma = \frac{\delta\nu_c}{\nu J_0(\beta)}\sqrt{\frac{h\nu}{8\eta P\tau}} \tag{2.9}$$

where: h is the Eisenberg's constant, P is the power incident on the resonator, η the quantum efficiency of the detector, ν the frequency of the incident light, $J_0(\beta)$ the zeroth order Bessel function of the phase modulation depth β (the optimum value for β is 1.08), and $\delta\nu_c$ is the cold oscillation linewidth of the laser resonator (about 100 MHz by Nd:YAG non-planar ring oscillator laser), and τ is the integration time.

If the level of the noise on the current of the photodetector is higher than the shot-noise level assumed above, then the minimum instability will be correspondingly higher. The Fig. 2.19 shows the lock instability estimated from these considerations.

Thermal noise

The influence of the thermal noise in an optical resonator was treated by Taylor *et al.* [50]. In a recent paper, Numata *et al.* [53] showed that thermal noise (Brownian motion) of the material the resonator is made of set a limit on the frequency stabilisation of a laser to a Fabry-Perot resonator. In particular, the one-side power spectrum of the displacement of a mirror (that determines through the length of the resonator the resonance frequency of the resonator, Eq. 2.1) is dominated by the mirrors themselves, because at the frequency region below the mechanical resonance (about 30 kHz for sapphire, [50]) only the losses around the beam spot contribute to the thermal noise. Therefore the loss of the spacer does not greatly contribute to the thermal noise.

The power spectrum $G_x(f)$ can be written as [53]:

$$G_x(f) = -\frac{4k_BT}{\omega}\mathrm{Im}[H(\omega)], \tag{2.10}$$

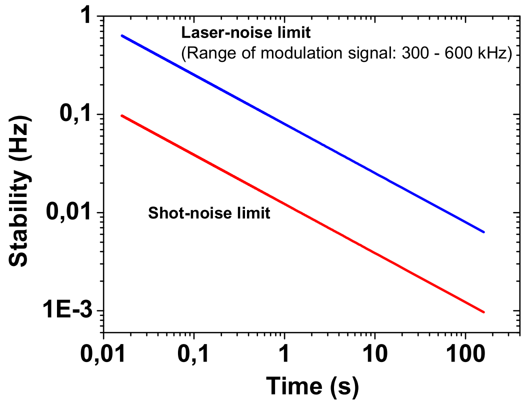

Figure 2.19: Expected frequency lock instability resulting from the noise produced by the photodetector, as a function of the integration time. The lower line plots the quantum noise of the laser power ('shot noise limit), and the upper line the actual level, as measured in Fig. 2.25.

where x is the displacement, k_B the Boltzmann constant, T the temperature, ω the angular frequency. $H(\omega)$ is the transfer function from the force $f(t)$ applied to the observing point to displacement $x(t)$ defined through the Fourier transforms $\tilde{X}(\omega)$ of $x(t)$ and $\tilde{F}(\omega)$ of $f(t)$, $H(\omega) = \tilde{X}(\omega)/\tilde{F}(\omega)$. $\mathrm{Im}[H(\omega)]$ is proportional to the loss of the system.

For a mirror with Poisson's ratio ν (see Sect. 2.3.1), beam radius w_0, loss ϕ_{sub} of the substrate and Young's modulus E we obtain:

$$G_{mir}(f) = \frac{4k_BT}{\omega}\frac{1-\sigma^2}{\sqrt{\pi}Ew_0}\phi_{sub}. \tag{2.11}$$

Here we see the advantage of using cryogenic sapphire resonator, because of the win of two order of magnitude at cryogenic temperatures respect to 300 K, and because of the high Young's modulus of sapphire (300 GPa compared to 68 GPa of ULE, for instance). Another consequence of Eq. (2.11) is that noise decreases with a larger beam radius, or lower loss substrate.

Uncertainty principle

Also the Eisenberg's uncertainty principle could be considered. In fact, the resonator is a unit of length. The uncertainty of the length of the resonator can be estimated considering the uncertainty in energy of the fundamental acoustic mode of its structure. The result is [50]:

$$\sigma_E = \sqrt{\frac{h}{2\pi EL^3\tau}} \tag{2.12}$$

where E is the Young's modulus of the material the resonator is made of. For our 3 cm long sapphire resonator this gives:

$$\sigma_E = \frac{9 \cdot 10^{-21}}{\sqrt{\tau}},$$

a value that is negligible compared to the shot noise.

2.5.1 Frequency stabilisation

Both lasers have two ways to control the output frequency, both relying on changes in the dimension of the laser crystal: one coarse and slow (time scale of seconds), having as actuator the temperature of the crystal, that was modulated by one output of the lock system we used (tuning coefficient 1 GHz/°C), and a fast one in which a piezoelectric actuator compressed the crystal in the vertical direction, obtaining consequently changes of the horizontal dimensions, thus of the path of the standing wave inside the crystal (tuning coefficient 1 MHz/V, range 0 - 150 V). The piezoelectric actuator was used also to produce the sidebands, adding a AC modulating signal to the DC signal of the control signal [54]. This configuration was preferred to the alternative of modulating the laser beam with an electro-optic modulator (EOM), because it produced a smaller residual amplitude modulation (AM) than the EOM, although a disadvantage is that is not possible to avoid the sidebands in the beat signal between the lasers. The residual amplitude modulation is generated by imperfections in the production of the phase modulation. The effect of AM is to shift the error signal of an offset, that the lock system interprets as a difference between the laser frequency and the resonance frequency of the resonator, even if the laser frequency exactly corresponds to the resonance. Since the AM can change in time due to intrinsic changes of the effect that generated it, it is highly desirable to avoid any additional source of AM, that's why modulation of the laser beam using the piezoelectric actuator was preferred.

The scheme of the optics is shown in Fig. 2.21. The scheme of the lock-box is shown in Fig. 2.22, and the corresponding Bode diagram in Fig. 2.23.

The lock-box was made in this configuration to achieve three characteristics:

1. high gain for low frequencies;

2. the gain for frequencies higher that 10 kHz be smaller than unity;

3. the slope of the Bode plot where the gain is unity is -6dB/octave.

The first requirement is necessary to improve the stability for low frequencies. The requirement that the gain for frequencies higher than 10 kHz be smaller than unity is a consequence of the presence of several mechanical resonances of the piezoelectric actuator at frequencies higher than 10 kHz. It is then necessary to avoid amplification at these frequencies, otherwise the system would oscillate. The requirement that the slope at unity gain be -6dB/octave comes from the stability criterion: a slope of -12dB/octave would result in a phase difference between input and output of 180 degrees, resulting then in positive feedback instead of negative feedback, that is, in oscillations in the system [55, 56].

The dispersion error signal produced by demodulation of the first harmonics of the sidebands is shown in Fig. 2.20. The signal shown is taken at room temperature. Demodulation at the third harmonics was also realised, but not used, because the signal-to-noise ratio was too small, then the beat frequency was too unstable for the goals of the experiment.

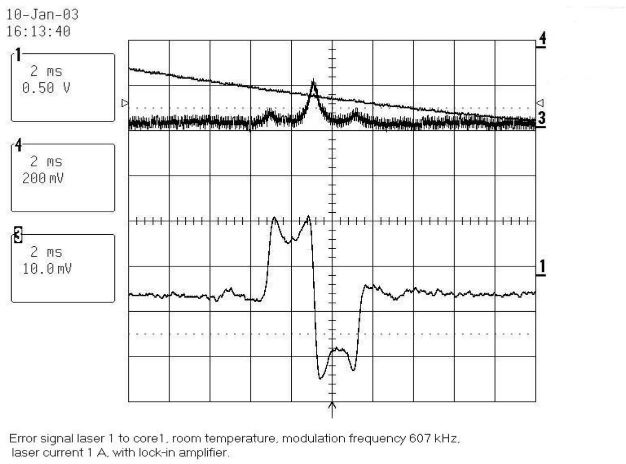

Figure 2.20: **Up:** signal transmitted through the resonator. **Down:** dispersion error signal generated by demodulation of the first harmonics of the modulation sidebands.

The setup for the frequency lock is shown in more detail in Fig. 2.24.

For a high precision Michelson-Morley experiment a very accurate lock of the lasers to the resonators is very important. This implies maximising the signal-to-noise ratio of the error signal, using photodetectors (photodiodes and preamplifiers) of low intrinsic noise. The preamplifiers were developed at the Institut für Experimentalphysik of the University of Düsseldorf. Their noise properties were measured, and plotted in Fig. 2.25.

The Pound-Drever-Hall [51] frequency-lock system operates at the frequencies 321 kHz and 308.5 kHz respectively for laser 1 and laser 2.

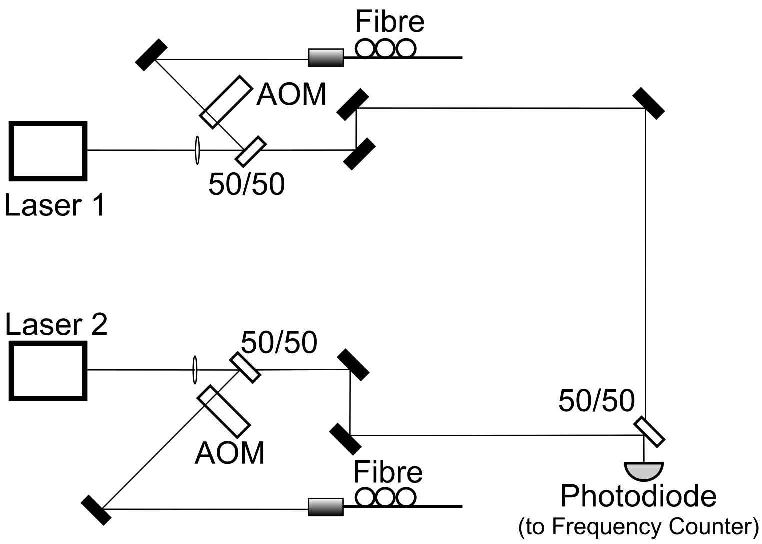

Figure 2.21: Optical scheme for the coupling to the resonators.

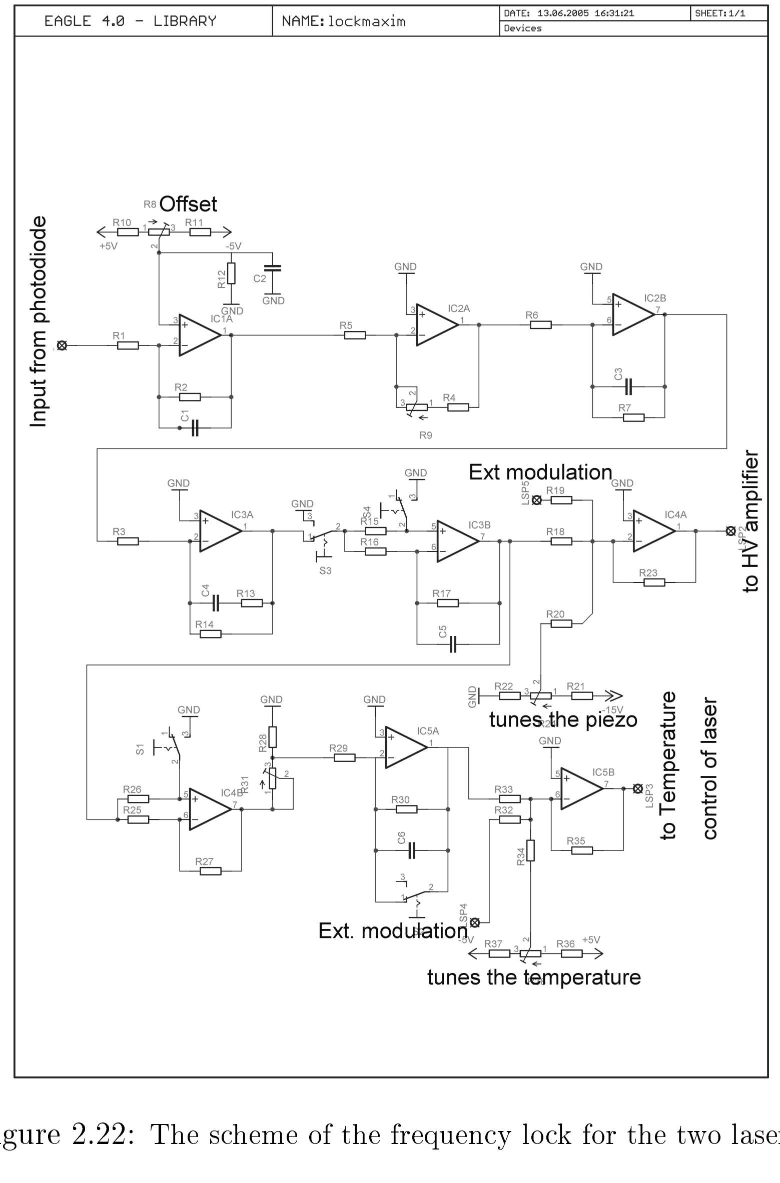

Figure 2.22: The scheme of the frequency lock for the two lasers.

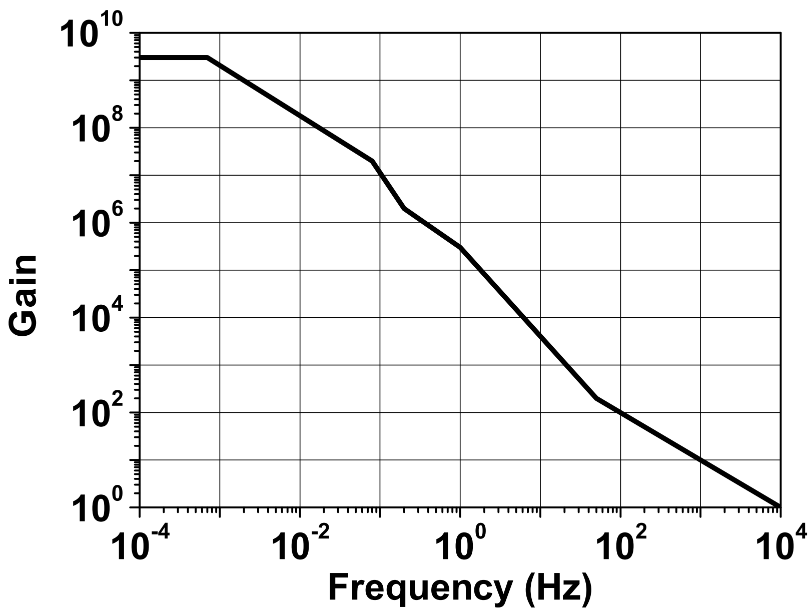

Figure 2.23: The calculated Bode diagram of the stabilisation system shown in Fig. 2.22.

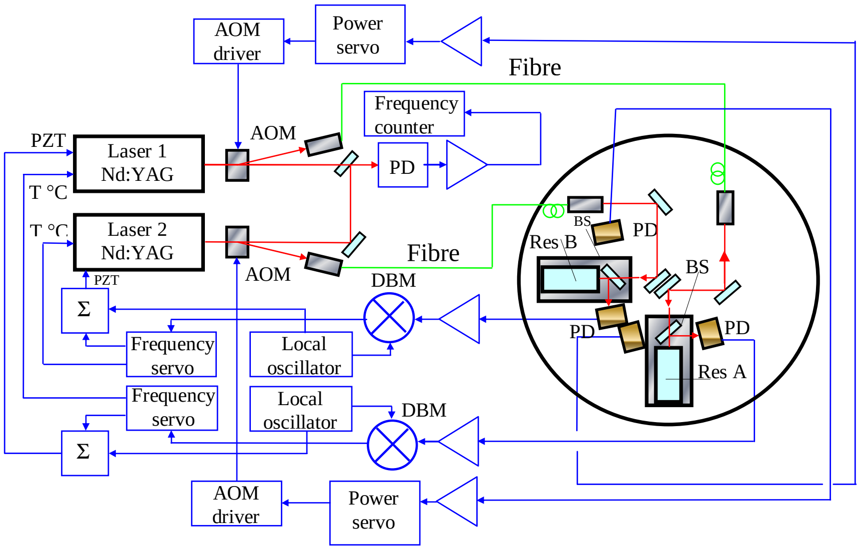

Figure 2.24: Setup for the frequency stabilisation of the lasers to the optical resonators. AOM: acousto-optic modulator; DBM: doubly-balanced mixer; BS: beams splitter; PD: photodiode; PZT: piezoelectric actuator; T: input for the temperature control of the laser crystal.

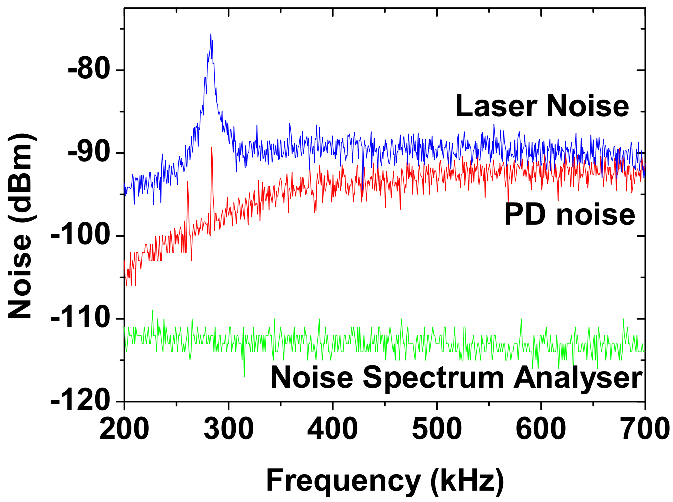

Figure 2.25: Noise of the photodetector as a function of frequency. The curve 'Laser noise' was measured with a power of 50 μW impinging on the photodiode. The curve 'PD noise' is the noise measured when the laser is off, and the lower curve is the proper noise of the spectrum analyser used for this measurement. The peak at 290 kHz is a measurement of the relaxation oscillation of the Nd:YAG laser. The resolution bandwidth is 1 kHz.

2.5.2 Power Stabilisation

The dependence of the resonator resonance frequencies on the power of the beam impinging to the resonators was measured (see Sect. 2.9.2 for details). The dependence was at level of 10 Hz/μW. The power of both beams were actively stabilized using acousto-optical-modulators (AOM) at a relative level of 10^{-4}. The scheme is shown in Fig. 2.26, and the corresponding Bode plot in Fig. 2.27.

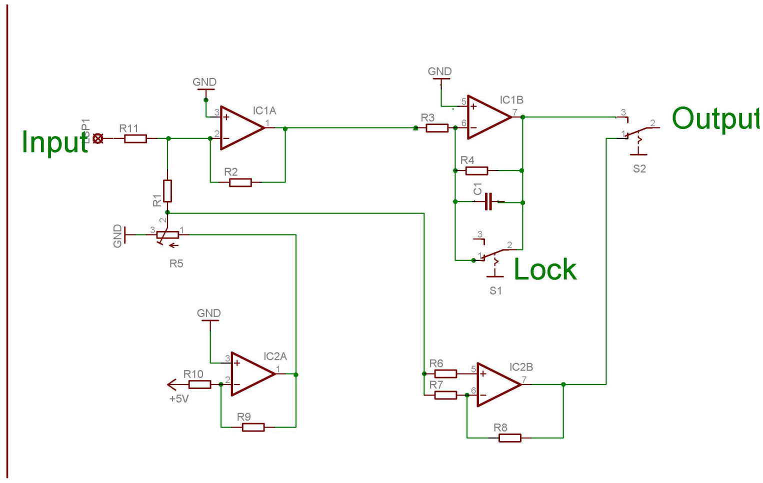

Figure 2.26: The scheme of the power lock for the two lasers through acousto-optic modulators.

The AOMs also served as optical isolators. The signals required to monitor the instantaneous laser powers were obtained from photodiodes placed inside the cryostat, just before the resonators. At a typical working power of 100 μW, the influence of residual power changes was thus reduced to the level of 1 Hz ($3.5 \cdot 10^{-15}$).

Fig. 2.28 shows the characterisation of the typical drift of the laser power at the output of the fibres, and the effect of the power stabilisation.

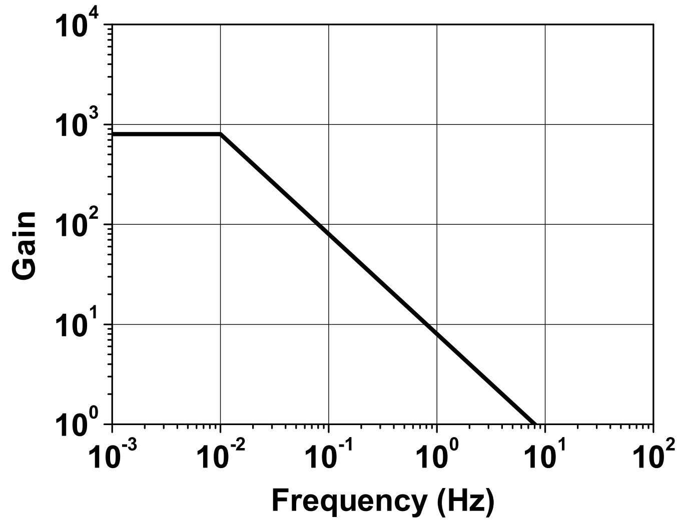

Figure 2.27: The Bode plot of the stabilisation of the power of the beam impinging to the resonators.

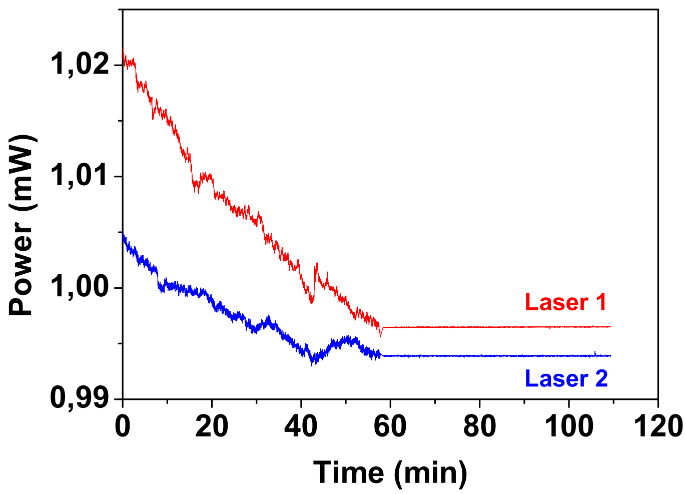

Figure 2.28: Active power stabilisation of the power of the laser power. In this plot is not the power impinging on the resonators (where powers at the level of 100 μW where used. This plot is made of data taken during the test of the lock. Before t = 60 min the stabilisation is off, afterwards they were turned on.

2.5.3 Results of the stabilisation

In the Fig. 2.29 the error signal of the lock of one resonator is shown, during a cryogenic run. The gain of the discriminator was $4{\cdot}10^{-5}$ V/Hz, and the error signal, over an integration time of 100 seconds (comparable with the time elapsed during a rotation) has a width of $1{\cdot}10^{-5}$ V, resulting in an instability of 0.25 Hz.

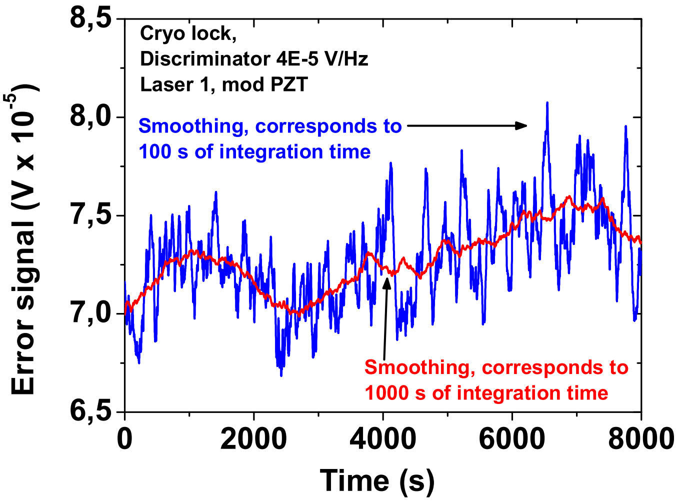

Figure 2.29: Error signal of stabilised laser

A similar measurement performed one year later over 60 000 seconds (16.7 hours) showed a similar behaviour, see Fig. 2.30. The lock signal compared to the temperature of the lab shows that the frequency-lock electronics is not very sensitive to the external temperature.

The Allan Variance of the beat frequency was measured with rotations (300 s for 90°). The result is in Fig. 2.31, solid line. It can be compared with the Allan Variance measured when the cryostat does not rotate, in the same Figure, dashed line.

The beat frequency between the two lasers was compared to the 5 MHz output of a hydrogen maser, by means of a phase lock of the frequency counter to the maser.

The hydrogen maser was supplied by the company Vremia-CH. The sensitivity of the maser from changes of the external temperature is $5 \cdot 10^{-15}/°C$, which is negligible in the time scale of a measurement run: 10 minutes for a rotation and 12 hours for a complete measurement. The relative drift of the maser output frequency in one day is less than 10^{-16}.

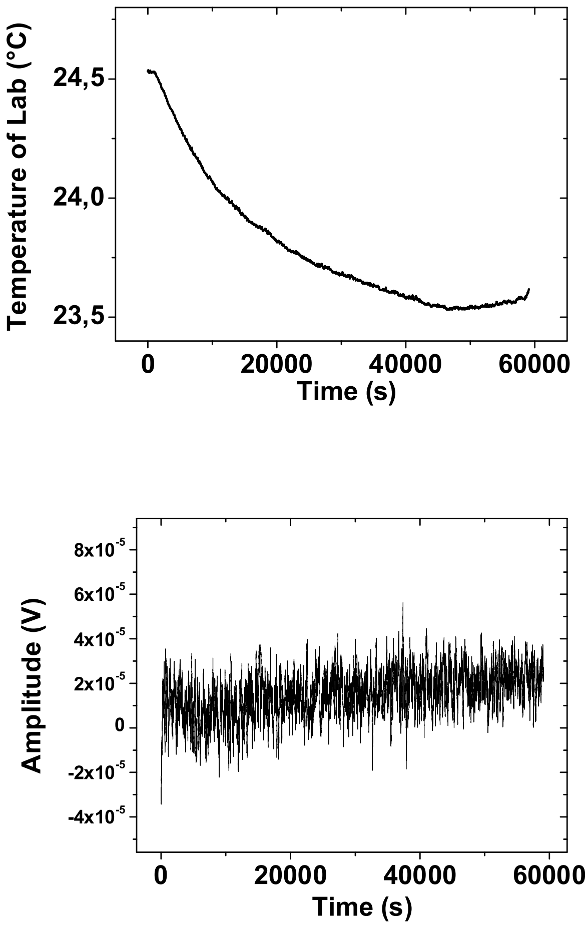

Figure 2.30: Error signal of stabilised laser, compared to the temperature of the lab.

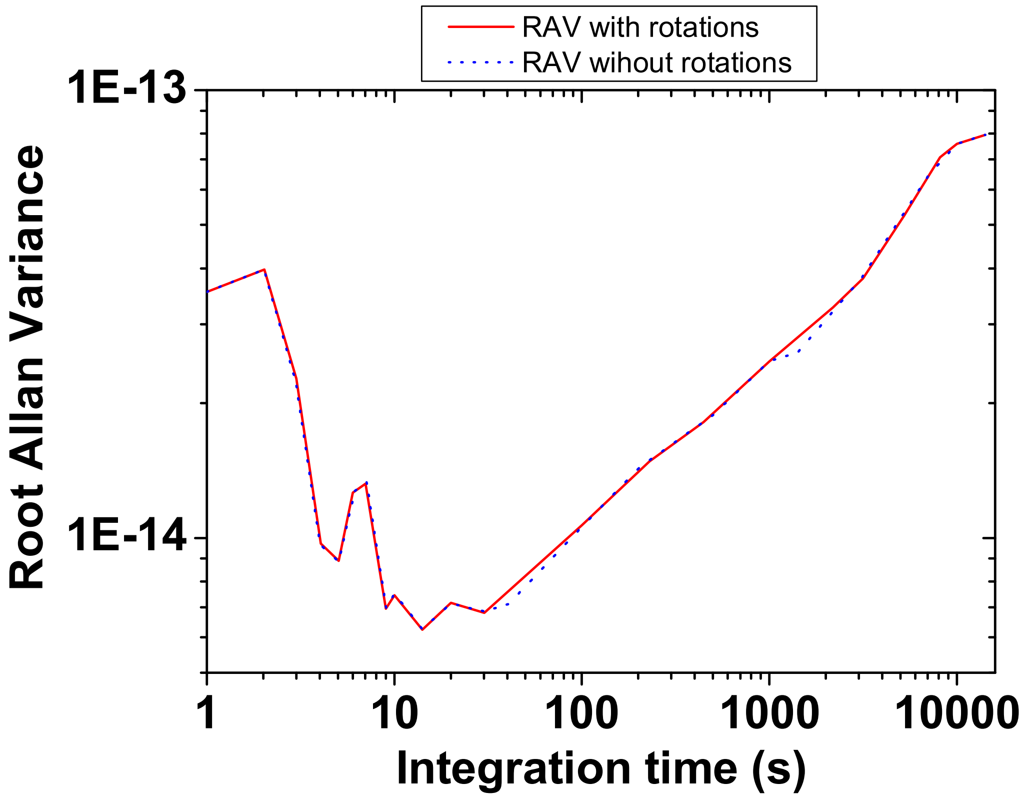

Figure 2.31: **Solid line:** The root Allan Variance of the beat frequency with rotations. **Dotted line:**The root Allan Variance of the beat frequency without rotations.

2.6 Drift of the resonators

The drift between the two resonators is of the order of 1 Hz just after the start of the cooling, and reduces to 0.02 Hz after some weeks of operation.

With the setup consisting of three resonators shown in section 2.6.1 the drift between different resonators was estimated.

2.6.1 Three resonators and two fibres

In order to characterise and understand the drift in the beat frequency for some time a third optical resonator, nominally identical to the other two was mounted in the same setup. It was mounted on a second platform, a copper disc identical to the one already described, under it, as it can be seen in Fig. 2.32. Also this third resonator was fibre-coupled, by means of a third optical fibre, similar to the other two already mounted. The TEM mode coupled to the resonator could be monitored though a window in the lower part of the cryostat and a CCD camera. In Fig.2.33 it can be seen in the center of the disc the mirror, tilted of 45°, that bent the beam from horizontal to vertical.

With this setup the drift of the different resonators was measured. In Figs. 2.34, 2.35, 2.36 the drifts between the different couples of resonators are shown:

of $D_{AB} = -\ 0.57$ Hz/s between resonators A and B,

of $D_{BC} = +\ 0.65$ Hz/s between resonators B and C,

of $D_{AC} = +\ 0.81$ Hz/s between resonators A and C.

The data used to plot the Figs. 2.34, 2.35 and 2.36 were recorded over a time span of two days.

It is to be noted that the relationship between the three drifts should be: $D_{AC} = \pm D_{AB} \pm D_{BC}$, the signs $\pm$ depending on which laser of the couple was locked to the mode of higher frequency. For instance, if the resonator A had (to simplify) no drift, and resonator B an absolute positive drift, the beat frequency between A and B would have a positive drift if the laser locked to A was stabilised at a lower frequency than the laser locked to B (the two frequencies diverge), and negative if the frequency of the laser locked to A would have a higher frequency (then laser B would approach laser A). From our data we do not have any of the combinations above, this is due to an instability of the temperature of the pulse-tube cooler at that time (the problem of the stability of the cooler was solved only later): this measurement is to be considered only as the estimate of the drift trends for the resonators, not as a precise measurement. This measurement was made to see whether there was some big difference of the drift or the stability between the resonators.

There was also the program to use the third resonator as alternative to one of the other two (or in presence of a third Nd:YAG laser, together) for the Michelson-Morley experiment, but it was seen that the presence of the second copper disc resulted in an increased mass that caused additional vibrations during the rotation of the cryostat. These vibrations spoiled the results of the experiment, for this

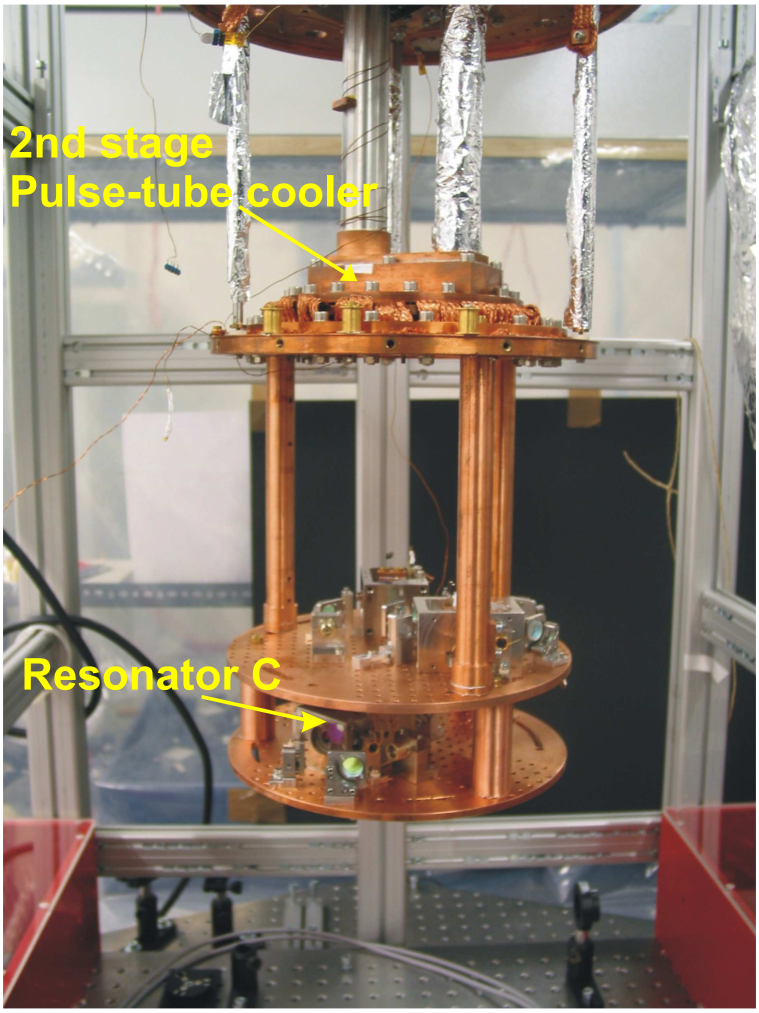

Figure 2.32: The setup with three resonators

reason after the measurements presented in this section the third resonator was unmounted.

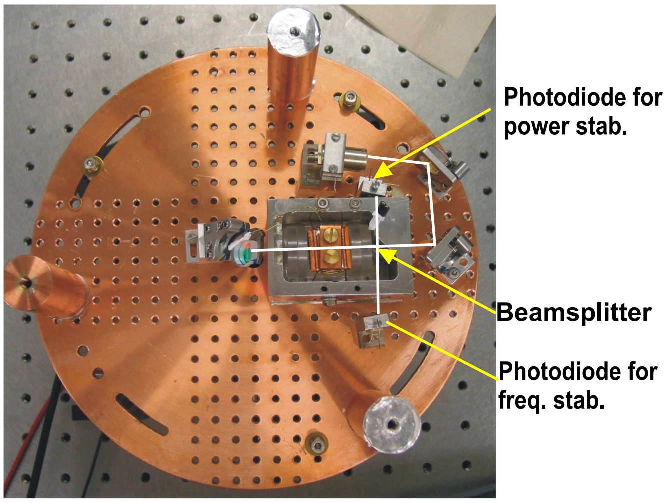

Figure 2.33: A detail of the setup: the third resonator.

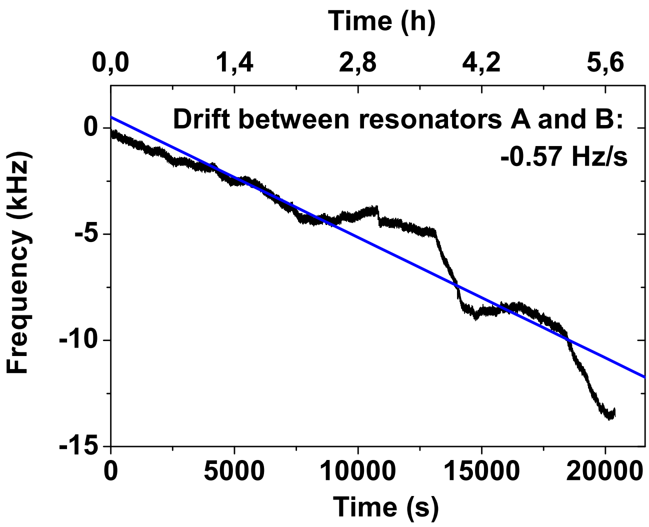

Figure 2.34: Drift between resonators A and B.

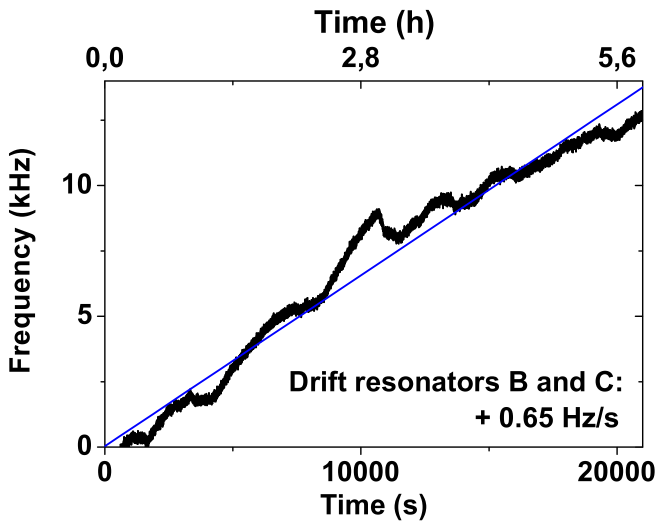

Figure 2.35: Drift between resonator B and resonator C.

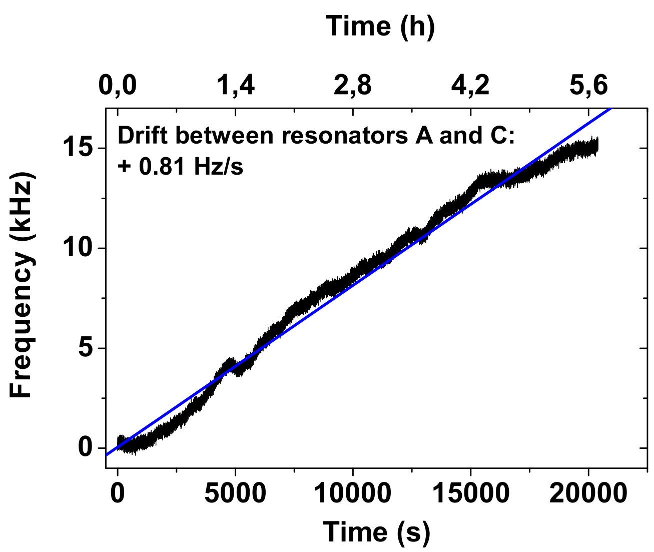

Figure 2.36: Drift between resonators A and C.

2.7 Comparison of a resonator with the frequency comb

A frequency comb provides a link between an ultra-stable microwave frequency (in the range of GHz), like the output of a cs clock or (like in our case) of a hydrogen maser and optical frequencies (THz). The basic idea is that the pulses circulating in the cavity of a pulsed laser can be Fourier-transformed in a series of frequencies, that represent a periodic spectrum in the frequency space with periodicity $f_r = 1/T$, where f_r is the repetition rate of the laser pulses, and $T = 2l/v_{gr}$ the pulse repetition time for a cavity of length l and a group velocity v_{gr} for the pulses. Stabilisation of the cavity's length and of an offset frequency f_{ceo} (through extension of the spectrum via self phase modulation in an optical fibre) provides an 'optical ruler' that links the radio frequencies f_r and f_{ceo} to the optical frequencies f_n, $f_n = nf_r + f_{ceo}$ [57, 58, 59].

The drift of one of the B resonator was estimated measuring its absolute frequency by means of a frequency comb locked to the hydrogen maser. The resonator was at 3.4 K since 4 months. The beam of the laser 2, locked to the resonator B was fed through a fibre to the frequency comb, that was operated in another lab, some 50 meters apart.

The experimental setup is shown in Fig. 2.37.

The result of the measurement is that the drift, 4 months after the cooling down, is at the level of 10 mHz/s, and it is shown in Fig. 2.38.

The Root Allan Variance of the beat frequency between the frequency comb and the resonator is plotted in Fig. 2.39.

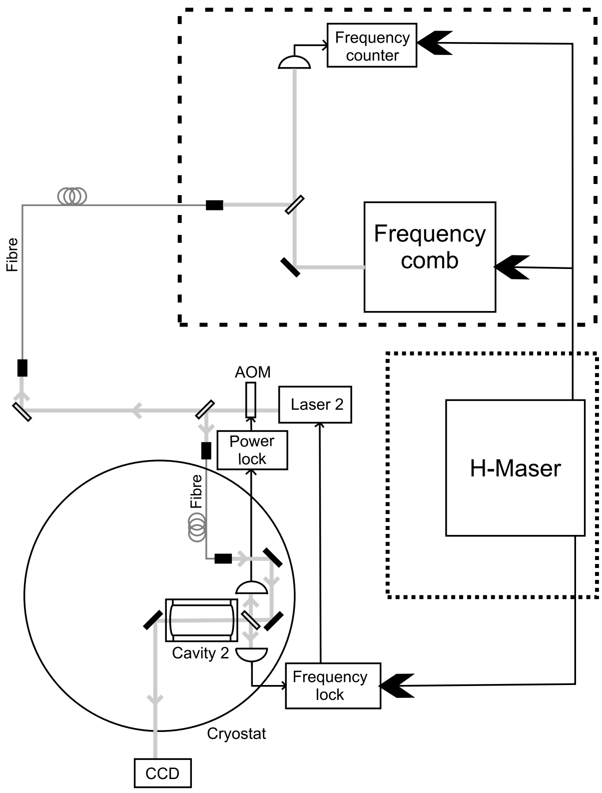

Figure 2.37: The experimental setup used to measure the drift of the resonator B with comparison to a frequency comb. The dotted lines mean that the frequency comb and the hydrogen maser were set-up in different labs that the cryogenic experiment described so far.

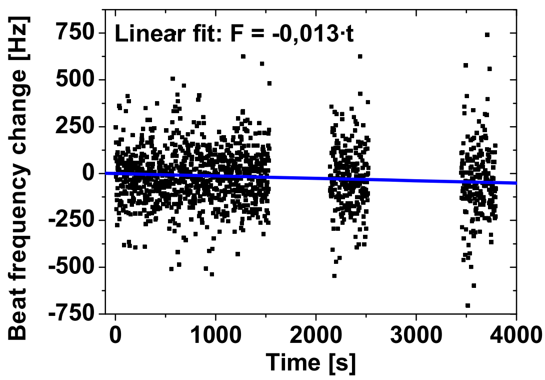

Figure 2.38: The frequency of the resonator B measured with the frequency comb. The drift of the frequency is reported on the plot: - 13 mHz/s. The measurement is short because of the limited stability of the frequency comb.

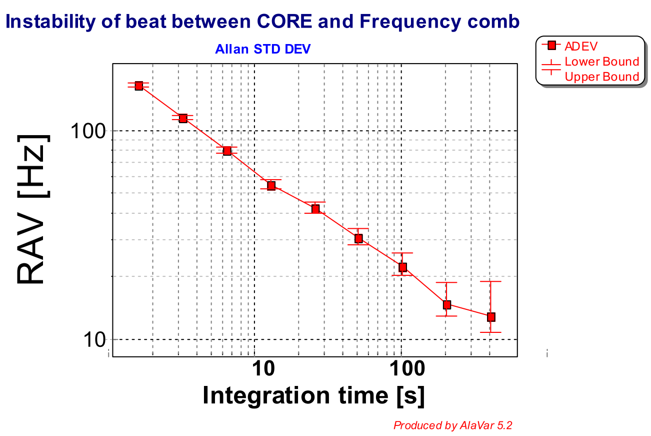

Figure 2.39: The Root Allan Variance of the beat frequency between the resonator B and the frequency comb.

2.8 Rotation table

The mechanical rotation stage consisted of a computer-controlled precision rotating table. The rotation stage itself rested on an optical table that was not floated. During rotations the set-up changes its axis, due to mechanical stress on the bearings of the rotation stage.

A vibration sensor was set up on the rotation stage, with the experiment mounted on it. The spectra of the vibrations were recorded for different rotation speeds, and plotted in Fig. 2.40.

The sensor was not calibrated, thus the spectra are not in units of g, but in mV. Important are the amplitudes as function of rotation velocity (frequency in number of rotation per hour, in the plot). These amplitudes are plotted in Fig. 2.41.

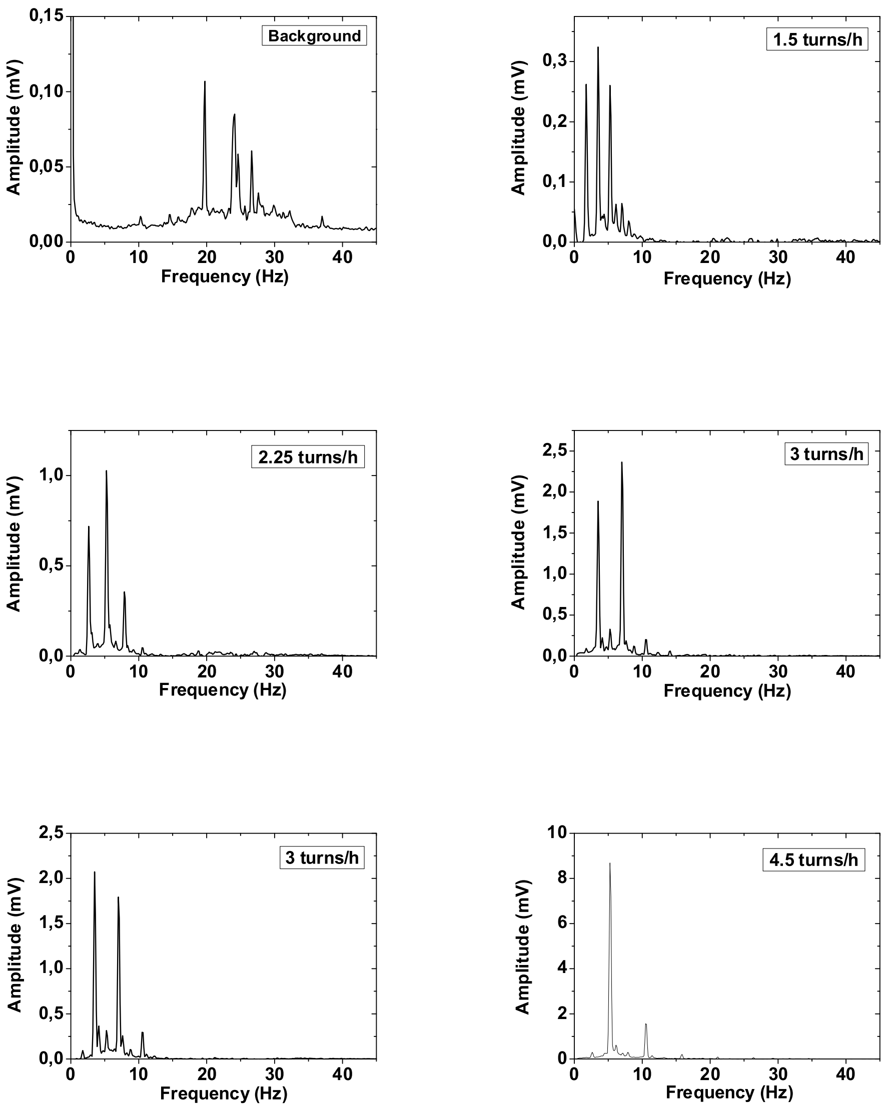

Figure 2.40: The spectra of vibrations of the experiment during rotations. The background was measured with the setup non rotating. To obtain the plots the background was subtracted from the measured spectra. The values are in mV, the sensor was not calibrated.

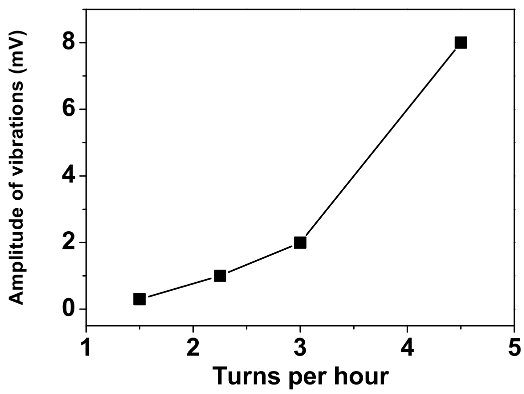

Figure 2.41: The amplitudes of vibrations, as function of the number of rotations per hour. It can be seen that when the frequency is higher than 3 rotations per hour the vibrations increase fast. For this reason we used for our rotations a frequency of about 3 rotations per hour (300 sec. per 90°).

2.9 Overall set-up: systematics

This sections is dedicated to the details of the various sources of systematic disturbances of the beat signal. Sources for systematic disturbances are:

1. shifts of the frequency due to changes of the temperature of resonators;
2. orientation of the resonators with respect to the gravity;
3. power of the laser beams impinging to the resonators;
4. vibration of the experimental apparatus due to the rotations or to the pulse-tube cooler;
5. the temperature in the lab.

The temperatures of the lab and at several points of the pulse-tube cooler can vary during the time of the rotations, and the tilts of the cryostat could only be minimised, not set to zero, due the absence of an active tilt compensation. Fig. 2.42 shows the temperatures of the second stage of the cooler (named 'KK2'), of the first stage (named 'KK1'), of the centre of the two pulse tubes, of the lab, and the tilts (1 mV corresponds to 0.5 μrad) in a typical measurement run.

Fig. 2.42 shows the measurements of the temperatures of various point of the pulse-tube cooler, of the tilts and of the external temperature. The corresponding change in beat frequency, and the temperatures of the resonators and of the lab, for the same data set, are plotted in Fig. 2.43. The difference in temperature between the cold stage and the resonators is due to an error in the calibration of the temperature sensor of the resonators.

The influence of the various effects are collected in the Table 2.1.

Table 2.1: The table of systematics. *Inst* means the instability of the system , it applies for the temperature in the lab, the temperature of the resonators and the power of the laser beams, *mod* is the range in which the tilt of the resonators modulated during a rotation.

Effect	Inst/mod	Sensitivity	Systematic	Relative
Tilt	50 μrad	0.06 Hz/μrad	3 Hz	$1.1 \cdot 10^{-14}$
Temp. in the Lab.	0.025 °C	75 Hz/°C	2 Hz	$0.7 \cdot 10^{-14}$
Temp. Resonators	45 μK	1.5 Hz/mK	0.1 Hz	$0.4 \cdot 10^{-15}$
Power Laser beam	10 nW	50 Hz/μW	0.5 Hz	$1.8 \cdot 10^{-15}$

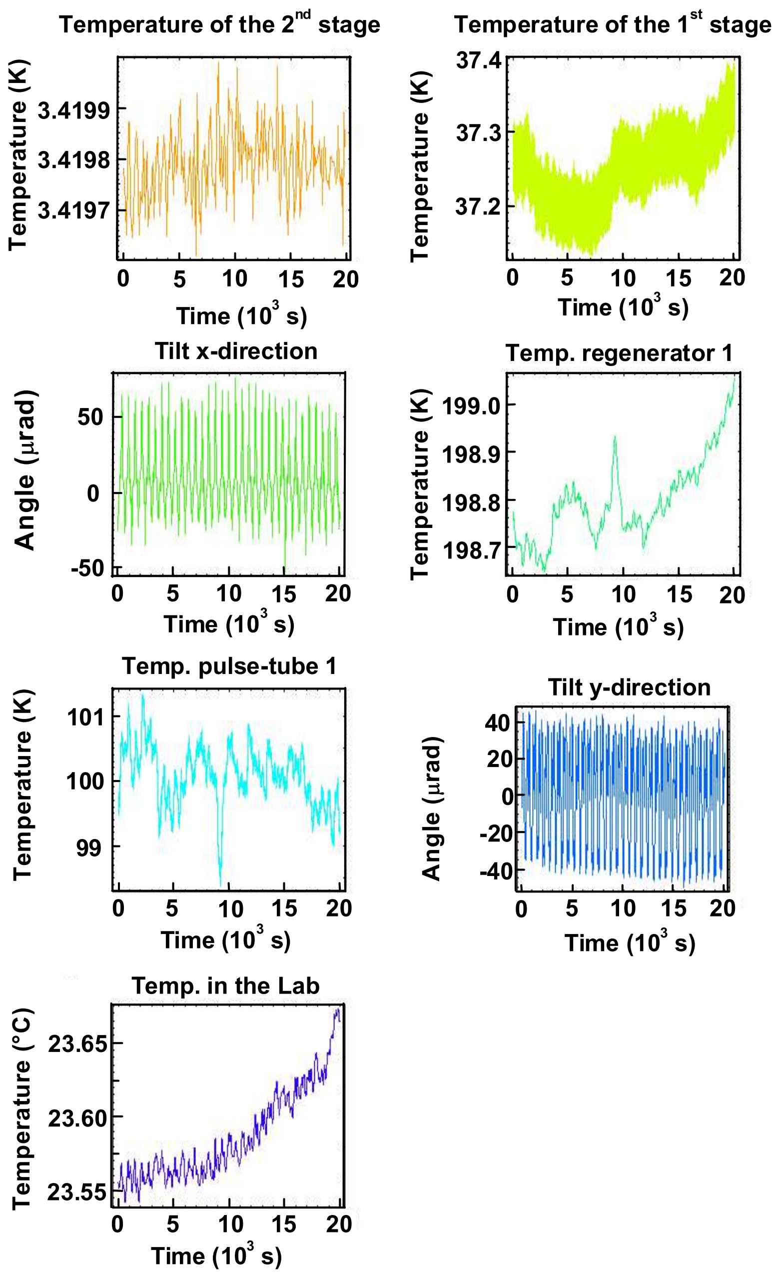

Figure 2.42: Temperatures of the 1^{st} and of the 2^{nd} stages, of the regenerator of the 1^{st} stage, of the middle of the second pulse-tube, and of the lab near the tilt-sensor. The tilts for a typical rotation are also plotted.

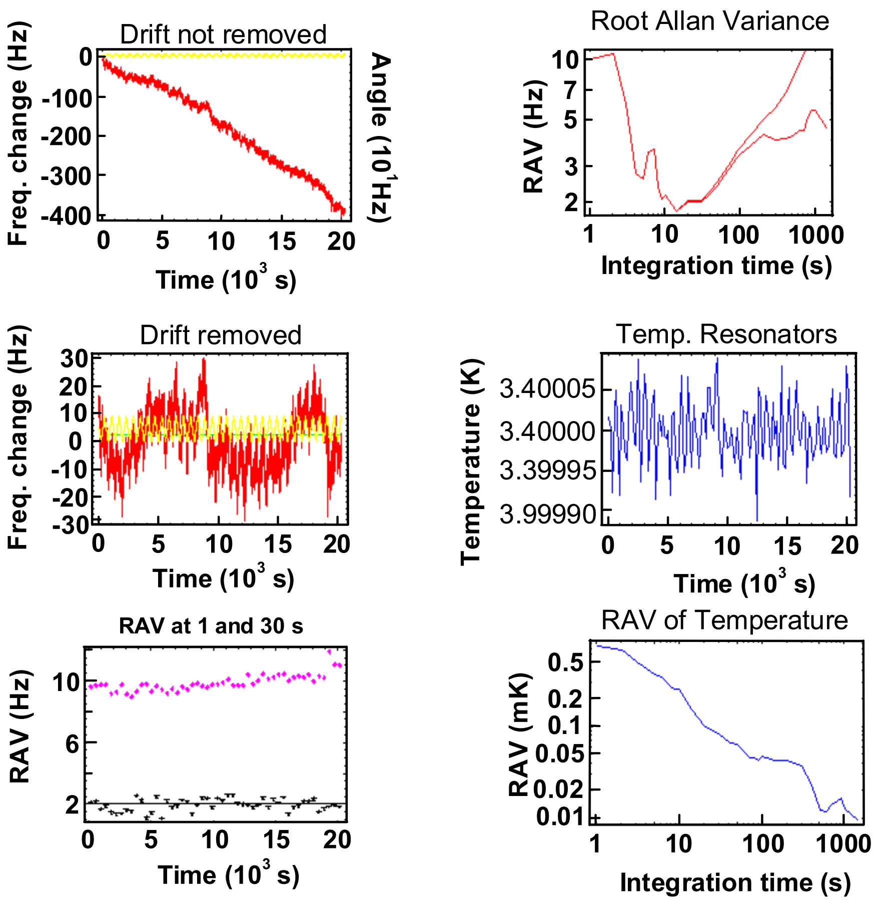

Figure 2.43: The raw data. The Allan variance of the frequency was calculated from raw data (upper curve) and from data after removing of the drift (lower curve, in the same plot). The linear drift is $-2{\cdot}10^{-2}$ Hz/s. Lower right is the Root Allan variance of the temperature of the resonators.

2.9.1 Tilt of the resonators

The importance of the tilt of the resonator in this experiment was explained in Sect. 2.3.1. The sensitivity of the beat frequency between the two resonators on the orientation of the cryostat was measured. As explained later in the data analysis, the frequency shift caused by this effect could be subtracted from the raw data before analysis.

The experiment lay on an optical table that was not floated. Instead of the common air-pressure controlled feet, the table lay on a metal frame. The length of the four feet of the table could be changed by acting on screws.

Before each measurement the frequency shift as a function of the change in the angle of the axis of the cryostat in two orthogonal directions (referred to as x and y in the plots) was quantified acting on these screws to change the orientation of the optical table and thus of the resonators, that were fixed inside the cryostat. The tilt-sensor (Applied Geomechanics, Miniature Sensor 755) was screwed to a platform fixed to the cryostat.

The Fig. 2.44 shows a typical measurement of this kind. From plots of this kind were measured the coefficients, in Hz/μrad, in both directions. After the measurement of the tilt sensitivity of the resonators the table was set in the configuration in which the variations of angle during a rotation were minimal.

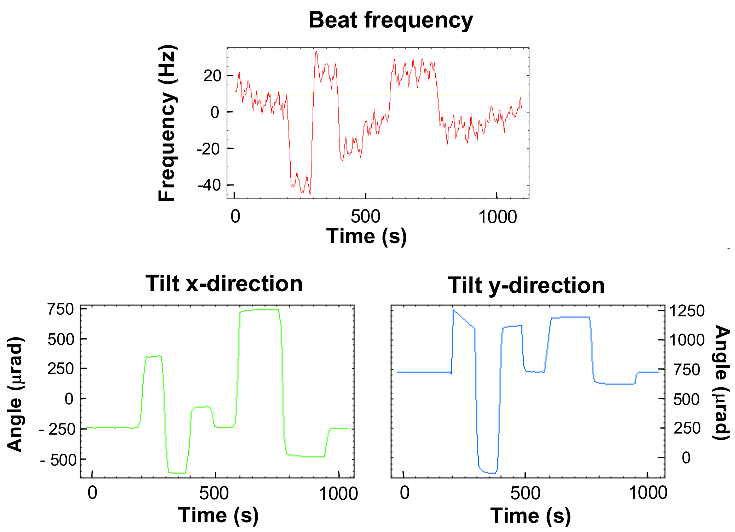

Figure 2.44: A typical measurement of the sensitivity of the beat frequency between the two resonators on the angle of the platform on which the cryostat was fixed.

We obtained a sensitivity of about 0.06 Hz/μrad. The value is the same for both resonators. The resolution of the tilt sensor is 0.1 μrad.

2.9.2 Power of the beam impinging on the resonators

The dependence of the beat frequency on the power of the beam impinging on the resonators was measured, keeping the power of one laser constant, and varying the power of the second one. The dependence could reliably be measured only for relativelylarge power changes ($> 5\ \mu$W).

The Fig. 2.45 shows the variations of the beat frequency for the resonator B as result of variations of the power of the laser beam impinging on the resonator.

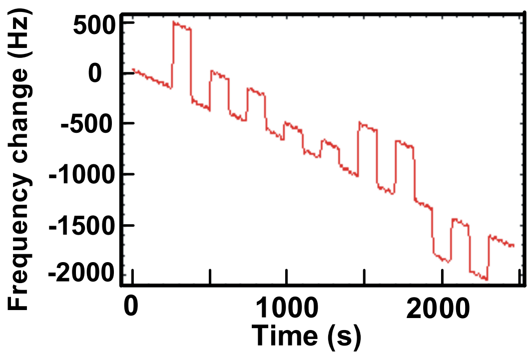

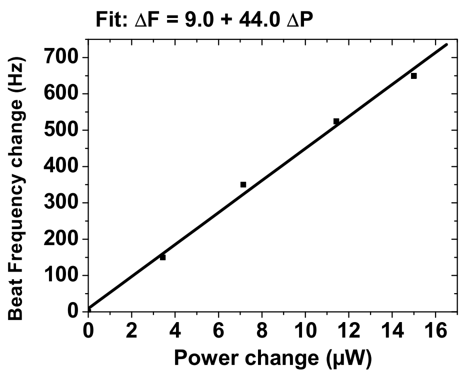

Figure 2.45: **Up:** Raw data from the measurement of the dependence of the beat frequency for variations of the power of the laser beam impinging on the resonator B. **Down:** The dependence of the beat frequency for variations of the power of the laser beam impinging on the resonator B.

For resonator A a smaller effect was observed. The differences between the coefficients for the two resonators are due to different coupling efficiency (mode coupling) of the beams in the resonators. We set then a conservative upper limit at 50 μW.

2.9.3 Vibrations

The displacements of the resonators due to vibrations of the pulse-tube cooler were measured, with a CCD camera fixed to the cryostat and pointing to the output beam from one of the resonators. The beam had a diameter of 1 mm, its image on the screen, produced by the CCD camera had a diameter of 10 cm. It was thus possible to detect lateral movements of about of $1 \pm 1\,\mu$m, and vertical movements of the same amplitude, resulting in a periodic movement at 45 degrees respect to the axis of the cooler at the frequency of the pulses of the cooler (1.1 Hz). This is in agreement with ref. [41], that reports that the longitudinal and transverse mechanical vibrations of a pulse-tube cooler are approximately of the same magnitude. This value is bigger than the value measured in [42], but in that case the measurement was performed on a one-stage pulse-tube cooler. It may be that a two-stage pulse-tube cooler has wider elongations, due to the longer tube it needs for the second stage. The displacement also depends on the pressure difference between the high and low pressure side of the compressor.

Since the optical fibres were fixed to the same copper disc where the resonator's housings were fixed to, it is not possible to estimate how much the resonators moved because of this modulation. Although the copper wire strap that fixed the resonators to the housings were not too tight, they were already at room temperature not loose enough to let the resonators move, and after cooling down they are expected to be even less loose (although still not tight), because of the bigger thermal expansion coefficient for copper than sapphire and invar. This gives a point to assume that the relative movements between the resonators and the laser beam be smaller than $1\,\mu m$. Müller *et al.* measured the frequency change of the laser locked to the resonator for a misalignment of the beam. From the graph plotted in [60] it can be interpolated a coefficient of about 0.3 Hz/μm. Then the frequency change due to misalignment is assumed here negligible.

The 200 Hz modulation signal seen in the beat frequency exactly at the frequency of the pumping of the pulse-tube cooler (1.1 Hz) is then probably originated by changes of the dimension of the resonator due to transfer of the vibrations to it. These are then calculated as:

$$\left(\frac{\delta L}{L}\right)_{vib} = \frac{\delta\nu}{\nu_0} = \frac{200\,\mathrm{Hz}}{3\cdot 10^{14}\,\mathrm{Hz}} = 6.7\cdot 10^{-13}.$$

That could be decorrelated by Fourier analysis of the beat signal, off-line.

From Eq. 2.6 we can calculate which acceleration to a single resonator would result in the same relative instability. We place a instead of g and rewrite (2.6) as:

$$\sigma = \frac{\Delta\nu}{\nu} = \frac{\rho a(0.5-\lambda)}{E} \tag{2.13}$$

we solve (2.13) for a and obtain:

$$a = \frac{\sigma E}{\rho(0.5-\lambda)} = 0.2\mathrm{m/s}^2 = 2\cdot 10^{-2} g \tag{2.14}$$

Thus the instability at the frequency of 1.1 Hz is due not only to vibrations of the cold end of the pulse-tube cooler, that are less than 10^{-4}g, see pag. 32. Other sources of instabilities related to the vibrations from the pulse-tube cooler are misalignment of the mode-matching coupling optics [50].

2.9.4 Temperature in the lab

As can be seen in Fig. 2.46, the temperature near the cryostat during one rotation had a modulation of about 0.025 °C. It was due to the temperature gradient inside the lab. This modulation resulted in a systematic effect observed in the beat signal. In contrast to the systematic caused by the variation of tilts, it was not possible to decorrelate this effect from the raw data. It is responsible for the greater part of the nonzero signal in the Lorentz violation signal.

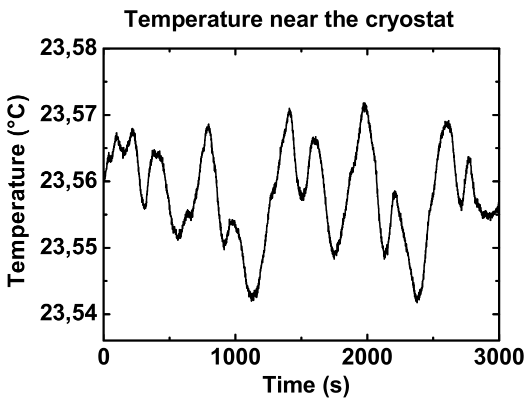

Figure 2.46: Temperature measured near the cryostat. The modulation period is of 300 s, the rotation half-period.

The sensitivity of the beat frequency to changes of the temperatures in the lab was measured modulating the room temperature acting on the air conditioning system of the lab. A change in the beat frequency of 75 Hz/°C was measured, see Fig. 2.47.

In Sect. 2.4.1 it was noted that a change of the temperature of the lab results in a change of the temperature of the cold stage.The frequency change measured here is not a consequence of this effect, because the temperatures of the resonators was stabilised, making them independent of the temperature of the room. This can be seen in the Fig.2.47,where the temperature of the resonators during the measurement is also plotted.

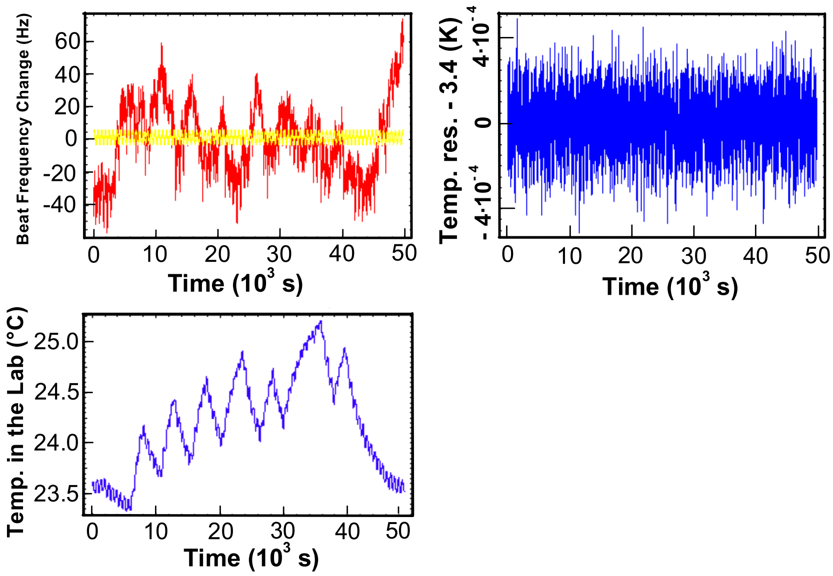

Figure 2.47: A change of the temperature of the lab results in a change of the beat frequency, most probably due to sensitivity of the optical fibres. During the measurement the temperature of the resonator remained constant, see plot up right.

2.10 Two resonators and one optical fibre

In a first stage of the experiment both lasers were coupled to the resonators through a single optical fibre. First the polarisations of the two beams were set orthogonal to each other, then they were superimposed via a beamsplitter to the fibre. Before each resonator was installed a polarisator, to block the undesired beam and let the other one through. A scheme of the setup is depicted in Fig. 2.48.

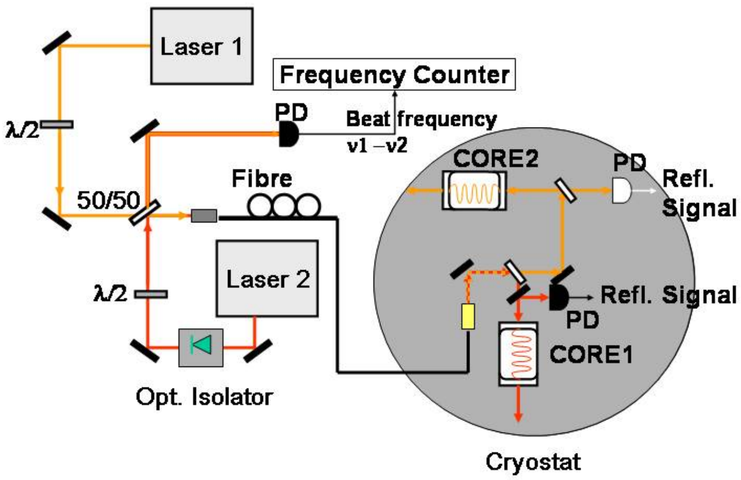

Figure 2.48: A scheme of the optical setup for the early experiment with two optical resonators and only one optical fibre. A picture of this scheme is in Fig. 2.49.

This configuration gives a common-mode rejection of systematic effects caused by external changes to the fibres. In fact such effects were later seen with the setup with two fibres, see Sect. 2.9.4. This scheme could not be used, because in the error signal of the frequency lock of the two lasers it was often possible to see the interference with the other beam. This means that although the beams were crossed-polarised, in each resonator there was also a part of the beam that had to be blocked. I believe that the strong temperature gradient in the cryogenic part of the fibre (300 K in two meters) caused mechanical stresses in the glass, that resulted in a rotation of the polarisations of the two beams. Thus in the fibre-outcoupler in the cryogenic part of the experiment the two beams were not orthogonal or not linear-polarised anymore. For this reason a second fibre were mounted to couple each laser through one fibre. A picture of the setup is shown in Fig. 2.49.

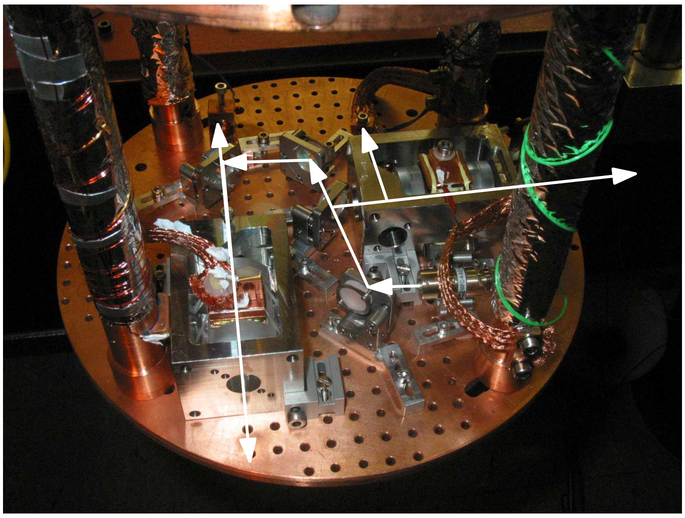

Figure 2.49: The optical setup with two optical resonators and one fibre

Chapter 3

Data analysis

The data set was collected at 1 s intervals during very stable operation from 4 February 2005 to 8 February 2005 for 76 hours.

Two computers were used to collect the data. The clocks of both computers were synchronised through the internet to the official time. One computer controlled the rotation angle and rotation speed of the experiment, recorded the beat frequency and the temperature of the optical resonators, by means of a program written in LabView. The second computer recorded the tilts values fed by the tilt sensor, and several temperatures at different points of the pulse-tube cooler. An example was plotted in Figs. 2.42 and 2.43. The tilt values were then used in the data analysis as explained below, the temperatures were used to monitor the system. Two temperatures in the lab were recorded, near the tilt sensor and near the optical fibres. In fact the optical fibres induced a temperature-dependent shift in the beat frequency, as explained in Sect. 2.9.4, and the tilt sensor showed a small dependence of the output on the temperature. The effect on the tilt sensor was suppressed by a passive temperature insulation of the sensor.

The two files produced by the two computers were synchronised and merged into a single file. The tilts of the cryostat were weighted with the measured beat frequency sensitivities and the resulting frequencies were subtracted from the beat frequency of the raw data. Then the beat modulation at 1.1 Hz caused the pulse-tube cooler was removed.

The edited beat frequencies were coupled to the corresponding angle of rotation, appearing in the form of Fig. 3.1 with the corresponding measurement without tilt decorrelation.

After manual removal of very few (less that 1%) clearly disturbed rotations, the remaining 432 rotation periods $\theta = [0°; 90°; 0°]$ (labeled by i) were each least-squares fitted with functions

$$a_i t + 2B(t_i)\sin 2\theta(t) + 2C(t_i)\cos 2\theta(t),$$

where the coefficients a_i quantify a (slowly varying) linear drift.

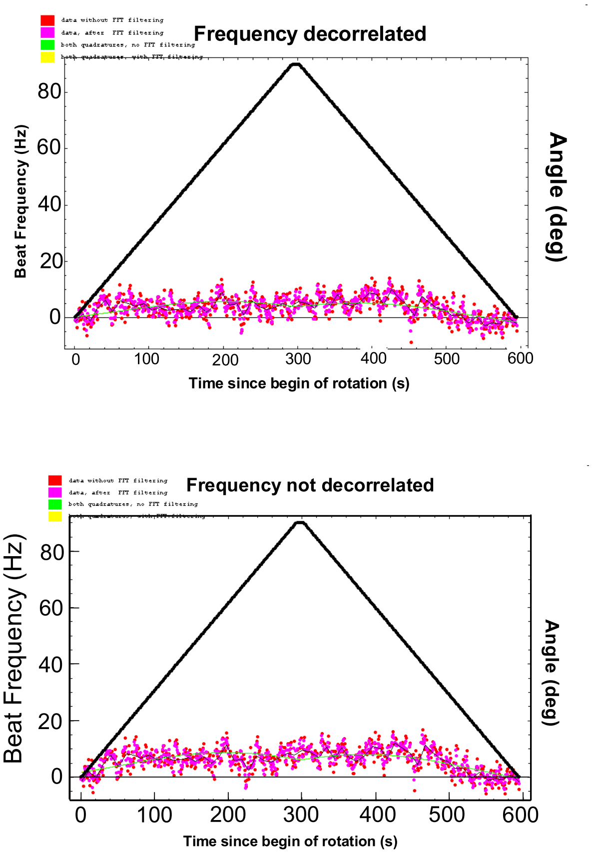

Figure 3.1: **Up:** The edited beat frequency: the frequency shift caused by the tilts (in the two directions, x and y) was subtracted from the raw data beat frequency, and the 1.1Hz modulation caused by the pulse-tube cooler was also subtracted by Fourier-analysis of the signal. The result of a typical beat frequency recorded during one rotation, and the rotation angle are shown here. **Down:** The same measurement, but without decorrelation. The tiny legend does not contain useful information.

The obtained amplitude sets $\{2B(t_i)\}$, $\{2C(t_i)\}$ are shown in Fig. 3.2. The data were analyzed following the Robertson-Mansouri-Sexl test theory, and according to the Standard Model Extension.

3.1 Analysis in the RMS framework

The amplitude sets $\{2B(t_i)\}$, $\{2C(t_i)\}$ were fitted with the functions (1.28) and (1.29), obtaining the coefficient for the violation of the isotropy of the speed of light: the results of the fit is $(\beta - \delta - \frac{1}{2}) = (+0.5 \pm 3) \cdot 10^{-10}$. Due to the experimental error in the determination of the tilt sensitivities there is an additional (systematic) error of $\pm 0.7 \cdot 10^{-10}$. We obtain then

$$\boxed{(\beta - \delta - \tfrac{1}{2}) = (+0.5 \pm 3 \pm 0.7) \cdot 10^{-10}}$$

This result is about factor 10 lower than the previous best results $(-1.2 \pm 1.9 \pm 1.2) \cdot 10^{-9}$ [14] and $(-2.2 \pm 1.5) \cdot 10^{-9}$ [5].[1]

A parameter $A = (\beta - \delta - \frac{1}{2}) = (+0.5 \pm 3 \pm 0.7) \cdot 10^{-10}$ corresponds to

$$\boxed{\frac{\delta c}{c} = 6.4 \cdot 10^{-16},}$$

taking $\beta^2 = v^2/c^2 = 1.52 \cdot 10^{-6}$ in Eq. (1.26).

3.2 Analysis in the SME test theory

Using all our data we can obtain a fit of the 5 Fourier amplitudes of $2C(t^*)$ at the time $t^* \simeq 6$ February 2005, see Table 3.1.

Table 3.1: Fourier amplitudes determined from the experiment. All quantities are in units of 10^{-16}.

	Basis	Value	Statistical error	Systematic error
C_0	1	−59	3.4	3.0
C_1	$\sin(\omega_\oplus T_\oplus)$	−3	1.5	0.5
C_2	$\cos(\omega_\oplus T_\oplus)$	11	2.0	0.5
C_3	$\sin(2\omega_\oplus T_\oplus)$	1	2.0	0.5
C_4	$\cos(2\omega_\oplus T_\oplus)$	0.1	2.0	0.2

These amplitudes are linear combinations of the $\tilde{\kappa}_{e-}$ and $\tilde{\kappa}_{o+}$ coefficients, where the weights of the latter depend on Earth's orbital phase (see Appendix E of [27]). For the fit the approximate relationship between the functions $B(t)$ and $C(t)$ was

[1] Note added in proof: after the submission of this thesis it was analysed a larger set of data, extending over 183 hours that contained 940 rotations, grouped in 5 sets. The 5 sets yielded the result:

$$(\beta - \delta - 1/2) = (-0.6 \pm 2.1 \pm 1.2) \times 10^{-10}.$$

Results published in [61, 62]

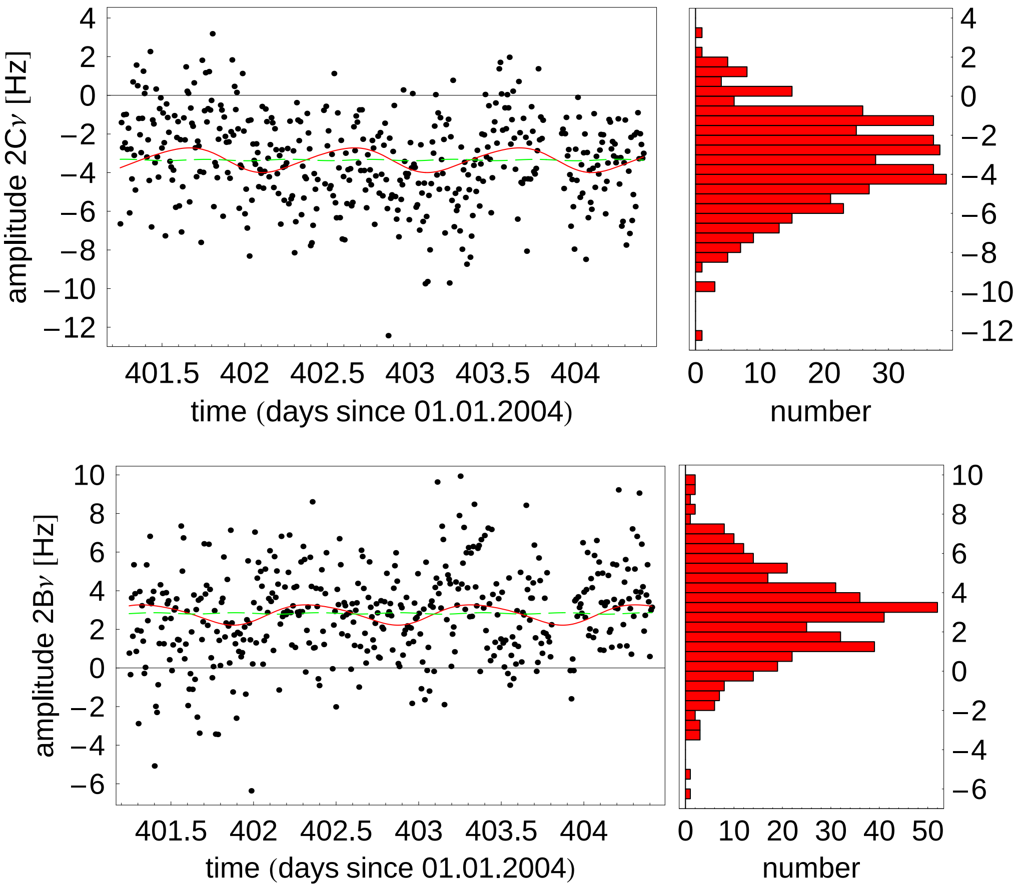

Figure 3.2: Measured $2B\nu$ and $2C\nu$ amplitudes of spatial anisotropy for individual rotations, and corresponding histograms. The fit error for each data point is less than 1 Hz. Full line: SME model plus systematic effect. Dashed line: RMS model plus systematic effect. Mean values: $\langle 2B\nu\rangle$= 2.8 Hz, $\langle 2C\nu\rangle$= -3.3 Hz.

used. The Fourier amplitudes of the B data can be obtained from the C amplitudes if the contributions due to the velocity of the laboratory with respect to the Earth's center, $\beta_L \approx 10^{-6}$, are neglected. Then $B_0 = 0$, $B_1 = -C_2/\cos\chi$, $B_2 = C_1/\cos\chi$, $B_3 = -2C_4\cos\chi/(1+\cos^2\chi)$ and $B_4 = 2C_3\cos\chi/(1+\cos^2\chi)$.

The coefficient b_0 in $B(t)$ takes into account the systematic effects. Due to the limited extent of the data over time, the frequencies $\omega_\oplus \pm \Omega_\oplus$ and $2\omega_\oplus \pm \Omega_\oplus$ cannot be distinguished and therefore it is not possible to extract the individual coefficients $\tilde{\kappa}_{e-}$ and $\tilde{\kappa}_{o+}$ from the C_i coefficients.

The results of the microwave cryogenic experiment [6] were used to set the elements of $(\tilde{\kappa}_{e-})$ (except for $(\tilde{\kappa}_{e-})^{ZZ}$) and the elements of $\beta_\oplus$ $(\tilde{\kappa}_{o+})$ to be zero, and used only the C_0-coefficient to determine $(\tilde{\kappa}_{e-})^{ZZ}$, *i.e.* Eq.(1.71) was truncated at the first term. The result is

$$\boxed{(\tilde{\kappa}_{e-})^{ZZ} = (-2.9 \pm 2.2) \cdot 10^{-14}}.[2]$$

The nonzero averages of the $2B$ and $2C$ amplitudes are due to a systematic effect of thermal origin that could not be modeled, as mentioned in section 2.9.4. The magnitude of the effect is consistent with the measured temperature sensitivity and the temperature modulation amplitude measured at the top of the apparatus. Thus we set for this parameter only an upper limit:

$$\boxed{|(\tilde{\kappa}_{e-})^{ZZ}| \leq 3 \cdot 10^{-14}}.$$

This experiment was limited firstly by the thermally induced systematic effects. Moreover, the laser frequency lock stability is limited by the small signal-to-noise ratio (low resonator throughput), which limits the ability to more precisely characterize the systematic effects.

[2] Note added in proof: in [26] a factor 2 was inadvertently omitted when calculating $(\tilde{\kappa}_{e-})^{ZZ}$ from 2C. The smaller value of the uncertainty in [26] was only statistic, whereas the uncertainty here is dominated by the systematic effects.

Chapter 4

Conclusions

Classic tests of Special Relativity were described, in order to introduce the kinematic test-theory of Robertson, Mansouri and Sexl. An extension of the Standard Model of particle physics, developed by A. Kostelecký and coworkers was also described. Then the experimental setup developed at the Institut für Experimentalphysik of the University of Düsseldorf and used to test experimentally the isotropy of the speed of light in both the test theories was described. In this experimental setup a pulse-tube cooler was used to cool two ultrastable cryogenic optical resonator down to 3.4 K. To my knowledge it was the first time that such a refrigerator was used for an experiment in optics. The pulse-tube cooler technique was used to avoid periodical changes on the mechanical dimensions of a cryostat using liquid helium as cryogen due to periodic refills. The pulse-tube cooler on the other hand produces vibrations at the frequency of gas helium waves used to cool the system. These vibrations were first decoupled from the resonators using a vibration insulation system, and then decorrelated from the signals used to test Relativity by Fourier analysis at the frequency of pumping. The temperature of the resonators were stabilised at the level of $60\,\mu$K, resulting in an instability of $13.6 \cdot 10^{-16}$.

The beat frequency between two Nd:YAG lasers stabilised at the resonance frequencies of the two optical resonators was measured and correlated with the position of the resonators and the time. The lasers were frequency stabilised using a Pound-Drever-Hall laser stabilisation technique, and the power of the beams impinging on the resonators was also stabilised. The laser beams were coupled to the resonators using optical fibres. This allowed a rejection of the instability caused by vibrations, but introduced a systematic effect to the system. The effect consisted in a sensitivity of the beat frequency on changes of temperature in the lab.

The complete setup, consisting of the cryostat, the lasers, the frequency stabilisation electronics, the temperature control, the frequency counter and the resonators was actively rotated.

Active rotation of the system was necessary for three reasons:

- to exploit the stability of the resonators, that is best between 10 and 100 seconds, instead of developing a frequency stabilisation system for very long integration time, and use the rotation of the Earth to change the direction of the axis of the resonators;

- to increase the statistics;
- to set a first limit to a previously unmeasured parameter of the dynamical test theory.

For the first two points a high rotation speed would be advantageous, but the system was limited by vibrations at high rotation speeds.

Rotations of the setup introduced a periodic tilt of the resonators due to mechanical instability of the rotation stage. The tilt of the resonators causes a change in its dimensions resulting in a change of the beat frequency that would mimic a violation of the Lorentz invariance, being at the same frequency of the rotations and in phase with it. To minimise this effect the cryostat was set in a position in which the variations of the tilts of the resonators were at minimum. The tilts were measured using a tilt sensor, and recorded. The calibration of the effect of a tilt of the resonators as a function of the angle allowed off-line decorrelation of the introduced systematic effect.

The data were analysed using the two test-theories described.

In the Robertson-Mansouri-Sexl test theory we obtained a violation of Lorentz invariance of $(\beta-\delta-1/2)=(0.5\pm3\pm0.7)\cdot10^{-10}$, which corresponds to a violation of the Lorentz invariance for the isotropy of space of $\frac{\delta c}{c}=6.4\cdot10^{-16}$. This was the most stringent limit at the time of the measurement.

The analysis of the experimental data led to the first determination of the upper limit to a previously unmeasured parameter $(\tilde{\kappa}_{e-})^{ZZ}$ of the dynamical test theory. The limit is $|\tilde{\kappa}_{e-}^{ZZ}|\leq 2\cdot10^{-14}$, a value confirmed by more recent measurements. The result is a nonzero value. This is due to the systematic effect due to the sensitivity of the beat frequency on the changes of temperature of the optical fibres. The temperature of the fibres changed during the rotations due to a temperature gradient in the lab. The effect was measured, but it was not possible to model it, so it could not be decorrelated. The order of magnitude of the effect is consistent with the nonzero value of the measured parameter.

4.1 Outlook

It was also proposed in [63] that the result of this experiment could be considered a first experimental check of the ether-drift observation reported by Miller in 1923 [64]. In [63] the results of our experiment are analysed considering the vacuum within the resonators as a physical medium whose refractive index is fixed by the general relativity. It is then stated that the frequency shift is consistent with the assumption of the presence of a preferred frame (Lorentz relativity instead of Einstein relativity), and that the Earth is moving with a velocity of ≈ 200 km/s in this system. However, the same author of [63] points out that a real precision test has still to consider the result of the same kind of measurement made a few months apart (August-September), where the frequency shift would increase of 70%.

The experiment described in this thesis will not take data in September, but other experiments are planned.

The results of this experiment and of the other experiments using cryogenic sapphire resonators showed that sapphire cryogenic resonators are still a promising technique. The results can still be improved, for instance setting up a more efficient temperature stabilisation of the lab, and an active control of the tilt of the resonators.

An active control of the fibre-coupling of the laser beams on the resonators would also be useful to improve the stability, although after cooling down from room temperature to 3.4 K the error signal decreases usually only of 10%. The use of optical fibres was necessary because of the vibrations caused by the pulse-tube cooler. To reduce the systematic effect caused by temperature gradients around the fibres (see Sect. 2.9.4), the length of the fibres should be reduced, the best would probably be to have the fibres only inside the cryostat, with coupling to the fibres either via feed-through or through optical windows in the cryostat. Another solution is of course an active beam stabilisation, as used in [5].

4.1.1 Room-temperature Michelson-Morley experiments

Room temperature experiments are very interesting because they allow to get rid of the cryogenic environment. This makes easier to implement new techniques and investigate on systematic effects.

With the availability of ULE resonators with a zero thermal expansion coefficient at or near room temperature the conditions on temperature stability are less stringent than in the past, and the construction of two resonators in a single block provides a common-mode rejection of the drift of the beat frequency between two resonators. The idea here is to put four mirrors in cross configuration in the same block of ULE. This gives common-mode rejection also of temperature instabilities of the block (within the temperature gradient of the block).

Working on a room temperature system permits to have a less heavy system. This is important because we have seen that the tilt and the vibrations have a dramatic effect on the signals. A more compact setup will be easier to integrate to an active vibration-insulation system, and tilt-control actuators.

Dr. A. Nevsky, Dr. M. Okhapkin and Mr. Ch. Eisele work on these ideas, also with an improved laser stabilisation system. The goal is to test Lorentz invariance improving the limits on kinematic and dynamic test theories under the 10^{-17} level that is set by the ratio between $m_w/m_P \simeq 10^{-17}$, where $m_w \simeq 100$ GeV is the electroweak scale and m_P the Planck's mass, see pag. 17.

4.1.2 OPTIS: a satellite-based test of Relativity

An improvement of the precision of tests of Special Relativity would be the result of satellite based experiments. The project OPTIS [65], started as a collaboration of the Center of Applied Space Technology and Microgravity (ZARM) of the University of Bremen (Germany) and the Humboldt-University in Berlin and the Institut für Experimentalphysik of the University of Düsseldorf, was planned to test Special and General Relativity, and supported by the German Space Agency (DLR).

The idea is to use three ULE resonators, in a single block, and compare the resonance frequencies between them, and between the resonators and an optical frequency comb, in dependence of the position and velocity of the satellite. The use of a satellite would permit to work in a microgravity environment. The goals of the mission are to test the isotropy of light propagation (Michelson-Morley experiment), the independence of the velocity of light from the velocity of the laboratory (Kennedy-Thorndike), the universality of the gravitational red-shift (comparing an optical resonator to an optical frequency comb).

The satellite should have a high eccentric orbit of 14 hours, with 5 months without shadows (useful for temperature stability) and 1 month with shadow phases:

	Apogee	Perigee
Height from Earth's centre	3600 km	10000 km
Velocity	2.28 km/s	5.93 km/s
Gravitational potential	$1.1 \cdot 10^{-10}$	$4.4 \cdot 10^{-10}$
Gravity gradient	$1.2 \cdot 10^{-8}$ s^{-2}	$0.8 \cdot 10^{-8}$ s^{-2}

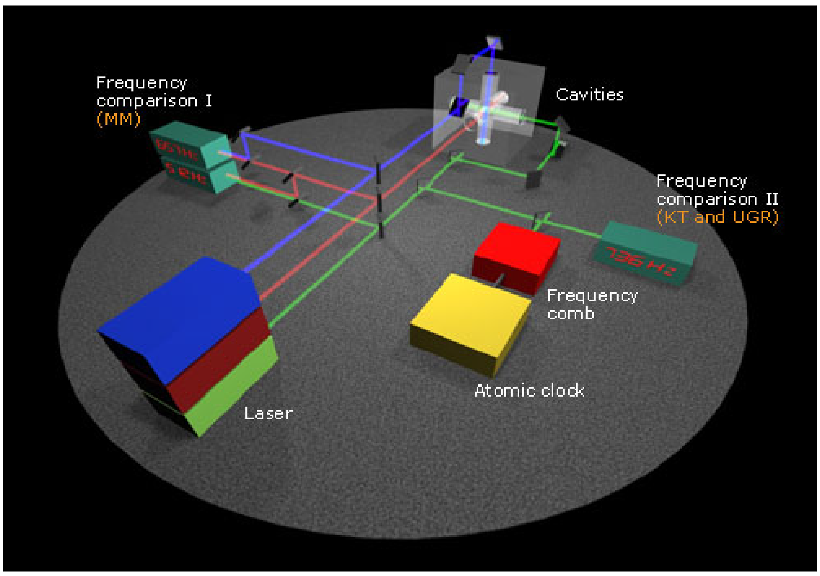

Figure 4.1: The basic setup for the OPTIS satellite mission. From [65].

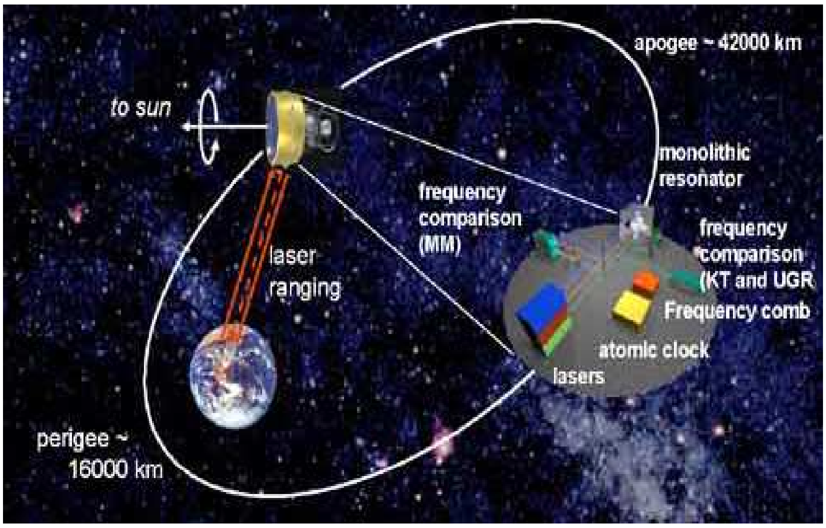

Figure 4.2: A scheme of the orbit of the mission OPTIS. From [65].

Appendix A

Allan Variance

A.1 Introduction

The use of the classical variance and the standard deviation of the mean can in some high precision measurements be unappropriate. The reason is basically that correlated random noise is as likely to occur as the uncorrelated random noise. Besides, the act of observing some physical quantity perturbs the quantity itself. The random deviations in a series of observations may be caused by the measurement system, by environmental coupling, or by intrinsic deviations of the measured quantity.

The assumption that each measurement of a series is independent because the measurements are taken in different times is sometimes not correct. If the series is not random and uncorrelated, the noise spectrum can not be considered 'white' [66].

In this case, more appropriated, and now universally accepted in metrology, is the use of the Allan Variance [67].

In the general case of a frequency measurement, it is useful to define:

$$y(t) = \frac{\nu_1 - \nu_0}{\nu_0} \tag{A.1}$$

as the fractional frequency difference or deviation of an oscillator, ν_1, with respect to a reference oscillator ν_0, divided by the nominal frequency ν_0. Conceptually, we can also consider the Eq. (A.1) as the free running frequency of an oscillator ν_1, with respect to its nominal value. The dimensionless quantity y(t) is useful in describing an oscillator performance: for instance the phase deviation x(t) of an oscillator over a period of time t is simply given by:

$$x(t) = \int_0^t y(t')\mathrm{d}t' \tag{A.2}$$

Almost all frequency measurements, with very few exceptions, are measurements of phase, or of the period fluctuations of an oscillator, not of frequency.

Note that time and phase deviations are proportional, $x = \phi/(2\pi\nu_0)$, where ϕ denotes the phase deviation of an oscillator.

Since it is impossible to measure instantaneous frequency, any frequency measurement involves some sample time τ: a time window through which the oscillators observed. The difference of two time deviations divided by the time τ gives the *fractional frequency* over the period τ:

$$\overline{y}(t) = \frac{x(t+\tau) - x(t)}{\tau} \tag{A.3}$$

A.2 Analysis of time domain data

Since phase is the integral of frequency, we may write:

$$S_y(f) = (2\pi f)^2 S_x(f) \tag{A.4}$$

where $y = dx/dt$ and x represents the time deviations. For discrete data the continuous derivative $y = dx/dt$ becomes $y_k = \Delta x_k/\tau_0$, where k is the counting index in the measurement time series, and $\Delta x_k = x_{k+1} - x_k$ is the first finite difference on the time deviation series x_k, with x_k spaced τ_0 apart.

If the fluctuations are characterized by power law spectra, that are more dispersive than classical white noise, then the standard deviation is a function of the number of data points in the set. It is also a function of the dead time and of the measurement system bandwidth. For instance, using flicker noise frequency modulation as a model, as the number of data points increases, the standard deviation monotonically increases without limit. The Allan variance is a statistical measure that does not depend upon the data length.

The Allan variance is estimated from a finite data set as follows:

$$\sigma_y(\tau) = \left[\frac{1}{2(M-1)}\sum_{i=1}^{M-1}(y_{i+1} - y_i)^2\right]^{1/2} \tag{A.5}$$

where the y_i are the discrete frequency averages on time τ.

If one wants to know how $\sigma_y(\tau)$ varies with the sample time τ, it is possible to average the values for y_1 and y_2, and call it a new y_1 and so on. This is possible only if there is no dead time.

We can combine the equations (A.3) and (A.5) to obtain $\sigma_y(\tau)$ in terms of the time difference or time deviation measurements: for N discrete time readings it may be estimated as

$$\sigma_y(\tau) = \left[\frac{1}{2(N-2)\tau^2}\sum_{i=1}^{N-2}(-x_{i+2} + 2x_{i+1} - x_i)^2\right]^{1/2} \tag{A.6}$$

here the i denotes the number of readings in the set of N and the nominal spacing between readings is τ. If there is no dead time in the data and the original data were taken with a sample time τ_0, a set of x_i's can be obtained by integrating the y_i's:

$$x_{i+1} = x_i + \tau_0 \sum_{j=1}^{i} y_j \tag{A.7}$$

Once we have the x_i's, we can pick τ in Eq. (A.6) to be any integer multiple of τ_0, i.e. $\tau = m\tau_0$:

$$\sigma_y(m\tau_0) = \left[\frac{1}{2(N-2m)m^2\tau_0^2} \sum_{i=1}^{N-2m} (-x_{i+2m} + 2x_{i+m} - x_i)^2 \right]^{1/2} \tag{A.8}$$

To understand why it is not correct to use the classical variance, first of all, let's compare the definitions of the two variances:

The Allan variance is defined as in Eq. (A.5)

$$\sigma_y(\tau) = \left[\frac{1}{2(M-1)} \sum_{i=1}^{M-1} (y_{i+1} - y_i)^2 \right]^{1/2} \tag{A.9}$$

and the standard deviation is defined as:

$$\sigma_y(N) = \left[\frac{1}{N-1} \sum_{k=1}^{N} (y_k - \overline{y})^2 \right]^{1/2} \tag{A.10}$$

where $\overline{y}$ denotes the mean value of the sample.

To show the divergent behaviour of the classical variance for correlated time series, we write from the Parceval's Theorem:

$$\sigma^2 = \frac{1}{\pi} \int_0^\infty S(\omega) \mathrm{d}\omega \tag{A.11}$$

where $S(\omega)$ is a symmetrical two-sided spectral density, and $\omega = 2\pi f$. If the variable being measured has random variations that have a power spectrum proportional to f^α, then for $\alpha = -1$ the classical variance is infinite at both limits of the integral. This means that unless there are both high- and low-frequency cutoffs to the process being analyzed, the classical variance is unbounded. A high-frequency cutoff always exists, and it is determined from the measurement system. However, a low-frequency cutoff is needed for $\alpha \leq -1$, and sometimes it is very difficult if not impossible to determine. If this is the case, then the classical variance is not useful in characterising f^α processes with $\alpha \leq -1$ [66].

In metrology we are often faced to processes which are correlated in time. Processes that can affect the measurements are coupling to the environment, or the aging of the physical device, or influence from the measurement process. As stated, in this case the random deviations are correlated, and to interpret the results a knowledge of the spectrum is necessary.

The normalized frequency y(t), defined in Eq. (A.1), will have systematic and random deviations. The spectral density of the random deviations is well modeled by $S_y(f) = h_\alpha f^\alpha$, with α = –2, –1, 0, +1, +2. The coefficient h_α is the intensity of the particular type α of power-law process. The value for α depends on the kind of clock considered, and on the region of Fourier frequency f or of averaging time τ of interest. In general, α tends to decrease increasing the averaging time.

If $S_y(f) = h_\alpha f^\alpha$, and α = –2, –1, 0, +1, +2, then using Eq. (A.4) we can write $S_x(f) = h_\alpha f^\beta/(2\pi)^2$, with corresponding values of β = –4, –3, –2, –1, 0. Table A.1 gives the names and Fourier relationships for the frequency and phase deviations, assuming $S_y(f) = h_\alpha f^\alpha$. Remember that time and phase deviations are proportional, $x = \phi/(2\pi\nu_0)$, where ϕ denotes the phase deviation of an oscillator.

Table A.1: Functional characteristics of different noise processes, from [66].

α	β	Frequency modulation	Phase modulation	$S_y(f)$	$S_x(f)$	$\sigma_y^2(\tau)$
+2	0	Super White	<u>White PM</u>	$h_2 f^2$	$\frac{h_2}{(2\pi)^2}$	$\frac{3f_h}{(2\pi)^2} h_2 \tau^{-2}$
+1	–1	Super Flicker	<u>Flicker PM</u>	$h_1 f$	$\frac{h_1}{(2\pi)^2} f^{-1}$	$\frac{1.3+3\ln(2\pi f_h \tau)}{(2\pi)^2} h_1 \tau^{-2}$
0	–2	<u>White FM</u>	<u>Random Walk PM</u>	h_0	$\frac{h_0}{(2\pi)^2} f^{-2}$	$\frac{1}{2} h_0 \tau^{-1}$
–1	–3	<u>Flicker FM</u>	Flicker Walk	$h_{-1} f^{-1}$	$\frac{h_{-1}}{(2\pi)^2} f^{-3}$	$2\ln(2) h_{-1}$
–2	–4	<u>Random Walk FM</u>	Random Run	$h_{-2} f^{-2}$	$\frac{h_{-2}}{(2\pi)^2} f^{-4}$	$\frac{(2\pi)^2}{6} h_{-2} \tau$

Bibliography

[1] A. Einstein, “Zur Elektrodynamik bewegter Körper,” *Annalen der Physik und Chemie*, vol. 17, p. 891, 1905.

[2] A. Brillet and J. L. Hall, “Improved laser test of the isotropy of space,” *Phys. Rev. Lett.*, vol. 42, no. 9, p. 549, 1979.

[3] P. Wolf, S. Bize, A. Clairon, A. N. Luiten, G. Santarelli, and M. E. Tobar, “Tests of Lorentz invariance using a microwave resonator,” *Phys. Rev. Lett.*, vol. 90, p. 060402, 2003.

[4] J. A. Lipa, J. A. Nissen, S. Wang, D. A. Stricker, and D. Avaloff, “New limit on signals of Lorentz violation in electrodynamics,” *Phys. Rev. Lett.*, vol. 90, p. 060403, 2003.

[5] H. Müller, S. Herrmann, C. Braxmaier, S. Schiller, and A. Peters, “Modern Michelson-Morley experiment using cryogenic optical resonators,” *Phys. Rev. Lett.*, vol. 91, p. 020401, 2003.

[6] P. Wolf, S. Bize, A. Clairon, G. Santarelli, M. E. Tobar, and A. N. Luiten, “Improved test of Lorentz invariance in electrodynamics,” *Phys. Rev. D*, vol. 70, p. 051902(R), 2004.

[7] C. M. Will, *Theory and experiment in gravitational physics.* Cambridge Univ. Press, 1993.

[8] V. A. Kostelecký, “Proceedings of the meetings on CPT and Lorentz symmetry,” 1999-2002.

[9] A. A. Michelson and E. W. Morley, “On the relative motion of the Earth and the luminifreous ether,” *American Journal of Science*, vol. XXXIV, p. 333, 1887.

[10] R. Resnick, *Introduction to Special Relativity.* Wiley, 1 ed., 1968.

[11] T. S. Jaseja, A. Javan, J. Murray, and C. H. Townes, “Test of special relativity or of the isotropy of space by use of infrared maser,” *Phys. Rev.*, vol. 133, p. A1221, 1964.

[12] A. Brillet and J. L. Hall, "An improved test of the isotropy of space using laser techniques," in *Laser Spec. IV*, Springer, 1979.

[13] C. Braxmaier, H. Müller, O. Pradl, J. Mlynek, A. Peters, and S. Schiller, "Test of relativity using a cryogenic optical resonator," *Phys. Rev. Lett.*, vol. 88, p. 010401, 2002.

[14] P. Wolf, M. E. Tobar, S. Bize, A. Clairon, A. N. Luiten, and G. Santarelli, "Whispering gallery resonators and tests of Lorentz invariance," *Gen. Rel. Grav.*, vol. 36, p. 2351, 2004.

[15] R. J. Kennedy and E. M. Thorndike, "Experimental establishment of the relativity of time," *Phys. Rev.*, vol. 42, p. 400, 1932.

[16] G. Saathoff, S. Karpuk, G. Huber, S. Krohn, R. Muñoz Horta, S. Reinhardt, D. Schwalm, A. Wolf, and G. Gwinner, "Improved test of time dilation in special relativity," *Phys. Rev. Lett.*, vol. 91, p. 190403, 2003.

[17] R. F. C. Vessot, M. W. Levine, E. M. Mattison, E. L. Blomberg, T. E. Hoffman, R. Decher, P. B. Eby, C. R. Bauger, J. W. Watts, D. L. Teuber, and F. D. Wills, "Test of relativistic gravitation with a space-borne hydrogen maser," *Phys. Rev. Lett.*, vol. 45, p. 2081, 1980.

[18] H. P. Robertson, "Postulate *versus* observation in the special theory of relativity," *Rev. Mod. Phys.*, vol. 21, p. 378, 1949.

[19] R. Mansouri and R. U. Sexl, "A test theory of special relativity: I. Simultaneity and clock synchronization," *Gen. Rel. Grav.*, vol. 8, p. 497, 1977.

[20] R. Mansouri and R. U. Sexl, "A test theory of special relativity: II. First order tests," *Gen. Rel. Grav.*, vol. 8, p. 515, 1977.

[21] R. Mansouri and R. U. Sexl, "A test theory of special relativity: III. Second-order tests," *Gen. Rel. Grav.*, vol. 8, p. 809, 1977.

[22] H. E. Ives and G. R. Stilwell, "An experimental study of the rate of a moving atomic clock," *J. Opt. Soc. Am.*, vol. 28, p. 215, 1938.

[23] H. E. Ives and G. R. Stilwell, "An experimental study of the rate of a moving atomic clock. II," *J. Opt. Soc. Am.*, vol. 31, p. 369, 1941.

[24] A. P. French, *Special Relativity.* Norton ed., 2 ed., 1968.

[25] G. F. Smoot, M. V. Gorenstein, and R. A. Muller, "Detection of anisotropy in the cosmic blackbody radiation," *Phys. Rev. Lett.*, vol. 39, p. 898, 1977.

[26] P. Antonini, M. Okhapkin, E. Göklü, and S. Schiller, "Test of constancy of speed of light with rotating cryogenic optical resonators," *Phys. Rev. A*, vol. 71, p. 050101(R), 2005.

[27] V. A. Kostelecký and M. Mewes, "Signals for Lorentz violation in electrodynamics," *Phys. Rev. D*, vol. 66, p. 056005, 2002.

[28] V. A. Kostelecký and S. Samuel, "Spontaneous breaking of Lorentz symmetry in string theory," *Phys. Rev. D*, vol. 39, p. 683, 1989.

[29] D. Colladay and V. A. Kostelecký, "Lorentz-violating extension of the standard model," *Phys. Rev. D*, vol. 58, p. 116002, 1998.

[30] R. Bluhm, V. A. Kostelecký, and N. Russell, "CPT and Lorentz tests in hydrogen and antihydrogen," *Phys. Rev. Lett.*, vol. 82, p. 2254, 1999.

[31] S. M. Carroll, G. B. Field, and R. Jackiw, "Limits on a Lorentz- and parity-violating modification of electrodynamics," *Phys. Rev. D*, vol. 41, p. 1231, 1990.

[32] V. A. Kostelecký and M. Mewes, "Cosmological costraints on Lorentz violation in electrodynamics," *Phys. Rev. Lett.*, vol. 87, p. 251304, 2001.

[33] M. E. Tobar, P. Wolf, A. Fowler, and J. G. Harnett, "New methods of testing Lorentz violation in electrodynamics," *Phys. Rev. D*, vol. 71, p. 025004, 2005.

[34] R. Bluhm, V. A. Kostelecký, C. D. Lane, and N. Russell, "Clock-comparison tests of Lorentz and CPT symmetry in space," *Phys. Rev. Lett.*, vol. 88, p. 090801, 2002.

[35] R. Bluhm, V. A. Kostelecký, C. D. Lane, and N. Russell, "Probing Lorentz and CPT violation with space-based experiments," *Phys. Rev. D*, vol. 68, p. 125008, 2003.

[36] E. Göklü, *Tests der Lorentzinvarianz mittels elektromagnetischer Resonatoren.* Diplomarbeit (German diploma thesis), Universität Düsseldorf. Germany, 2004.

[37] C. Lämmerzahl and M. P. Haugan, "On the iterpretation of Michelson-Morley experiments," *Phys. Lett. A*, vol. 282, p. 223, 2001.

[38] H. Müller, C. Braxmaier, S. Herrmann, A. Peters, and C. Lämmerzahl, "Electromagnetic cavities and Lorentz invariance violation," *Phys. Rev. D*, vol. 67, p. 056006, 2003.

[39] G. K. White and P. J. Meeson, *Experimental Techniques in Low-Temperature Physics.*

[40] C. Wang, G. Thummes, and C. Heiden, "A two-stage pulse tube cooler operating below 4 K," *Cryogenics*, vol. 37, p. 159, 1997.

[41] C. Wang, G. Thummes, C. Heiden, K.-J. Best, and B. Oswald, “Cryogen free operation of a niobium-tin magnet using a two-stage pulse tube cooler,” *IEEE Trans. Appl. Superconductivity*, vol. 9, p. 402, 1998.

[42] C. Lienerth, G. Thummes, and C. Heiden, “Progress in low noise cooling peformance of pulse-tube cooler for HT SQUID,” *IEEE Trans. Appl. Superconductivity*, vol. 11, p. 812, 2001.

[43] D. Gedeon, “DC flows in Stirling and pulse tube coolers,” *Cryocoolers*, vol. 9, p. 385, 1997.

[44] R. Karunanithi, S. Jacob, S. Kasthurirengan, U. Behera, and D. S. Nadig, “Development of a reliable and simple pressure wave generator for pulse tube refrigerators,” *Rev. Sci. Instrum.*, vol. 75, p. 2479, 2004.

[45] S. Seel, R. Storz, G. Ruoso, J. Mlynek, and S. Schiller, “Cryogenic optical resonators: a new tool for laser frequency stabilization at the 1 Hz level,” *Phys. Rev. Lett.*, vol. 78, p. 4741, 1997.

[46] R. Storz, C. Braxmaier, K. Jäck, O. Pradl, and S. Schiller, “Ultrahigh long-term dimensional stability of a sapphire cryogenic optical resonator,” *Opt. Lett.*, vol. 23, p. 1031, 1998.

[47] H. Müller, C. Braxmaier, S. Hermann, O. Pradl, C. Lämmerzahl, J. Mlynek, S. Schiller, and A. Peters, “Testing the foundation of relativity using cryogenic optical resonators,” *IJMPD*, vol. 11, p. 1101, 2002.

[48] M. Lucht, M. Lerche, H. C. Wille, Y. V. Shvyd’ko, H. D. Rüter, E. Gerdau, and P. Becker, “Precise measurement of the lattice parameters of α-Al_2O_3 in the temperature range 4.5-250 K using the Mössbauer wavelength standard,” *J. Appl. Cryst.*, vol. 36, p. 1075, 2003.

[49] K. Jäck, *Charakterisierung eines kryogenen Referenzresonator-Systems zur Nd:YAG-Laser-Frequenzstabilisierung.* Diplomarbeit (German diploma thesis), Universität Konstanz. Germany, 1997.

[50] C. T. Taylor, M. Notcutt, and D. G. Blair, “Cryogenic, all-sapphire, Fabry-Perot optical frequency reference,” *Rev. Sci. Instrum.*, vol. 66, p. 955, 1995.

[51] R. W. P. Drever, J. L. Hall, F. V. Kowalski, J. Hough, G. M. Ford, A. J. Munley, and H. Ward, “Laser phase and frequency stabilization using an optical resonator,” *Appl. Phys. B*, vol. 31, p. 97, 1983.

[52] T. Day, E. K. Gustafson, and R. L. Byer, “Sub-hertz relative frequency stabilization of two-diode laser-pumped Nd:YAG lasers locked to a Fabry-Perot interferometer,” *IEEE J. Quantum Electron.*, vol. 28, p. 1106, 1992.

[53] K. Numata, A. Kemery, and J. Camp, "Thermal-noise limit in frequency stabilization of lasers with rigid cavities," *Phys. Rev. Lett.*, vol. 93, p. 250602, 2004.

[54] G. Cantatore, F. D. Valle, E. Milotti, P. Pace, E. Zavattini, E. Polacco, F. Perrone, C. Rizzo, G. Zavattini, and G. Ruoso, "Frequency locking of a Nd:YAG laser using the laser itself as the optical phase modulator," *Rev. Sci. Instrum.*, vol. 66, p. 2785, 1994.

[55] P. Horowitz and W. Hill, *The Art of Electronics.* Cambridge University Press, 2 ed., 1989.

[56] G. F. Franklin, J. D. Powell, and A. Emami-Naeini, *Feedback Control of Dynamic Systems.* Addison-Wesley ed., 3 ed., 1995.

[57] S. A. Diddams, D. J. Jones, L. Ma, S. T. Cundiff, and J. L. Hall, "Optical frequency measurement across a 104-THz gap with a femtosecond laser frequency comb," *Opt. Lett.*, vol. 25, p. 186, 2000.

[58] S. A. Diddams, T. Udem, K. R. Vogel, C. W. Oates, E. A. Curtis, R. S. Windeler, A. Bartels, J. C. Bergquist, and L.Hollberg, "A compact femtosecond-laser-based optical clockwork," *Science*, vol. 293, p. 825, 2001.

[59] T. Udem, J. Reichert, R. Holzwarth, and T. W. Hänsch, "Accurate measurement of large optical frequency differences with a mode-locked laser," *Opt. Lett.*, vol. 24, p. 881, 1999.

[60] H. Müller, *Modern optical tests of Relativity.* Phd thesis, Humboldt-University, Berlin. Germany, 2004.

[61] P. Antonini, M. Okhapkin, E. Göklü, and S. Schiller, "Reply to "Comment on 'Test of constancy of speed of light with rotating cryogenic optical resonators' "," *Phys. Rev. A*, vol. 72, p. 066102, 2005.

[62] S. Schiller, P. Antonini, and M. Okhapkin, "A precision test of the isotropy of the speed of light using rotating cryogenic optical cavities," *arXiv:physics/0510169*, 2005. To appear in: Lect. Notes Phys. (2006).

[63] M. Consoli, "Precision test for the new Michelson-Morley experiments with rotating cryogenic cavities," *arXiv*, vol. physics, p. 0506005, 2005.

[64] D. C. Miller, "The ether-drift experiment and the determination of the absolute motion of the Earth," *Rev. Mod. Phys.*, vol. 5, p. 203, 1923.

[65] C. Lämmerzahl, I. Ciufolini, H. Dittus, L. Iorio, H. Müller, A. Peters, E. Samain, S. Scheithauer, and S. Schiller, "OPTIS– an Einstein mission for improved test of special and general relativity," *Gen. Rev. Grav.*, vol. 36, p. 2373, 2004.

[66] D. W. Allan, "Should the classical variance be used as a basic measure in standard metrology?," *IEEE Trans. Instr. Meas.*, vol. IM-36, p. 646, 1987.

[67] D. B. Sullivan, D. W. Allan, D. A. Howe, and F. L. Walls, "Characterization of clocks and oscillators," *NIST Technical note*, vol. TN1337, 1990.

Thank you

It is a very big pleasure for me to thank the people who helped me during this work.

First of all, Prof. Stephan Schiller, who decided to give me this task, and always found the time to guide and motivate me through my PhD. He also took active part in the work in the lab and in the data analysis. For all what I have learned from him I am really very thankful.

Dr. Maxim Okhapkin worked as post-doc at this experiment. I was very lucky to work with such a skillful scientist, and very happy to have found in him also a very good friend.

Ertan Göklü developed together with Prof. Schiller the routines for the analysis of the data of the experiment for his diploma thesis. Without his work my experimental work would have been useless.

In the Institut für Experimentalphysik of the University of Düsseldorf I had the pleasure to work together with many other people, who made here a very good atmosphere: Prof. A. Görlitz, Prof. Andreas Wicht, Dr. Alexander Nevsky, Dr. Helmut Wenz, Pr. Doz. Claus Lämmerzahl, the postdocs Bernhard Roth, Peter Blythe and Alex Wilson, the PhD students Luca Haiberger, Alexander Ostendorf, Ulf Fröhlich, Frank Müller, Christian Eisele, Ingo Ernsting, Chaobo Zhang, Roland Wilke, Sven Kroboth, Nils Nemitz... the diploma students David, Heiner, Hartmut, Michael, Thomas, Ulf. Ms. Barbara Nolte always assigned me the best students to teach at the undergraduate courses.

Other people did essential work for my research: Peter Dutkievicz who prepared a lot of electronic stuff, Willi Rockrath who had always the time to fix problems with the computers, Rita Gusek, Waldemar Kussmaul, Mr. Hoffmann and Jens Bremen in the mechanical workshop, Günter Ziethen and Silke Frye.

They didn't take active part in my research, but even from the distance I felt them always very near: my wonderful family and Federica who had the goodness to wait for my coming back home. There are no words to thank all of them.

Piergiorgio Antonini

Erklärung:

Die hier vorgelegte Dissertation habe ich eigenständig und ohne unerlaubte Hilfe angefertigt. Die Dissertation wurde in der vorgelegten oder in ähnlicher Form noch bei keiner anderen Institution eingereicht. Ich habe bisher keine erfolglosen Promotionsversuche unternommen.

Düsseldorf, den 15.02.2006

(Piergiorgio Antonini)